Stress Analysis of Pressurized Water Reactor Steam Generator Tube Denting Phenomena

EPRI

EPRI NP-828
Project 700
Interim Report
July 1978

Keywords:
Steam Generator
Tube Denting
Pressurized Water Reactor
Corrosion
Support Plate

Prepared by
Failure Analysis Associates
Palo Alto, California

ELECTRIC POWER RESEARCH INSTITUTE

Stress Analysis of Pressurized Water Reactor Steam Generator Tube Denting Phenomena

NP-828
Research Project 700

Interim Report, July 1978

Work Completed, October 1977

Prepared by

FAILURE ANALYSIS ASSOCIATES
750 Welch Road, Suite 116
Palo Alto, California 94304

Principal Investigators
Jerrell M. Thomas
Russell C. Cipolla
Ganapathy V. Ranjan
George Derbalian

Prepared for

Electric Power Research Institute
3412 Hillview Avenue
Palo Alto, California 94304

EPRI Project Manager
Floyd Gelhaus
Nuclear Power Division

EPRI PERSPECTIVE

PROJECT DESCRIPTION

In 1976, EPRI became aware of the phenomena associated with nuclear steam generator tube denting. These generators are vertical shell, inverted U-tube heat exchangers with over 3000 Inconel-600 tubes. The primary water inside these tubes is typically at 2000 psi pressure and at a temperature such that the tube wall average temperature is near 525°F. At various elevations, the tubes pass through drilled holes in carbon steel plates. "Denting" of tubes (reduction in diameter where tubes pass through support plates) has occurred in a number of steam generators. Most commonly this has occurred in plants with seawater cooling, with prior use of phosphate water treatment followed by all-volatile chemistry, and which have had considerable history of condenser leaks. A common cause of the tube denting is now believed to be the acidic chloride attack of these support plates which causes rapid corrosion on the surfaces of the tube support plate holes through which the tubes pass. Even small traces of chloride (<1ppm) in feedwater are ample to initiate denting due to the concentrating effect of the heated crevice between the tube and the support plate. Copper and oxygen also influence the rate of corrosion in the crevice. Since the corrosion product has a larger volume than the metal from which it forms, the tube becomes compressed, the plate hole is expanded, and the support plate deforms and cracks.

A number of utilities with nuclear steam supply systems which utilize this design of steam generator formed a PWR Owners Group late in 1976 for the specific task of determining the best solutions to steam generator problems and to augment the rate of effort possible within EPRI budgets. EPRI subsequently established a Steam Generator Project Office to manage the PWR Owners Group Steam Generator program. A broad and comprehensive technical program has now been defined by the EPRI Project Office and many projects have been initiated, as well as continuing or accelerating the EPRI-funded work.

PROJECT OBJECTIVE

Late in 1976, as part of the RP700 contract scope of work, Failure Analysis Associates staff met with utility and manufacturer personnel. Out of this and subsequent similar meetings came the beginning of the work plan formulation for EPRI-funded activities directed at mechanical and stress analysis of the denting phenomenon. The RP700 Contract was used to initiate some of the critical scoping analyses.

In plants where the tube denting is most severe, deformations of the support plate flow slots and tube U-bends and cracking of support plate ligaments have been observed. In a few instances, tube denting has caused leaks to develop in tubes in the vicinity of the support plate. In one instance, leaks have developed in a tube U-bend. Elastic-plastic analyses have been performed to determine the stresses, strains, and deformations in the tubes and support plates which are associated with these denting phenomena. These analyses are mainly applicable to the Westinghouse Series 44 and 51 designs.

CONCLUSIONS AND RECOMMENDATIONS

This report summarizes these preliminary analysis results. As in any mathematical modeling of physical events, there are limitations on how well the models represent reality. Sensitivity studies to quantify the effects of changes in assumptions and in input data are desirable to guide future modeling efforts and work to characterize the denting, deformation, and cracking effects more precisely. This is expected to be a continuing effort with progressively more refined models, more accurate input information, and with a variety of uses; for example, to guide operating and inspection decisions, to estimate useful lifetimes, and to provide inputs for licensing analysis.

Floyd E. Gelhaus
EPRI Project Manager
Nuclear Power Division

ABSTRACT

In some Pressurized Water Reactor (PWR) steam generators, a corrosion product has formed on the carbon steel support plate in the crevice between the tube and support plate. The corrosion product occupies more volume than the original metal; the tube-to-support plate crevice volume is thus consumed with corrosion product, and further corrosive action results in a radially inward force on the tube and a radially outward force on the corroding support plate. This has resulted in indentation ("denting") of the tube, accompanied by occasional cracking. Large in-plane deformation and cracking of support plates has also been observed in the most severely affected plants along with some serious side effects, such as deformation and cracking of inner row tube U-bends caused by support plate movement.

Mechanical aspects of the tube denting phenomena have been studied using analytical models. The models used ranged from closed form analytical solutions to state-of-the-art numerical elastic-plastic computer program for moderate strains. It was found that tube dents, such as those observed in operating steam generators, are associated with yielding of both the tubes and support plates. Also studied were the stresses in tube U-bends caused by support plate flow slot deformation.

Blank Page

ACKNOWLEDGEMENTS

The authors gratefully acknowledge the cooperation of Consolidated Edison Company, Florida Power and Light Company, Southern California Edison Company, Virginia Electric and Power Company, Westinghouse Electric Corporation, and the Electric Power Research Institute (EPRI) in furnishing information necessary to accomplish this analysis. Mr. Louis Martel of EPRI and Dr. Charles A. Rau, Jr., of Failure Analysis Associates were especially helpful in formulating and guiding the program. The authors further acknowledge the assistance of Cathy Rogers and Darlene Sinibaldi in typing the manuscript and Jeanne Weir in drawing the illustrations.

Blank Page

TABLE OF CONTENTS

(TABLE OF CONTENTS - Continued)

ILLUSTRATIONS

SUMMARY

Extensive elastic-plastic analyses have been performed to determine stresses, strains, and deformations in Pressurized Water Reactor (PWR) steam generator tubes and support plates relevant to tube "denting" phenomena. These analyses (with qualifications as stated throughout the report) are applicable to the Westinghouse Series 44 and 51 designs. The scope of the denting problem and the essential mechanical features were determined in consultation with the EPRI staff, affected utilities, and steam generator vendors. A fraction of PWR steam generators are experiencing some tube denting which sometimes results in leaking tubes. Large deformations and some cracking of support plates have been observed. Support plate deformations have resulted in straining and cracking of some tube U-bends.

An elastic analysis of the tube U-bend shows that circumferential strains above yield occur due to ovalization of the tube even with small support plate flow slot deformations on the order of 40 mils compared to observed deformations of more than 800 mils in the most severely affected plants. These strains contribute to the cracking of small bend radius U-bend tubes.

Normal operational stresses for the tubes are far below the yield stress, but once the clearance annulus is closed, additional corrosion can readily cause yielding of the tube. The diametral dent depth at tube yielding is on the order of one mil for axisymmetric dents and ten mils for oval dents. For axisymmetric dents, the maximum stress is longitudinal, and for oval dents, it is circumferential.

Yielding in the support plate precedes yielding of the tube and occurs first near free edges, then later near rigid supports after yielding of the tube. Near rigid supports, local yielding of the plate is predicted, but large tube deformations are expected to precede gross yielding of the plate. As material wastage occurs in the plate due to corrosion, gross yielding of the weakened plate may also occur near rigid supports, but this wastage effect is not included in this analysis. For this reason, results of the support plate ligament analysis may not be applicable to the most seriously affected plants.

Field observations show that large deformations have occurred in the tubes (up to 0.23 inch diametral dent depth) and support plates (up to 1.75 inch flow slot closure). The major features of the field observations are quantitatively reproduced analytically by separate models of the tube and support plate. A more refined model of the combined tube, support plate, and crevice oxide has been applied in the elastic range and is expected to give a closer approximation to the interaction between the tube, plate, and oxide when applied in the plastic range.

Further development of the combined model should include the effects of the significant plate metal losses due to corrosion, and a similar model should be developed for other designs. Failure criteria for the tube and plate should be developed for use in conjunction with the models to predict conditions under which failure will occur. Analytical models should be used to evaluate the effects of proposed corrective actions.

1.0 INTRODUCTION

1.1 Background

The "denting" of PWR steam generator tubing has been identified as a problem of high economic impact. In some PWR plants, an interaction among the tube hole crevice environment, tube, and support plate has caused a corrosion product to form on the carbon steel support plate. The corrosion product occupies more volume than the original metal; the tube-to-support plate crevice volume is, thus, consumed with corrosion product, and further corrosive action results in a radially inward force on the tube and a radially outward force on the corroding support plate. This has resulted in indentation ("denting") of the tube, accompanied by occasional cracking. Large in-plane deformation and cracking of the support plate has also been observed in the most severely affected plants. Some serious side effects, such as deformation and cracking of tube U-bends caused by support plate deflections, have been observed.

The essential mechanical features of the "tube denting" problem are illustrated in Fig. 1.1. A schematic of an overall steam generator is shown in Fig. 1.1(a), with a normal tube-support plate intersection shown in Fig. 1.1(b). The tube denting is illustrated in Fig. 1.1(c).

In plants where the tube denting is most severe, deformations of the support plate flow slots and tube U-bends and cracking of support plate ligaments have been observed as illustrated in Figs. 1.1(d), 1.1(e), and 1.1(f). In a few instances, tube denting has caused leaks to develop in tubes in the vicinity of the support plate. In one instance, a leak has developed in a tube U-bend. There is evidence which indicates the leaks are caused by longitudinal cracking initiating on the inside (primary side) tube surface. It is generally assumed that tube leaks at dents are caused by stress corrosion cracking, a phenomenon that occurs in some materials under sustained tensile stress in an adverse environment. Figure 1.2 illustrates the denting process phenomenology as related to this report. The support plate material reacts with the tube hole crevice environment to cause corrosion of the support plate. The oxide which grows in the crevice

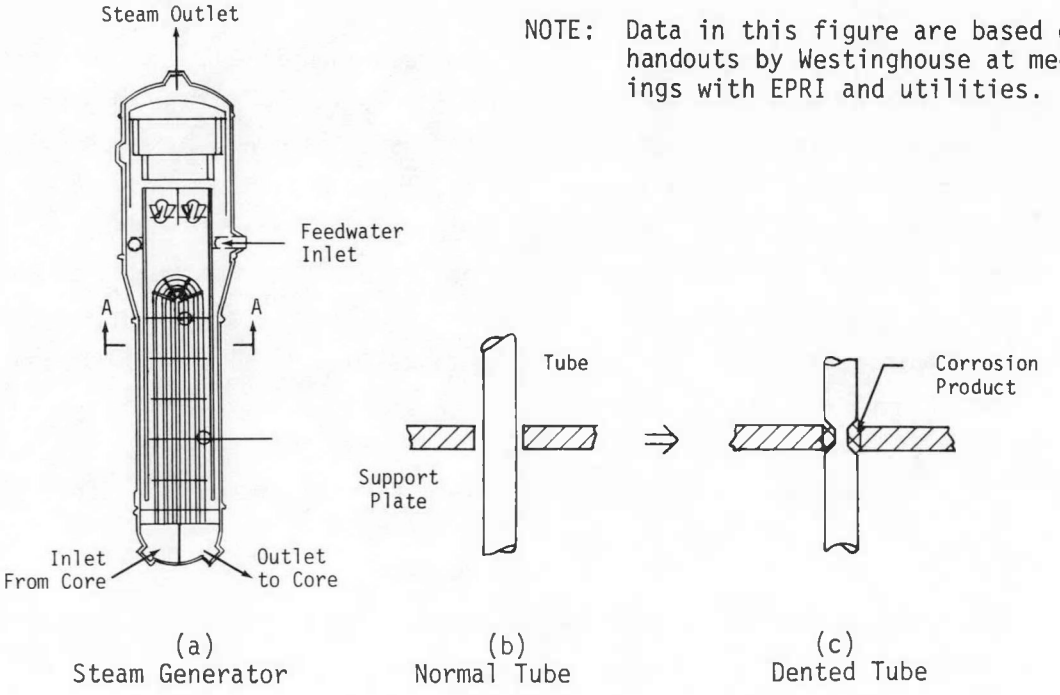

NOTE: Data in this figure are based on handouts by Westinghouse at meetings with EPRI and utilities.

Figure 1.1 - Schematic Representation of Various Aspects of PWR Steam Generator (a) and Denting (b-c). (Continued on next page)

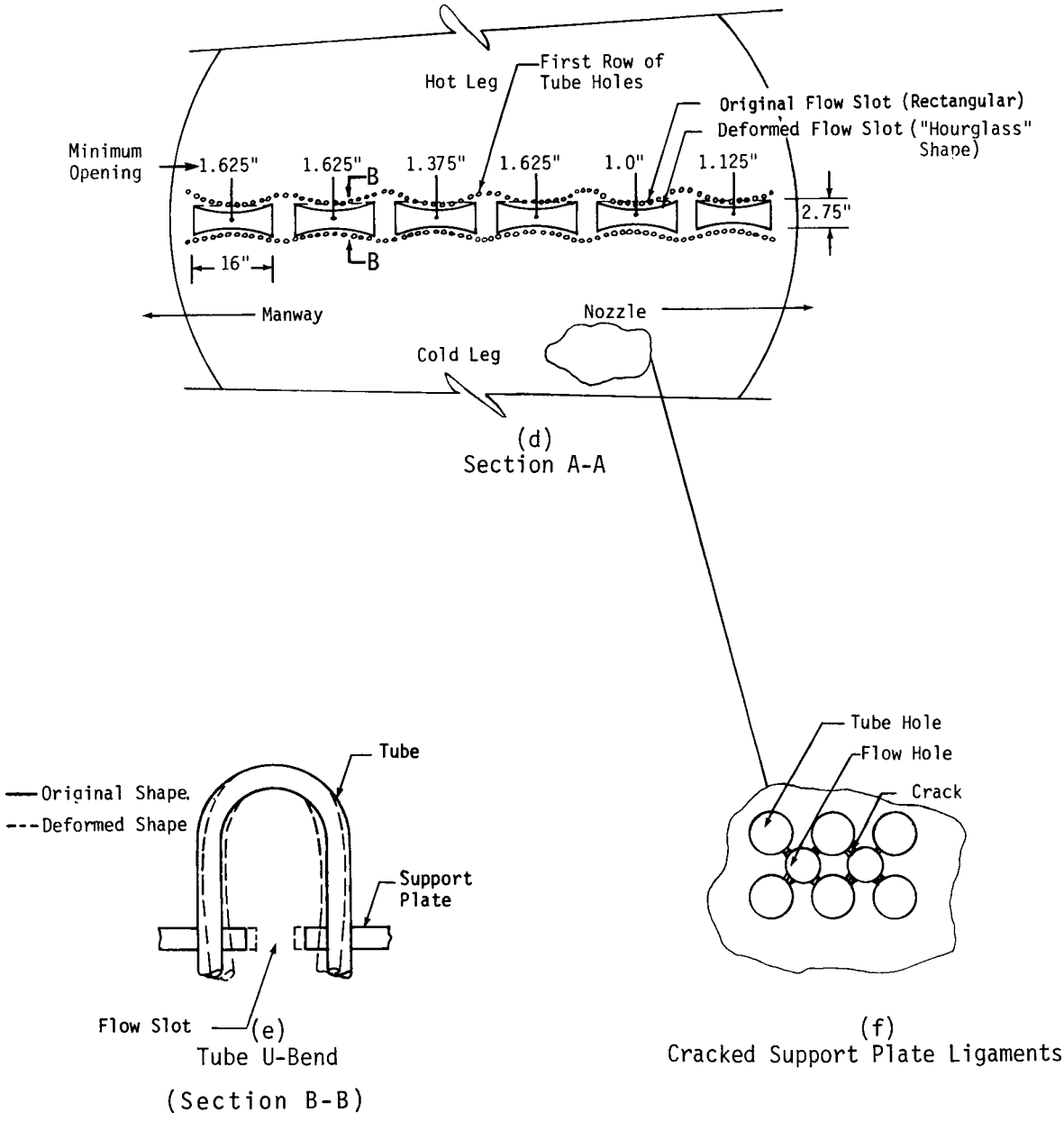

Figure 1.1 - (continued) Consequences of Denting (d-f).

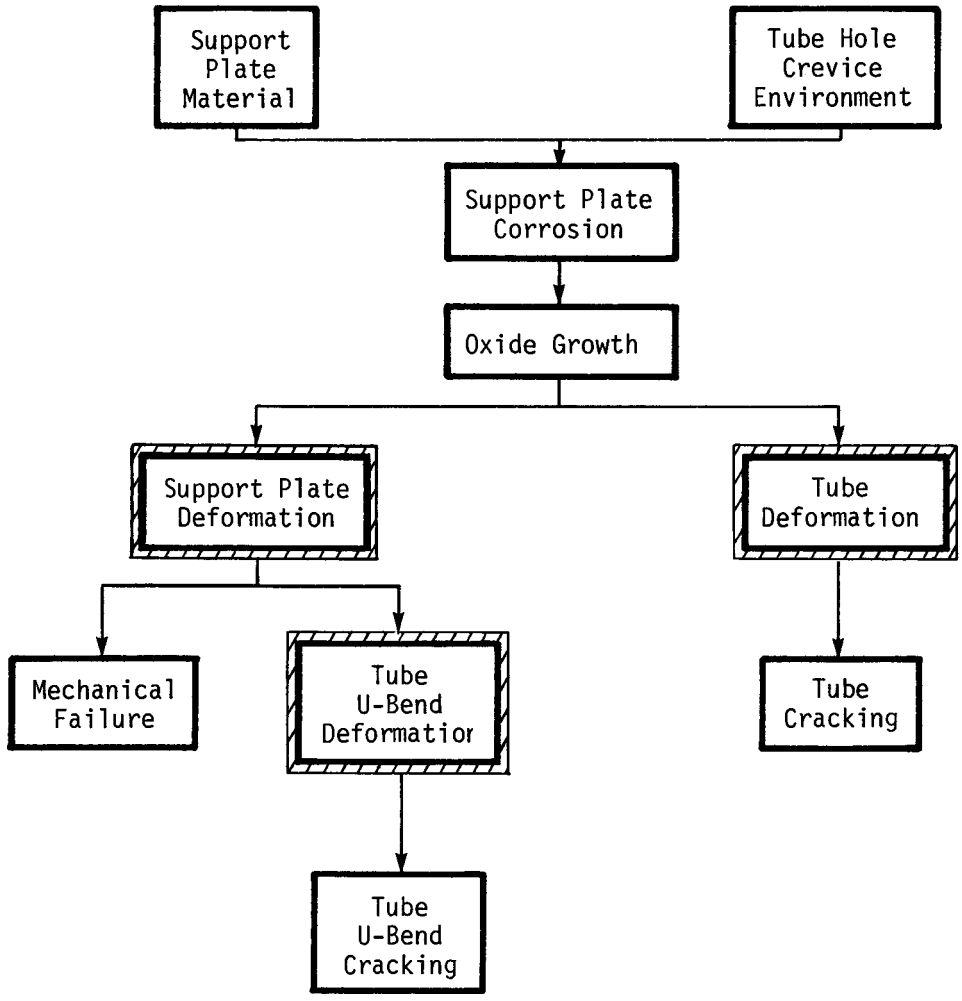

Note: Shaded boxes represent scope of analyses in this report.

Figure 1.2 - Steam Generator Tube Denting Process Phenomenology

between the tube and support plate causes deformations of the tube and support plate which can result in tube cracking, mechanical failure of the support plate, and deformation of tube U-bends which can then lead to tube U-bend cracking.

In June 1976, Failure Analysis Associates (FAA) initiated a general review to determine (1) the frequency of tube leaks and preventative plugging, (2) the location and probable cause of problems, and (3) methods for nondestructive inspection of tubing. Our review included the open literature, utility semi-annual reports, and telephone and personal discussions with utility and vendor personnel. The review indicated a variety of different failure locations and causes. The review revealed that most tubes were plugged based on the eddy current inspection signal before leaking and without detailed examination. The survey also showed that many utilities were changing from phosphate to all-volatile (AVT) water treatment.

In late 1976, Failure Analysis Associates met with Westinghouse and four utilities experiencing significant tube denting to define the problem unknowns and to assist EPRI and FAA in formulation of necessary work plans. The major observations were:

1) A large fraction of steam generators belonging to the four utilities are experiencing some tube denting.

2) Leaks have developed at some dents.

3) The detailed shapes of dents were not known.

4) Westinghouse had initiated a substantial analysis effort to assist the utilities in making decisions on near term corrective actions.

5) When a tube leaks, the corrective action has been to plug the leaking tube; in some instances, utilities have elected to preventatively plug tubes in the most susceptible areas before leaking occurs.

6) Extensive plugging could result in a decreased steam generation capacity and derating of the nuclear power plant to assure sufficient margin under postulated accident conditions.

Because of the number of steam generators which have experienced some degree of denting and the potential consequences of continued denting, EPRI requested that FAA initiate analyses of denting development. The analyses were to be coordinated with and supplementary to the vendor efforts, where possible.

1.2 Scope of Analyses

This report presents results of the analyses of denting development that have been completed through September 1977. This is expected to be a continuing effort with progressively more refined models, more accurate input information, and more diverse questions to be answered. The analyses presented herein were performed on steam generator designs typical of Westinghouse nuclear steam supply systems.

The initial analytical effort concerned only the Westinghouse systems because most plates affected utilize this design; of the three basic steam generator designs (i.e., Series 27, 44, and 51 models), the Series 44 geometry was selected for study. However, due to the general nature of the applied boundary conditions and the fact that the most critical dimensions of the tube and support plate are nearly the same, the analysis results presented would apply also to the behavior of the Series 51 design. The resulting error would be well within the accuracy of the results obtained by the available analytical tools that were used. Tube analysis results, especially for shallow dents, may also be applicable to other vendor designs.

1.3 Objectives and Technical Approach

Determination of stresses and strains in the tubes and support plates is an essential step to an understanding of the denting problem and evaluation of potential solutions. The intergration of this step into a failure prediction model is shown in Fig. 1.3. For stress corrosion cracking problems, a knowledge of stresses and strains is not sufficient to define conditions required for cracking. A failure criteria, which quantifies the interaction of stresses, strains, time, and environment required to produce cracking of tube and plate materials, is also essential. However, this report is essentially devoted to calculation of stresses, strains, and associated deformations of the tube and support plate.

Strains produced in the steam generator tubes and support plates by the denting phenomena are far in excess of the material yield strenghts. Therefore,

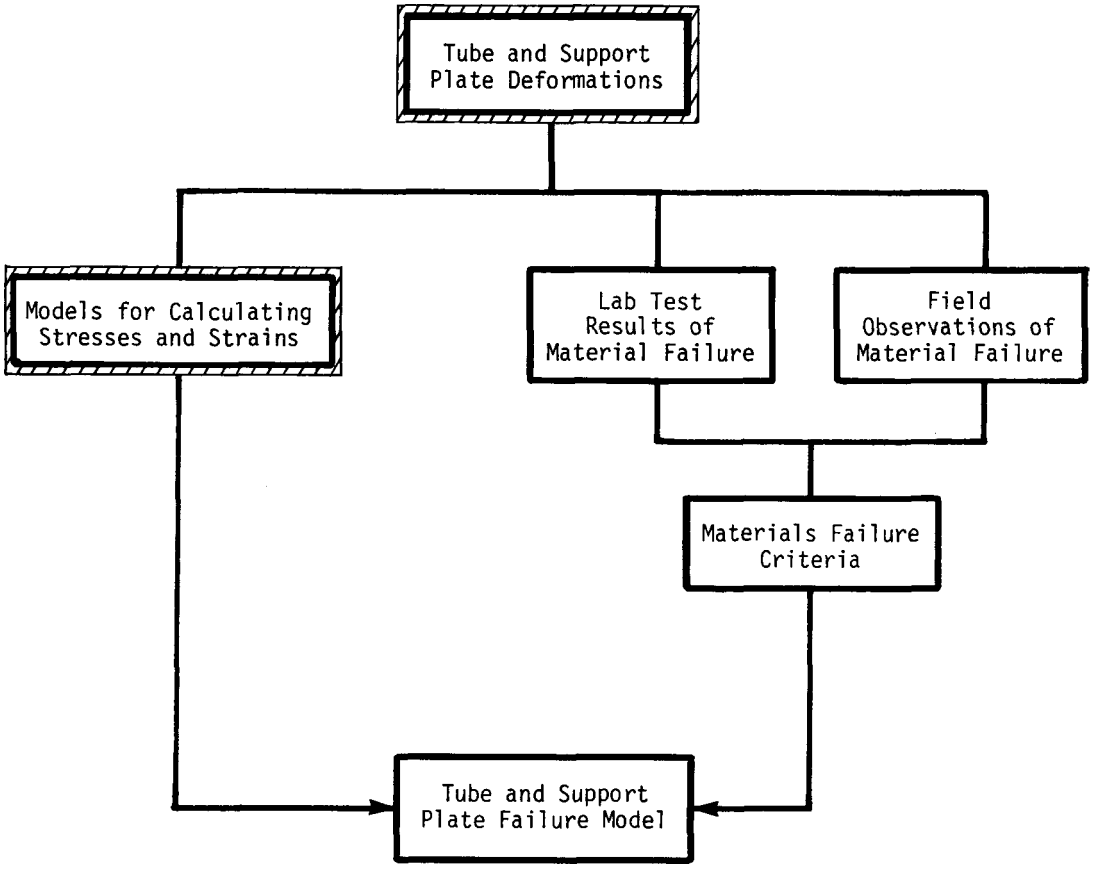

Note: Shaded boxes are within scope of this report.

Figure 1.3 - Steam Generator Tube and Support Plate Failure Model

elastic-plastic analysis involving state-of-the-art computer codes are required in the problem solution. However, "hand" calculations in the elastic and the elastic-plastic ranges can give considerable insight into the problem and reveal the areas where more refined analyses should be concentrated.

The approach used was to start with the simplest analyses relevant to the problem and progress to more refined analyses where the need was indicated by the simplified analyses. Therefore, hand calculations were first performed for the tube and support plate, separate computer models for the two were then developed, and, finally, a model combining the tube, plate, and oxide corrodent was developed. Tube analysis results are contained in Section 2.0, plate results in Section 3.0, and combined model results in Section 4.0. In most cases, prolific results are developed in the elastic range, and more selective results are developed in the plastic range where computer costs become an important consideration.

The "local" computer models of support plate ligaments in this report were developed by FAA with the viewpoint that they would eventually be interfaced with "global" models of the entire support plate by the vendor as illustrated in Fig. 1.4 and explained more fully in Section 3.0. However, analyses to date have been completed using only idealized boundary conditions as discussed in Section 3.0. These idealized boundary conditions give considerable insight into behavior in certain regions of the support plate without the need of using boundary conditions from vendor global models.

1.4 Applicability of Results

As in any mathematical modelling of physical events, there are limitations on how well the models represent reality. The models in this report are typical in this respect and contain many of the usual engineering assumptions that must be made to construct a tractable model. In general, sensitivity studies have not yet been done to quantify the effects of changes in assumptions; therefore, at this time, the effect of modelling assumptions remains largely a matter of engineering judgement. The applicability of results is presented below in terms of lists of the scope, limitations, and uncertainties of the analysis.

Numerous assumptions are made in the detailed models in Sections 2.0, 3.0, and 4.0. These assumptions and their effect on applicability of the analysis to the field are stated at the points where the assumptions are made.

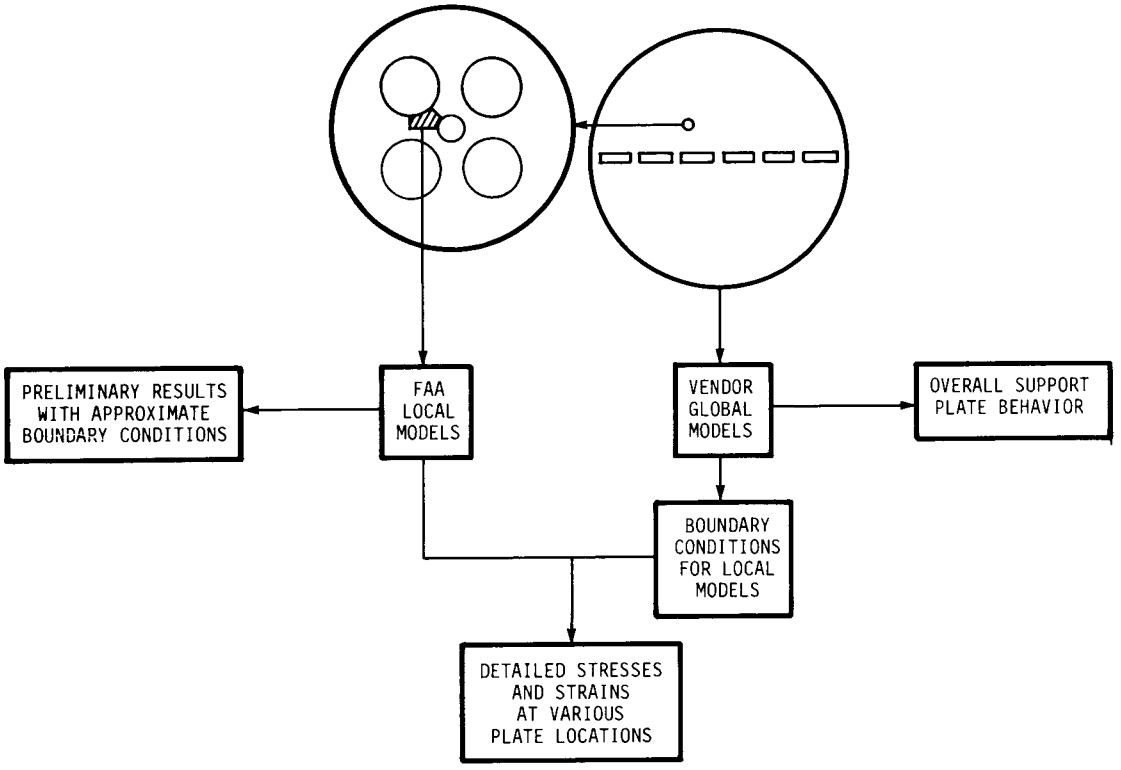

Figure 1.4 - Interface of Local Models With Global Models

1.4.1 Scope

1) The analyses in this report (with qualifications as stated in this Section and throughout the report) are applicable to the Westinghouse Series 44 and 51 steam generator designs.

2) The report is concerned only with the mechanical behavior of the tubes and support plates, assuming that denting is taking place. Causes of the corrosion that results in denting are not addressed.

3) The analysis does not directly consider time as a variable and, therefore, yields no information on how much time is required for the events analyzed to take place.

4) For operational parameters such as pressures and temperatures, design values were used in the analysis. Typical operational values would have been preferred had they been available. However, in the problems analyzed in this report, deviations in these operational parameters are likely to have much less influence than some of the modelling assumptions and should be regarded as within the accuracy of the analysis.

5) The consequences of tube or plate failure are not addressed.

1.4.2 Limitations

1) From pictures in informal PWR Owner's Group meeting handouts, some cracked support plates accompanied by very large deformations of the cracked plate ligaments have been observed in the most severely affected plants. The models in this report do not treat these extreme cases. Maximum strains of 5% in the support plate have been analyzed. It is not known whether support plate cracking occurs due to tensile over-stress alone at high strains or whether some complex failure mechanism permits cracking to occur at lower strains. In the former case, strains calculated in this report are not large enough to predict the failure event. In the latter case, the analysis presented here may be directly applicable to predicting failure when coupled with appropriate material failure criteria.

2) Similarly, tube cracking and some extremely deep tube dents of up to 235 mils have been observed in the field. Analyses in this report do not cover cracked tubes or these extremely deep dents. The deepest dent analyzed was 140 mils, and generally the analysis was terminated at smaller dent depths when the computer program approached its maximum range of strain applicability.

3) The effect of corrosion in removing support plate material is not considered. The effect of this limitation is discussed in Section 3.0.

4) Any mechanical constraint or load-carrying ability of the oxide is not considered except in the elastic analysis in Section 4.0.

5) Actual failure could not be predicted because a failure criteria relating strain, time, and environment to tube or plate cracking is not available.

1.4.3 Uncertainties

1) The behavior of the oxide in the crevice between the tube and support plate as a structural member is uncertain. Except for the elastic model in Section 4.0, the oxide was assumed to transmit forces between the tube and support plate without supporting any load (i.e., as if it were a fluid). Actual behavior depends on the oxide mechanical properties which have not been determined.

2) It is uncertain how well the idealized shapes of tube dents assumed in the analysis represent reality. The dent shapes analyzed are shapes typically encountered in the behavior of cylindrical shells and are idealizations of the actual dents. Field data on dent shapes is very limited, and the specific causes (i.e., buckling of the tube wall, local growth of oxide, penetration by broken plate ligaments) of localized dents is unknown.

3) How well the idealized boundary conditions (i.e., edge constraints) used for analyzing support plate ligaments represent the actual boundary conditions is uncertain. The boundary conditions used represent

actual conditions of either complete constraint or complete freedom to expand for the entire support plate, neither of which is precisely true. The boundary conditions used approximate certain areas of the support plate, as explained in Section 3.0, but the degree of approximation is uncertain.

2.0 ANALYSIS OF TUBE

2.1 Introduction

2.1.1 Analysis Objectives

"Tube denting" which has been observed in PWR Steam Generator tubing causes high stresses and strains in tubes at the support plate elevations. It is generally believed that tube failure is caused by a stress corrosion cracking mechanism. However, ductile rupture due to large scale plastic straining by the denting process and cracking after a local elastic-plastic buckling type instability (local inward bulging of the tube wall) occurs are also possible failure modes.

From the above statements, the objectives of this analysis are to (1) determine the stresses and strains in the tube for different denting conditions and final tube shapes, and (2) differentiate between the conditions which could cause longitudinal cracking or circumferential cracking. Although in several instances longitudinal cracks have been observed, there can be conditions when circumferential cracking is plausible. An evaluation of stresses and strains in dented tubes along with certain specific field and laboratory data could give the required input necessary to analytically describe the tube failure mode(s). Results from these tube analyses will also aid in predicting the potential consequences of continued denting in existing plants which have experienced some degree of denting. In addition, the results may suggest changes in operating conditions to prolong plant life.

2.1.2 Problems of Interest

A typical 30 mils diametral dent is shown in Fig. 2.1. Minimum I.D. dimensions as small as 0.540 inch (235 mil dent) have been measured in the field. Tubes containing such deep dents are plugged and occur only in the most seriously affected plants. Here the maximum diametral dent depth (δ_d) denotes the dent size, and this convention is followed throughout this Section. Figure 2.2 shows

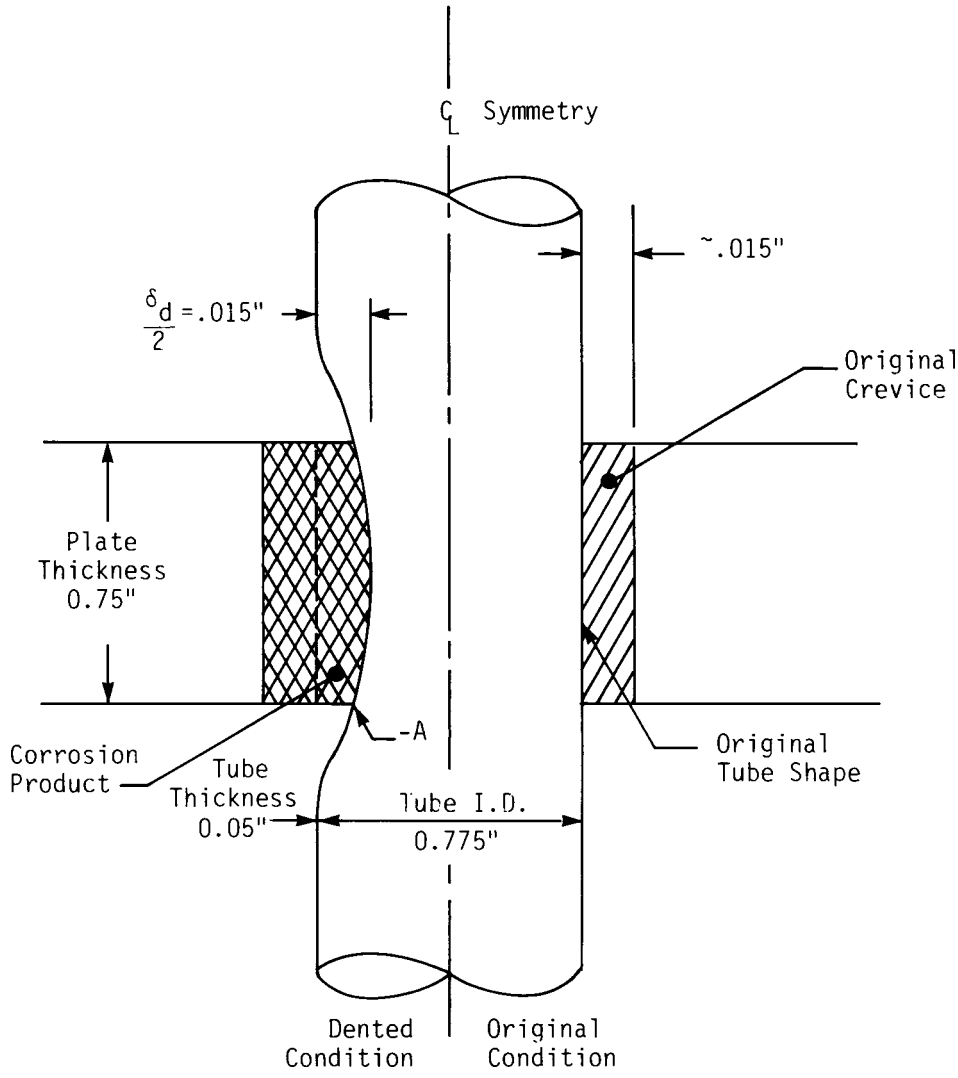

Figure 2.1 - Schematic of a Typical
30 mil Dent.

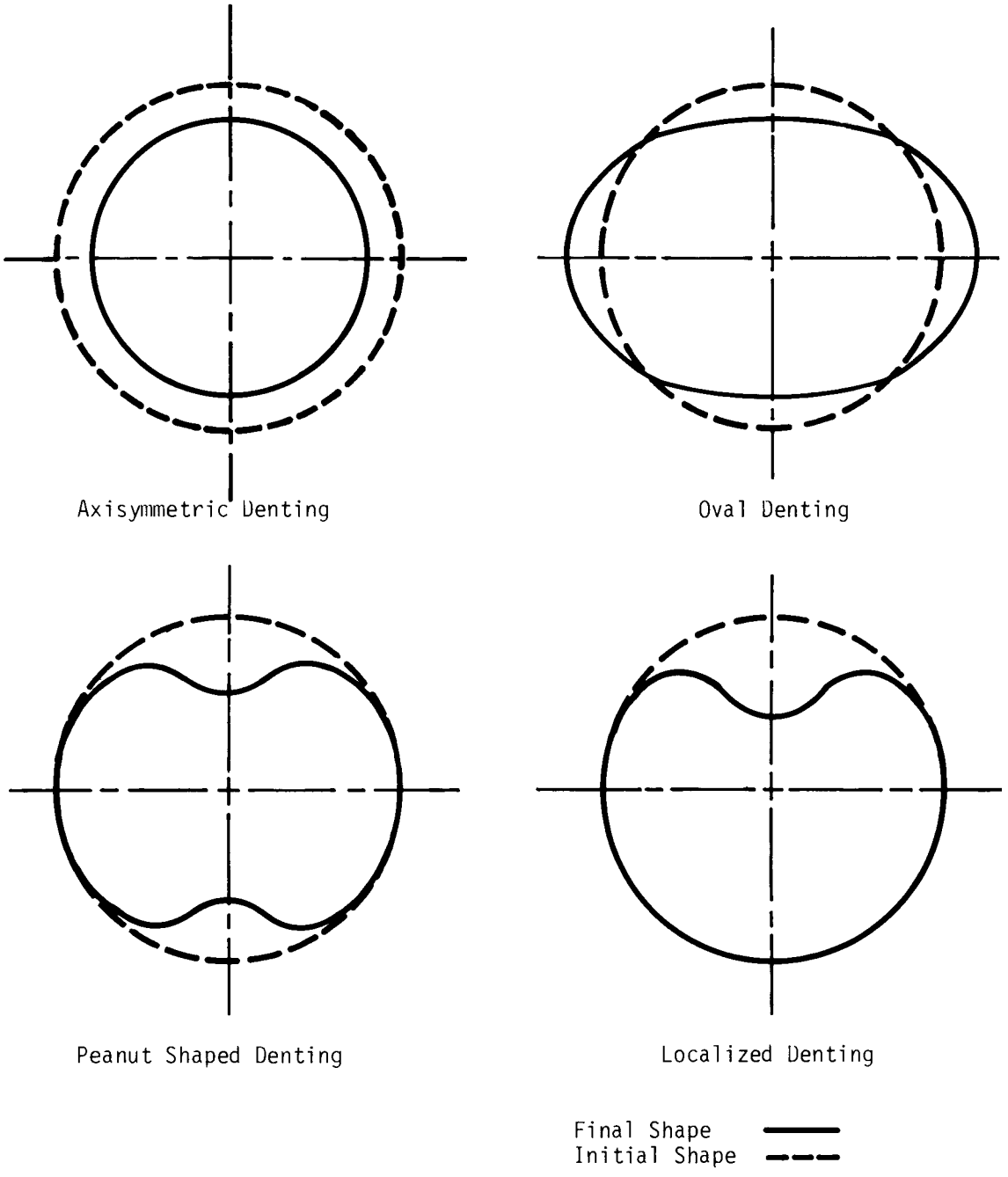

Figure 2.2 - Denting Shapes Under Investigation

some of the tube cross-sections analyzed at dented regions. Although no perfectly axisymmetric or perfectly oval dents may occur in the field, these are believed to be important cases which approximate field conditions in some instances. In addition to these two dent shapes, a peanut-shaped or two-lobed cross-section as well as localized denting or one-lobed cross-section are observed in tubes removed from operating steam generators. Both an elastic and an elastic-plastic analysis are to be carried out to compute the stresses and strains developed in tubes under these four denting conditions. These results along with the field and laboratory data would be useful in formulating a failure criterion and predicting future behavior.

The growth of corrosion products in the crevice between the tube and support plate produces an outward radial force on the support plate. This results in in-plane deformation of the plate. The deformation is greatest in the region of the flow slots, and the flow slots themselves deform significantly which is termed "hourglassing" (see Fig. 1.1(d)).

The tube segments in the U-bend region at the first two or three rows of the top support plate are deformed as illustrated in Fig. 1.1(e). The deformation is maximum for tubes which are located toward the center of flow slot. This inward movement of legs at U-bend sections causes the tubes to ovalize significantly, thus, developing rather high circumferential stresses at the extrados and intrados of the bend section. Axial cracks have been observed at these U-bend sections in the first row of tubes where the bend radius is small. Also, the tubes with cracks were located toward the center of the flow slots, where the deformation is maximum. These cracks were found to be I.D. initiated. It is desirable to evaluate the stresses and strains developed at the apex of U-bend sections, for a known amount of "hourglassing" at flow slots. Since the hourglassing at flow slots of the top support plate that caused the tubes to crack is measurable, these analyses will provide stresses and strains at which tube cracking has occurred in the field. This will be useful in developing a tube failure criterion and in predicting the behavior of adjacent rows of U-bend tubes.

2.2 Methods of Approach

The generic problem of U-bend tube ovalization due to in-plane bending moment has been extensively investigated in the past. Closed form solutions exist for the elastic case and include the effect of net internal pressure on the ovalization

of curved tubes. These solutions will be used here to evaluate the amount of deformation required at the top support plate to cause yielding of the U-bend section at its apex.

Numerical analysis is applied to analyze tube denting under four different conditions. Each tube model is analyzed using a computer code called STAGS (Structural Analysis of General Shells). This code was developed at the Lockheed Palo Alto Research Laboratory and is extensively used in aircraft and aerospace industries (2.1). The code is based on a theory which combines energy principles and finite difference methods to obtain a system of nonlinear equations. The theory includes the two important geometric nonlinearities due to prestress and moderately large rotation. Although the deformation can be large, the analysis is valid only for small strains. In other words, the large strain terms which are important for thickness change (i.e., necking) are not included. The stress-strain curve for SB-163 Inconel 600 tubing analyzed in this Section is shown in Fig. 2.3. It is seen that the strain hardening is fairly gradual, and the necking is substantial only after a strain of about 25%. This suggests that the STAGS code will provide accurate results for tube denting analyses, even for values of strain as large as 10%. The code uses a modified Newton-Raphson technique to solve the system of nonlinear equations. For greater economy and flexibility in the analysis, a capability is provided for use of variable spacing finite difference grids. Inelastic material behavior as predicted by the White Bessling theory (2.2, 2.3) is incorporated into the analysis. This theory retains the important features such as strain hardening and the Bauschinger effect. Yielding is according to von Mises, and, for thin shells, the radial stresses are small in comparison with axial and circumferential stresses. The shear stresses are zero in the axisymmetric case, and, for the nonaxisymmetric problems considered in this Section, they are an order of magnitude smaller than the axial and circumferential stresses. Hence, for negligible radial and shear stresses, the von Mises yield condition is

$$\sigma_1^2 - \sigma_1 \sigma_2 + \sigma_2^2 = \bar{\sigma}^2$$

where σ_1 and σ_2 are the axial and circumferential stresses and $\bar{\sigma}$ is the equivalent flow stress for the material. This criterion is used to determine the onset of tube yielding under various conditions.

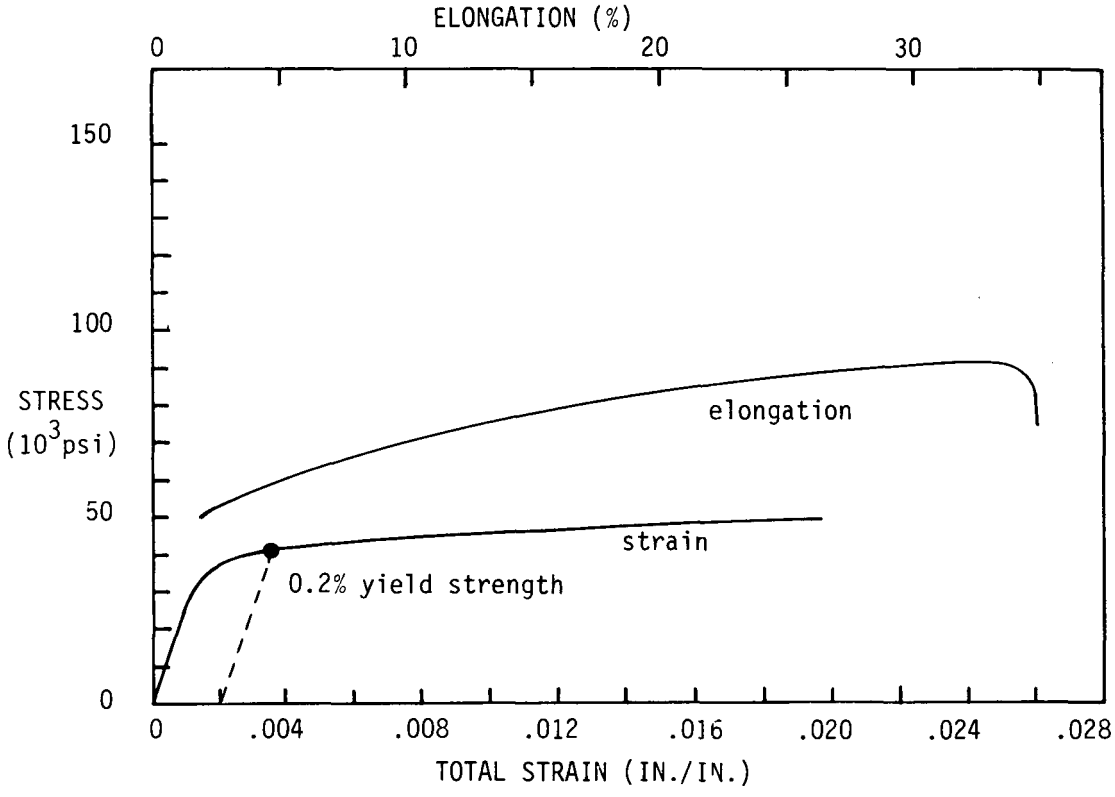

Figure 2.3 - Stress-Strain Curve for SB-163 Inconel 600 Tubing at 600°F.

In the present investigation, STAGS is used for both linear and inelastic stress analysis in which the geometric nonlinearities are included. Any combination of point forces, line loads, and distributed surface tractions can be applied. Loading by specification of displacements or thermal gradients through the shell wall and over the shell surface is also permitted. The code can also accept any configuration of boundary conditions or other displacement constraints.

The linear elastic results determined by STAGS for all problems under consideration are checked against closed form analytical solutions obtained using the mathematical technique called Asymptotic Integration Method (2.4, 2.5, and 2.6). This check is done to make sure that the finite difference mesh used is finite enough to pick up the high stress gradients encountered near shell edges yet coarse enough to avoid numerical instability.

In the following subsections, important results for the various problems of interest are presented, and their implications to the tube denting problems as a whole are discussed.

2.3 Tube Geometry and Material Properties

The nominal tube dimensions for the cross-section whether in the straight legs or the U-bend regions are shown in Fig. 2.4. The dimensions shown are the values used in the present analyses and are typical for either a Series 44 or 51 steam generator design. However, actual tube tolerances indicate the tube wall thickness could be as low as 0.045 inch, and the tube O.D could vary between 0.8675 and 0.88 inch. The support plate geometry and its dimensions are presented in Section 3.2, and the pertinent dimensional values are given in Fig. 3.2.

The tubes are made of SB-163 Inconel 600 material. The ASME Code (2.7) values for modulus of elasticity, E, and Poisson's ratio, ν, at $600^{o}F$ are 29.2×10^{6} psi and 0.3, respectively; and these values are used in the analysis. The ASME Code specification for the minimum value of yield stress is 35,300 psi. However, a value of 41,000 psi, which is the 0.2% offset yield stress (Westinghouse data), is used in the analysis to compute the load at which the tube begins yielding. The stress-strain behavior of Inconel 600 at $600^{o}F$ is shown in Fig. 2.3.

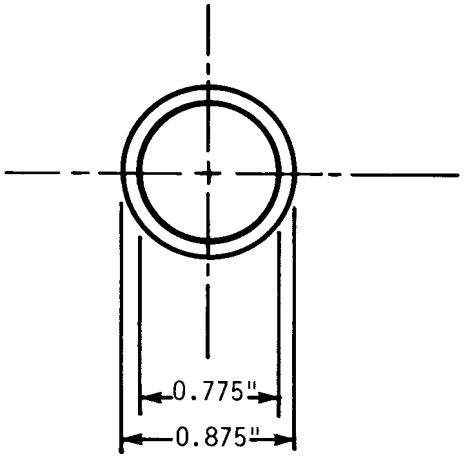

(a) Inconel Tube Cross Section

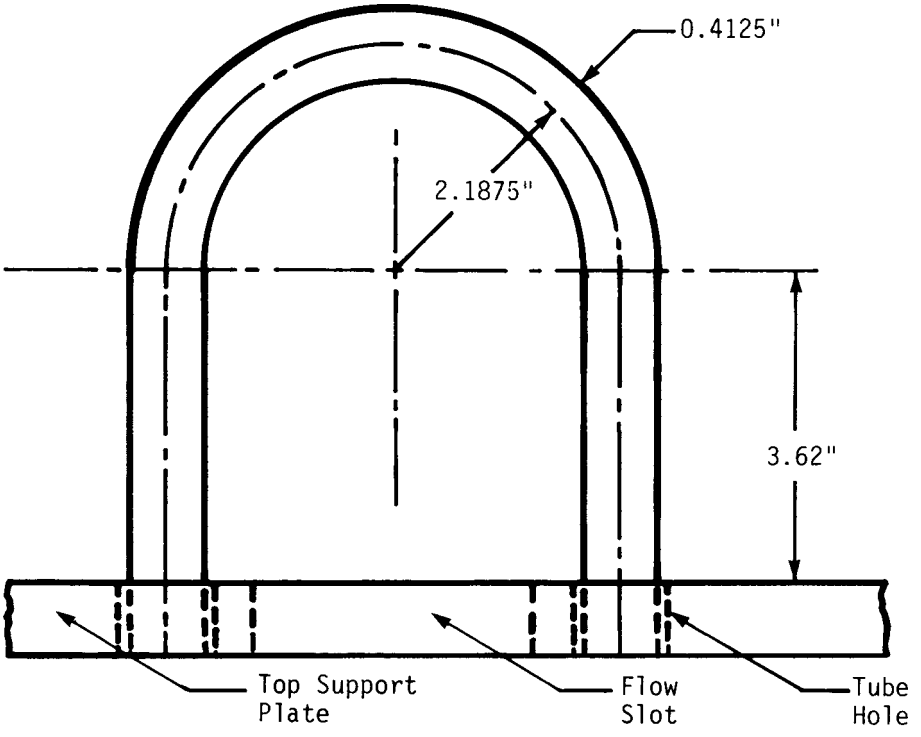

(b) U-Bend Geometry

Figure 2.4 - Tube Cross-Section and U-Bend Geometry at First Row of Series 44 Westinghouse Steam Generator.

2.4 Elastic Analysis of U-Bend Sections at First Row

For both in-plane and out-of-plane bending, a curved tube is much more flexible than a straight tube of the same cross-section because there is a tendency for a curved cross-section to ovalize (often called von Karman flattening). When flattening takes place, the strain in the outermost fibers of the tube, for a given change of curvature of the centerline of the tube, is less than it would be if there were no flattening of the cross-sections. Consequently, a smaller bending moment is required to produce a given change of curvature. The ratio of the resulting increased deflection to that predicted by conventional beam theory is termed the "flexibility factor" for that tube. This increase in flexibility alters the bending stress distribution given by the elementary beam theory. In reality, the longitudinal bending stresses in the extreme fibers are greatly relieved by the ovalization (flattening). At the same time, the maximum longitudinal stress is shifted nearer the neutral axis, as shown in Fig. 2.5(b). Circumferential bending stresses are developed due to the tube flattening, as shown in Fig. 2.5(c) and (d).

The ratio of the maximum stress in the curved pipe bend to the maximum longitudinal stress that would exist in straight tube subjected to the same moment is termed "stress intensification factor." Clark and Reissner (2.8) obtained the dependence of these factors on geometry by asymptotic methods. Figure 2.5(c) illustrates this dependence for the circumferential stress, from which it is clear why tubes with a small bend radius are more likely to develop axial cracks than tubes with a larger bend radius. Rodabaugh and George (2.9) included the effect of internal pressure on these factors. These results are summarized in a compact form in (2.10). They are now applied to the U-bend tube cracking problem encountered in PWR steam generators.

Due to the in-plane deformation of the top support plate by corrosion, the flow slots "hourglass." This, in turn, pinches the U-bend section legs toward each other. This inward movement develops an in-plane bending moment at the apex of the U-bend section, causing it to flatten. A relation for the in-plane bending moment in terms of the leg pinching, δ (shown in Fig. 2.5(a)), is obtained using the elementary beam theory for the straight section and the curved tube theory for the semicircular portion of the U-bend tube. The circumferential stress intensification factors at the various locations of the cross-section for the present U-bend geometry are shown in Fig. 2.5(d). Circumferential stresses as a function of the leg pinching, δ, have been determined. The values on the tube

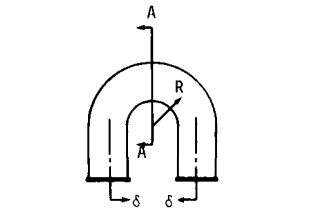

(δ = inward displacement of legs)

a) Tube U-Bend

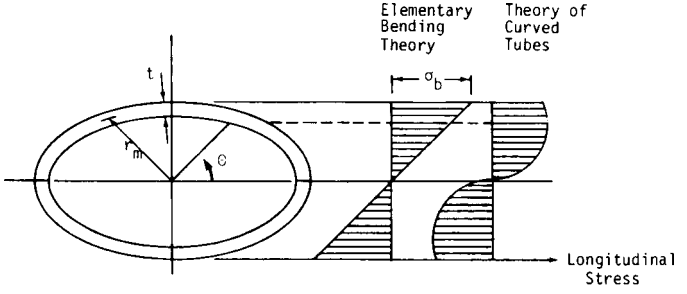

b) Illustration of Curved Tube Behavior (Section A-A)

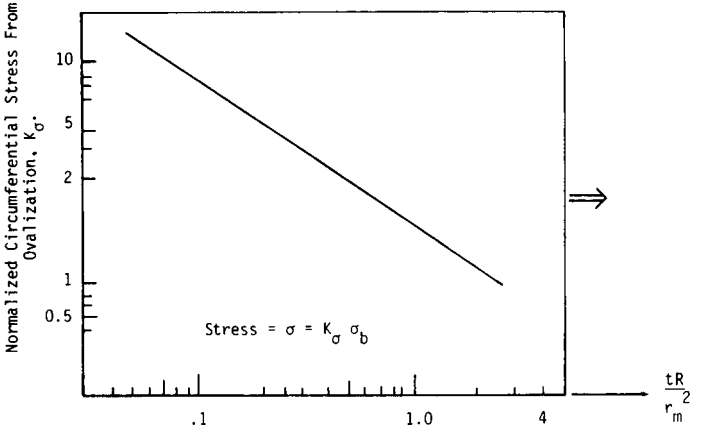

c) Dependence of Stresses on Geometry

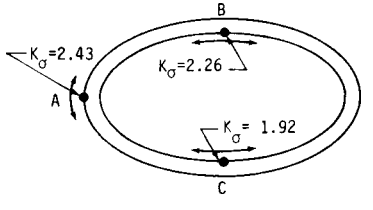

d) Normalized Circumferential Stress (Section A-A)

Figure 2.5 - Effect of Von-Karman Flattening at U-Bend Due to Leg Pinching.

inner surface are shown in Fig. 2.6, from which it is clear that even for a small amount (40 mils) of leg pinching, the tube is stressed to its yield point. For larger amounts of flow slot closure such as those shown in Fig. 1.1(d), an elastic-plastic analysis is needed to compute the circumferential strains developed at the extrados and intrados of the U-bend. These high sustained strains in a corrosive environment are responsible for the stress corrosion cracking. However, without a proper quantification of the residual stress distribution and the initial ovality, it would be difficult to predict these strains accurately.

2.5 Stresses in Tube Due to Operating Pressures Alone

Before proceeding with an analysis of tubes under the abnormal conditions of denting, it is appropriate to calculate stresses in the tubes as designed (without denting). At normal operating conditions, the primary water pressure is 2250 psi, and the secondary water pressure is 785 psi. To compute the stresses developed in the tube due to the net internal pressure of 1465 psi, a tube model, which is shown in Fig. 2.7, is analyzed by the shell analysis code STAGS.

In establishing the model dimensions, specifically the effective shell height above the support plate to retain in the model, analytical relations were developed using shell theory (2.4). For axisymmetric loading on a cylindrical shell, the distance from the shell edge (in the present problem, from the edge at the surface of the support plate) at which the bending stresses decay to about four percent of their edge values is given by

$$\delta_{n=0} = \pi \left(\frac{2Rt}{\left[12(1 - \nu^2)\right]^{\frac{1}{2}}} \right)^{\frac{1}{2}} \tag{2.2}$$

where R is the mean radius of the cylindrical shell, t is the thickness, and ν the Poisson's ratio. For the axisymmetric problem under consideration,

$$\delta_{n=0} = 0.351 \text{ inch} \tag{2.3}$$

To eliminate the influence of the top edge boundary conditions on the bending stresses developed at the support plate portion of the tube, the tube length above the support plate is taken to be one inch for all the axisymmetric problems considered in this Section. In addition, since the support plate thickness is 0.75 inch (which is greater than 2 x 0.351 inch), there is little interaction between the two shell edges at the support plate surfaces.

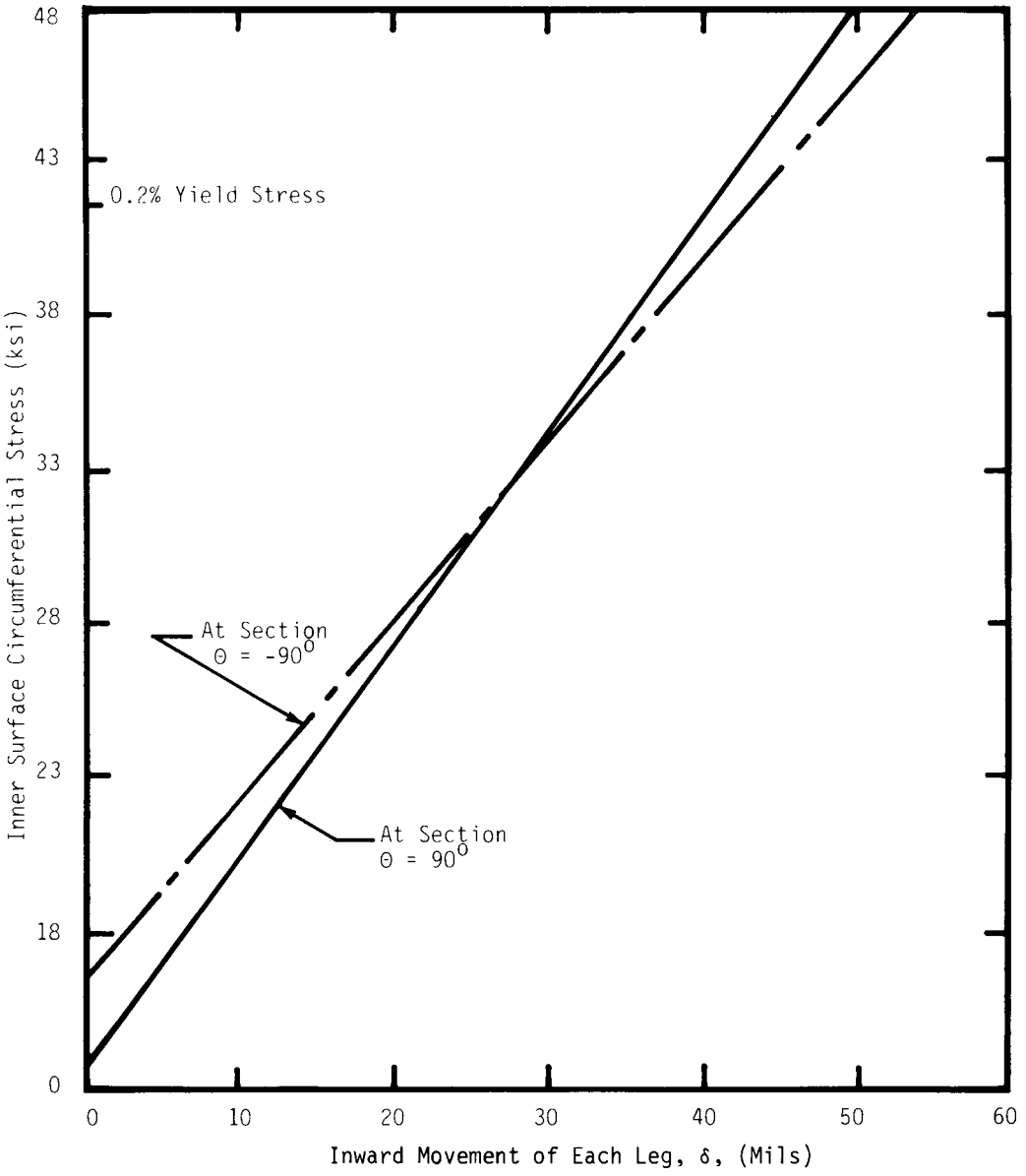

Figure 2.6 - Maximum Circumferential Stress at U-Bend Due to Leg Pinching.

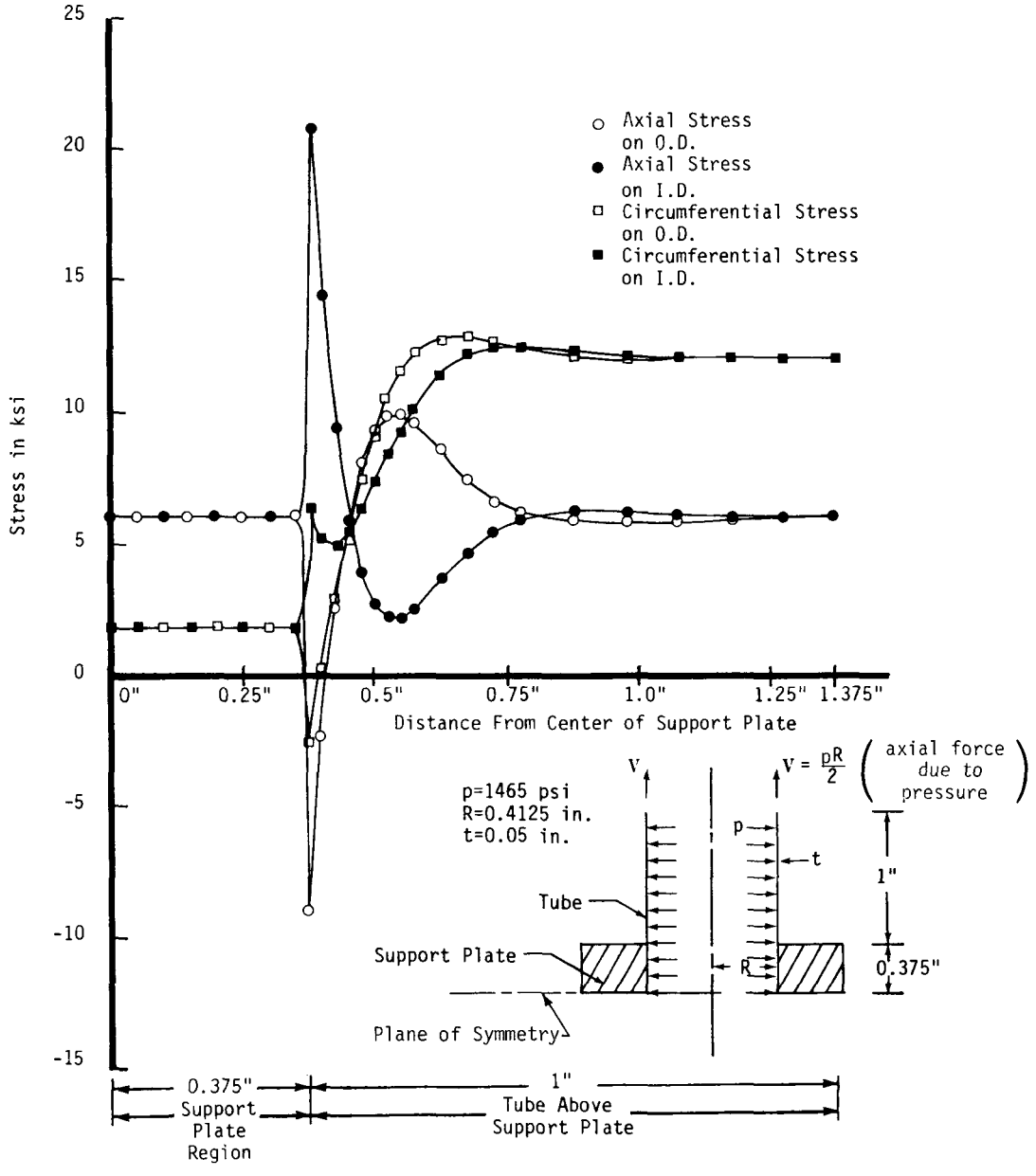

Figure 2.7 - Linear Analysis Results for Stresses Due to Internal Pressure.

When corrosion product fills the annular gap, tube deformation is restricted along the length through the support plate. This aspect of denting is partially considered here by imposing the boundary condition that the radial displacement of tube at the plate region is zero. This condition develops bending stresses in the tube at the plate surface edges. These bending stresses are absent if a clearance is maintained between the tube and support plate. It is seen from Fig. 2.7 that the maximum axial and circumferential tensile stresses are 21,000 psi and 12,500 psi, respectively, which are much lower than the 0.2% yield stress of 41,000 psi. As discussed in the next subsections, the stresses and strains developed due to operating pressures are much lower than those caused by the dent itself.

2.6 Axisymmetric Dent Analysis

Because the support plate surrounding a tube does not provide axisymmetric boundary conditions, it is unlikely that purely axisymmetric dents will occur in the field. However, any dent in which the tube circumference is smaller than the original circumference has an axisymmetric component. This is expected in virtually all dents, and the analyses that follow pertain to stresses and strains caused by the axisymmetric component of deformations. The axisymmetric dent problem is analyzed here from the viewpoint of two limiting situations. The first case assumes a normal, radially inward imposed displacement on the tube by the oxide with some prescribed axial profile. In the second case, the same geometric model was utilized, but inward imposed uniform pressure by oxide was assumed. The first model is believed to more accurately represent the field conditions, but the second model will provide results which will be useful in correlating tube and plate stresses in Section 3.0. The same STAGS tube model used in Section 2.5 is implemented herein.

2.6.1 Imposed Displacement Analysis

A typical axial profile for an axisymmetric dent is given in Fig. 2.8. The diametral dent depth of 24 mils denotes the dent size (Fig. 2.1), and the profile was determined from dented shapes from actual field samples. Any dent investigated using this model is assumed to have the same relative profile as in Fig. 2.8 Of course, a variety of profiles would be expected in the field, so this analysis must be regarded as typical only. It was mentioned in Section 2.5 that the distance from the tube edge at which the bending stresses decay to about four percent of their edge values is 0.351 inch. Hence, the edge which is one inch from the

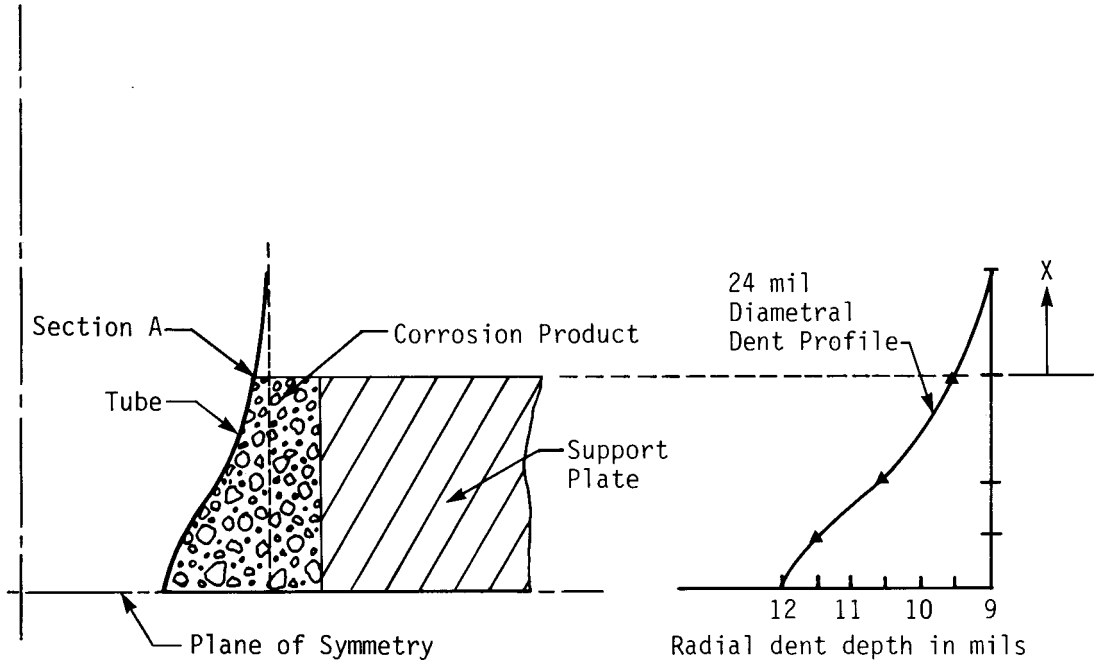

Section A - Location of Maximum Axial Stress

Figure 2.8 - Axial Variation of Axisymmetric 24 mils-Dent. (Same Relative Axial Profile is Considered for Dents of Different Depths).

support plate surface can be taken to be either clamped or free (Figs. 2.7 and 2.9), and this boundary condition will not influence the stresses in the dented portion of the tube.

STAGS results with the prescribed displacement assumption are given in Figs. 2.10 through 2.12. The elastic results shown in Fig. 2.10 compare well with the asymptotic expansion solution, which is not presented here. This helps to confirm that the finite difference mesh selected is appropriate to carry out an elastic-plastic analysis. High tensile axial stresses and strains are developed on the tube I.D. surface near the shell edges at the support plate surface. In fact, Fig. 2.12 shows that a dent of diametral depth of 40 mils results in a tensile axial strain of 12 percent on the tube I.D. surface. These highly localized stresses and strains could develop circumferential cracks in the tube near the support plate surfaces. The circumferential stresses and strains were found to be compressive everywhere except in the portion of the tube away from the plate surface (Fig. 2.10). The maximum circumferential stresses are so small for axisymmetric dents that they are not expected to cause longitudinal cracks. However, longitudinal cracks have been observed, suggesting that asymmetric denting had taken place.

A tube indentation has both axisymmetric and asymmetric components. Even if the tube leaks due to a longitudinal crack caused by the asymmetric part of the denting and is plugged, continued denting if it occurs, may develop large axial strains due to the axisymmetric component, increasing the susceptibility to branching of the existing longitudinal cracks into circumferential cracks at the elevation of the support plate surface.

2.6.2 Imposed Uniform Pressure Analysis

The elastic-plastic results for the external pressure load axisymmetric STAGS model (see Fig. 2.9) are shown in Fig. 2.13. A pressure of 4720 psi is required to initiate yielding (0.2% offset) in the tube. The elastic results agree well with the closed form solution obtained using the asymptotic integration method. The normal displacement profiles at the onset of yielding are compared for several models in Fig. 2.14. Among these are the results for a cylinder under an external pressure for plane strain and plane stress conditions. These results are computed from

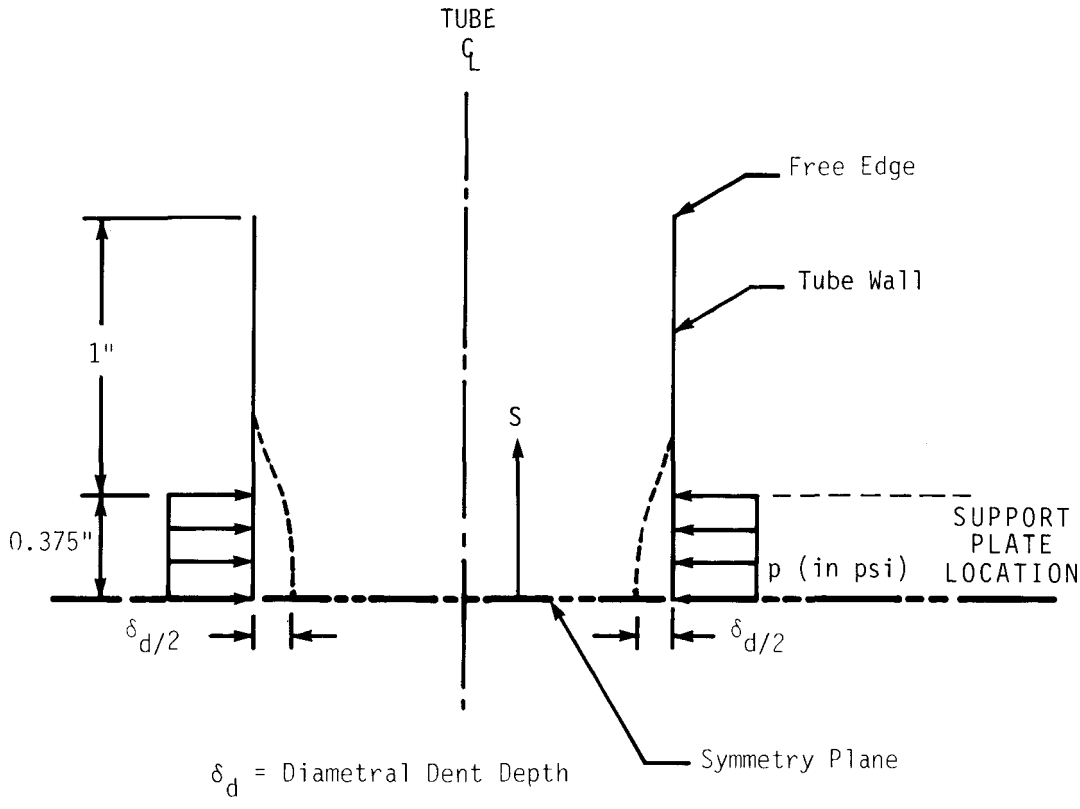

Figure 2.9 - Local External Pressure Load Model for Axisymmetric Dent.

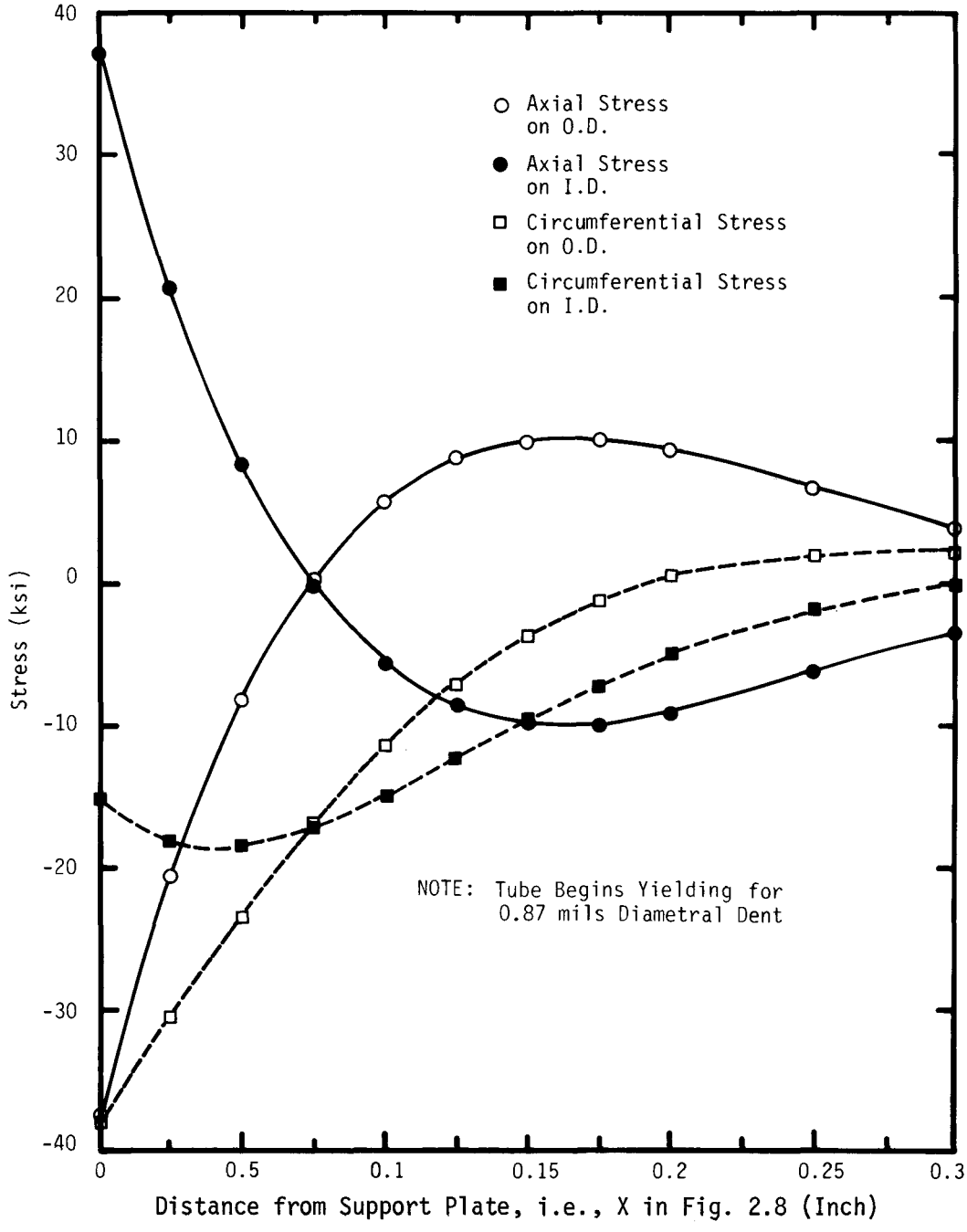

Figure 2.10 - Linear Analysis Results for Axisymmetric 1 mil Diametral Dent (Prescribed Displacement Assumption With Dent Profile Shown in Fig. 2.8).

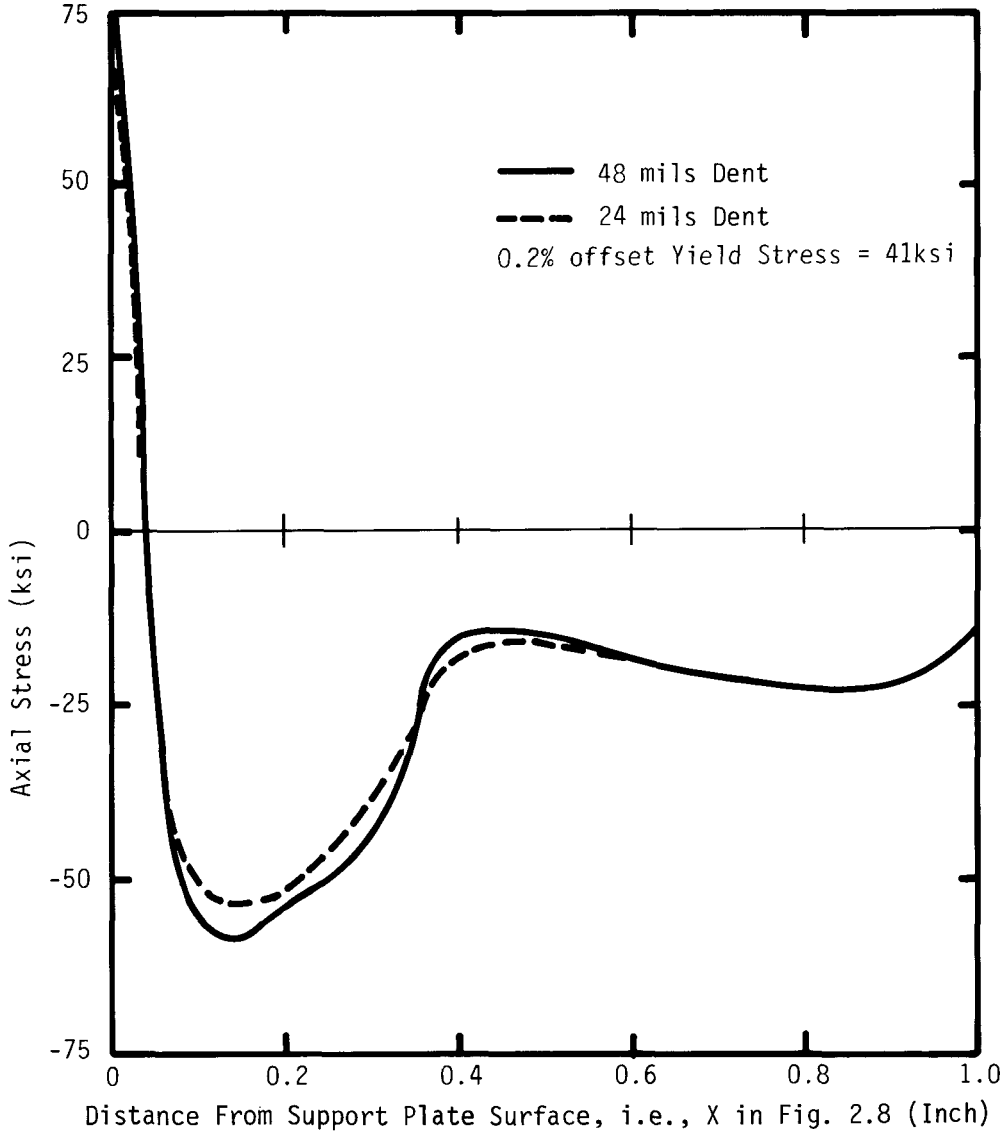

Figure 2.11 - Elastic-Plastic Axial Stress Variation at I.D. Surface for Axisymmetric Dent, (Prescribed Displacement Assumption).

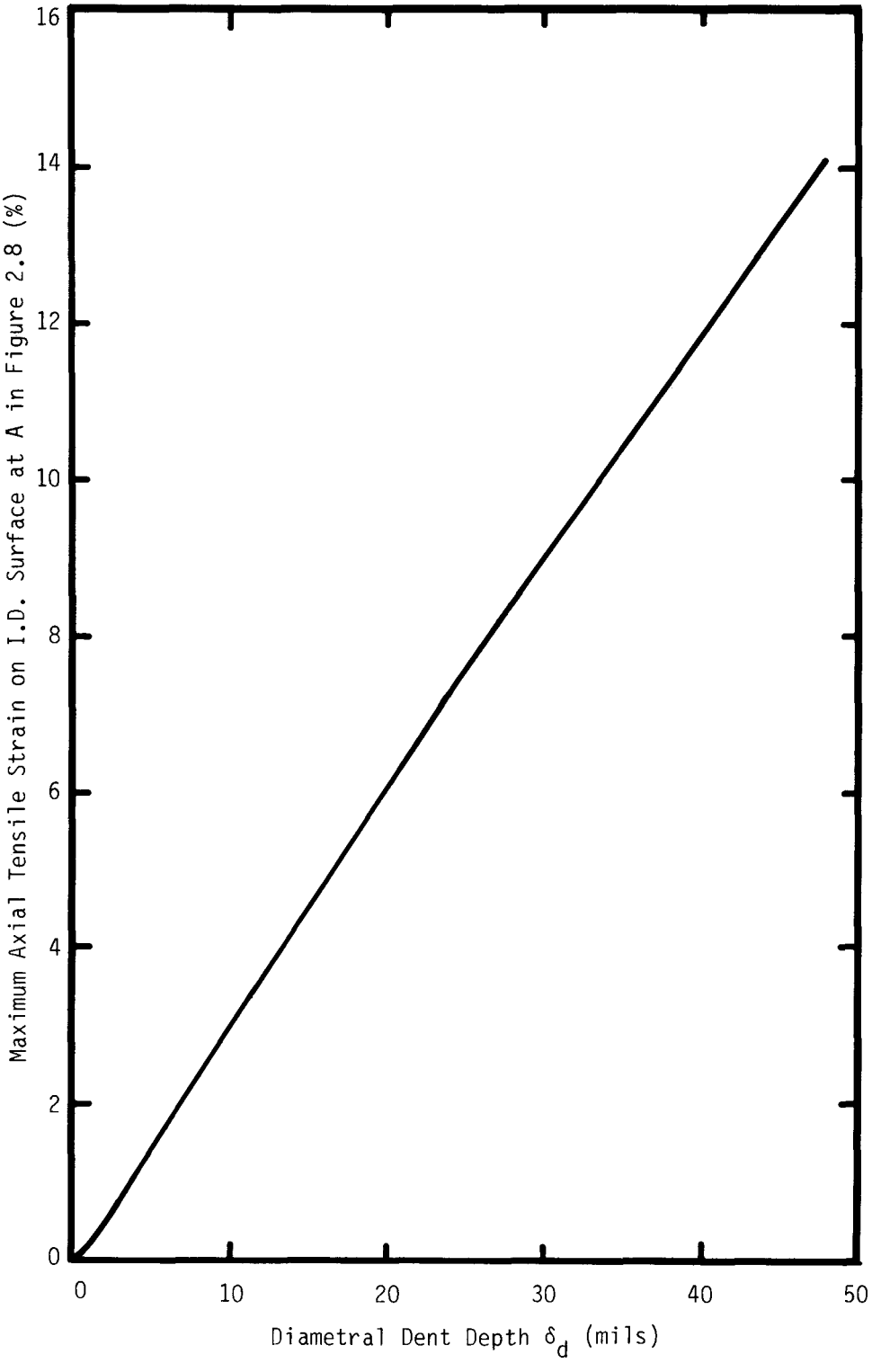

Figure 2.12 - Elastic-Plastic Results for Maximum Axial Tensile Strain for Axisymmetric Dent (Prescribed Displacement Assumption).

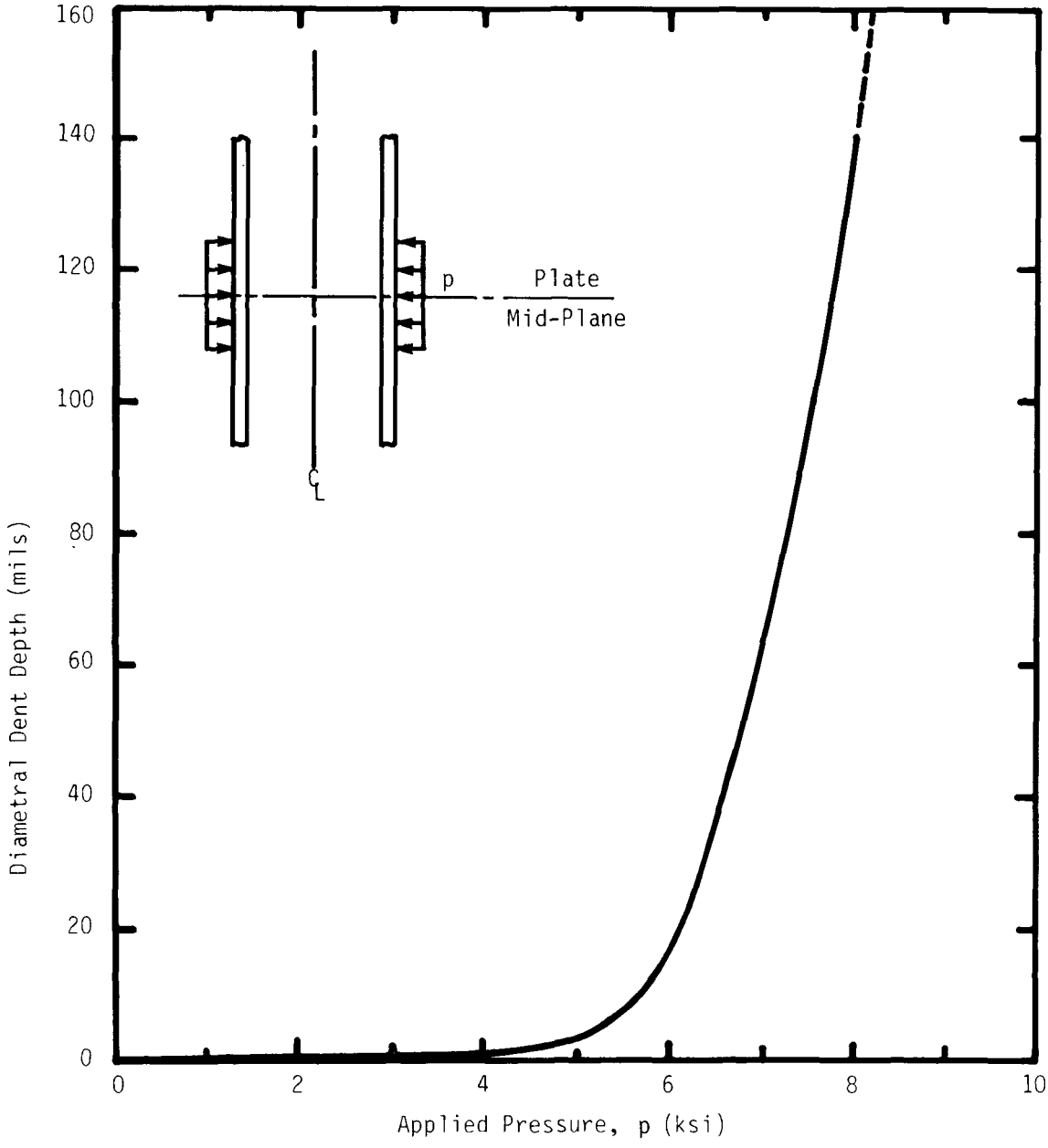

Figure 2.13 - Correlation Between Applied Tube Pressure and Diametral Dent Depth at the Plate Mid-Plane for the Axisymmetric Case.

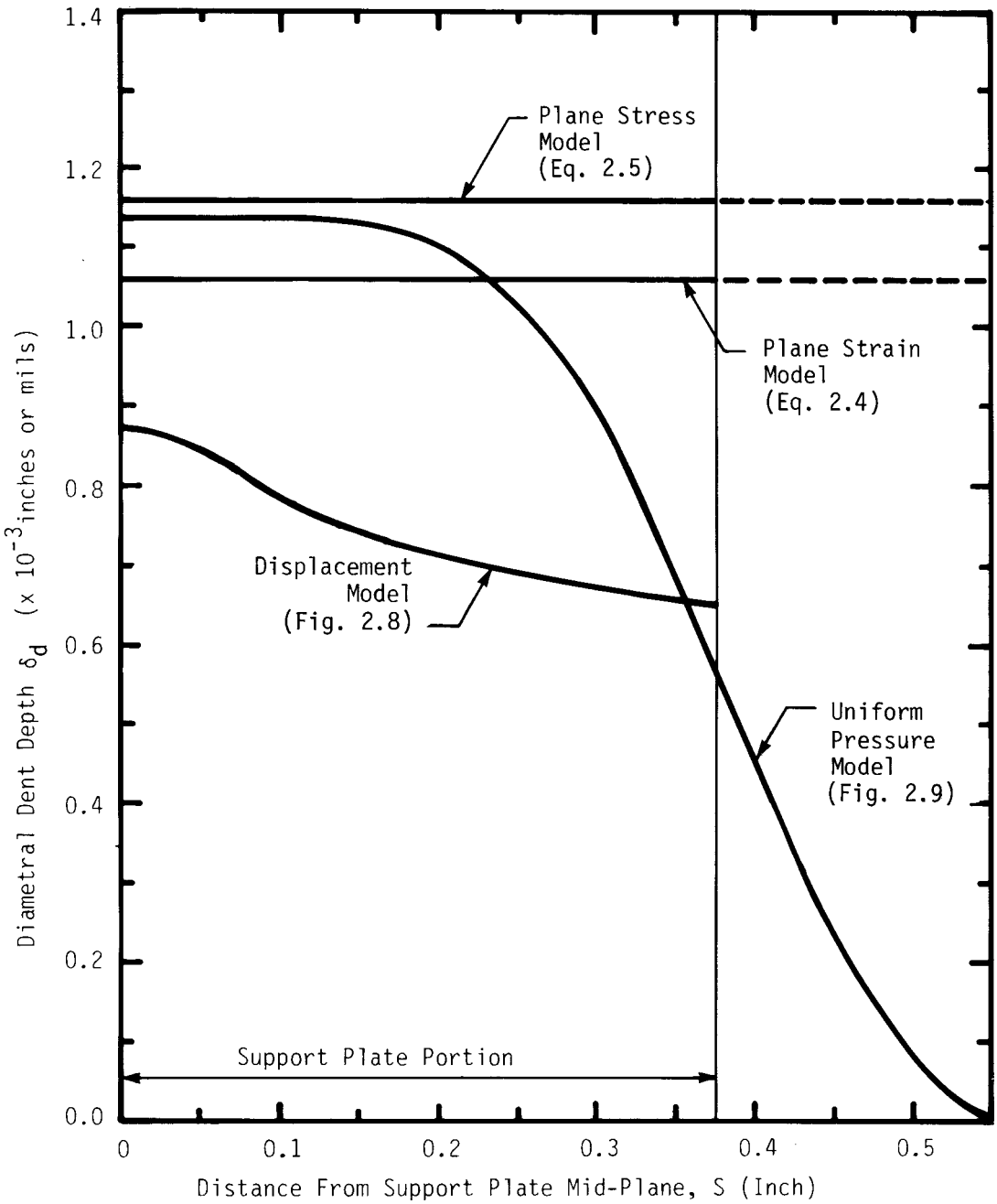

Figure 2.14- Comparison of Axial Variation of Inward Radial Deflection for Several Assumptions When Tube Initially Yields.

$$\delta_d = \frac{4a(1 - \nu^2)p}{E(1 - a^2/b^2)} \qquad \text{(plane strain)} \qquad (2.4)$$

and

$$\delta_d = \frac{4ap}{E(1 - a^2/b^2)} \qquad \text{(plane stress)} \qquad (2.5)$$

where dimensions a and b and elastic properties E and ν all pertain to the tube and

$a = 0.3875$ in.

$b = 0.4375$ in.

$E = 29.2 \times 10^6$ psi at 600^oF

$\nu = 0.3$

$p = 4720$ psi

A comparison of these calculations shows that a plane stress analysis provides a good approximation to the tube deformation behavior at the plate mid-plane under pressure boundary conditions. Furthermore, the tube behavior along the center of the plate region is bracketed by the plane strain and plane stress results, and these results differ by only 9%. This information provides background for the tube behavior assumptions necessary in Section 4.0.

Figure 2.13 provides the correlation between the applied tube pressure and the diametral dent depth from the STAGS model. This correlation will be used in Section 3.0 to relate the dent size to the strains calculated for in the support plate using the ligament models.

2.7 Oval-Shaped Dent Analysis

The model utilized to investigate the effects of tube ovalization due to denting is shown in Fig. 2.15. Both the undeformed and deformed cross-sections are shown. If u, v, and w are the meridional, circumferential and normal displacements, and β is the meriondal rotation of a shell of revolution undergoing asymmetric deformation, the values of u, v, w, and β at a shell edge need to be prescribed to make the problem well-defined. Figure 2.15 shows the model in which the symmetry plane

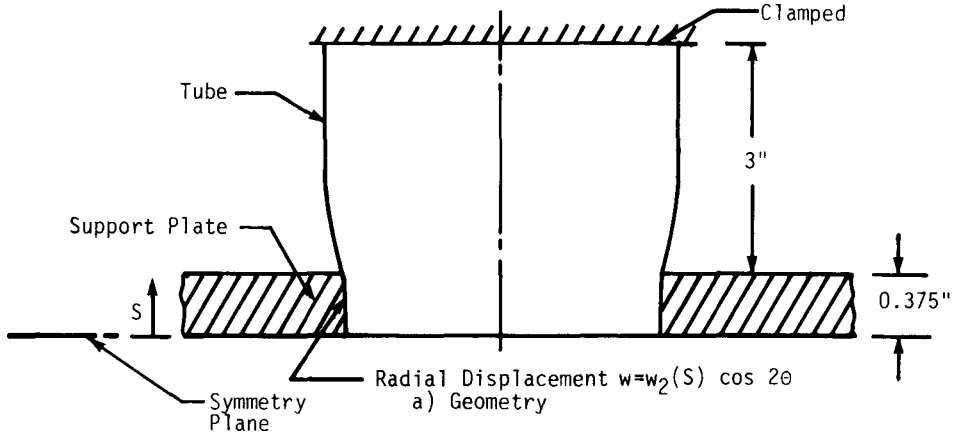

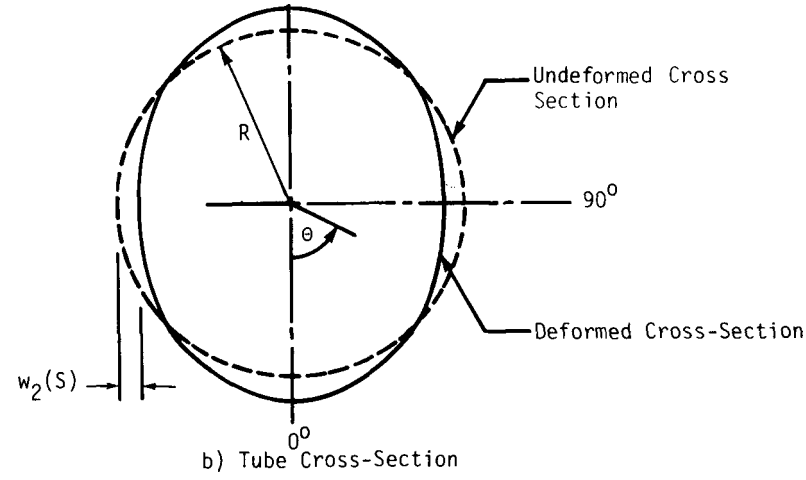

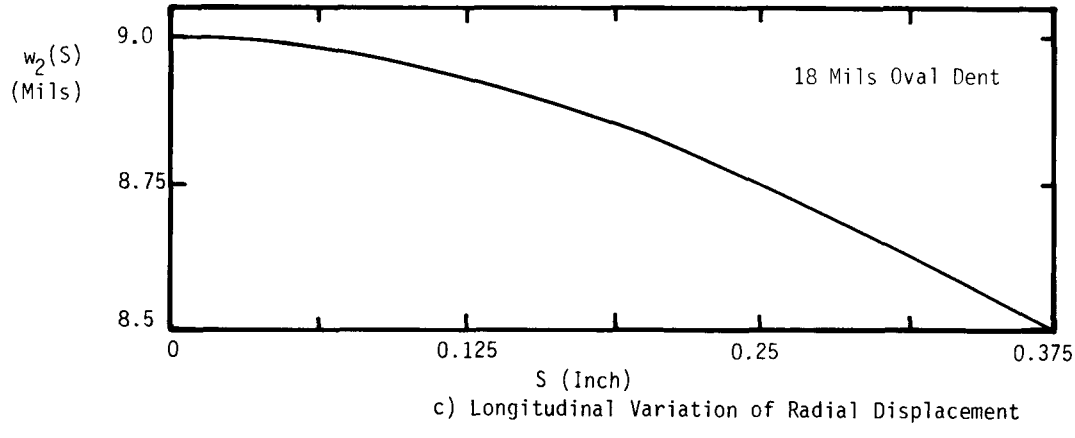

Figure 2.15 - Oval Denting Model Geometry and Assumptions.

edge is prescribed with $u = \beta = o$, and the normal displacement w is as prescribed at all points within the support plate elevations

$$w = w_2 (S) \cos 2\theta \tag{2.6}$$

This is one of the many oval shapes that could have been assumed to be consistent with field measurements of w which were available only at 0^o, 90^o, 180^o, and 270^o. The following analysis must, therefore, be regarded as typical only. To specify v, it is assumed that the shell mid-surface does not stretch so that the mid-surface hoop strain is given by

$$\varepsilon_\theta = \frac{\partial v}{R\partial\theta} + \frac{w}{R} = 0 \tag{2.7}$$

where θ is the circumferential angle, and R is the radius of the tube. Integrating, it is found that

$$v = -\frac{w_2(S)}{2} \sin 2\theta + v_o \tag{2.8}$$

Since v_o implies a pure twist of the tube cross-section, which is not present here,

$$v_o = 0 \tag{2.9}$$

In this way, all the four necessary values are specified at the symmetry plane edge.

The axial profile for w, consistent with field data and prescribed only at the plate region of the tube, is shown in Fig. 2.15. The maximum diametral dent depth 18 mils at the support plate mid-plane denotes the oval dent size. This profile is taken as the reference profile for an oval dent of any size. The circumferential displacement profile which is also specified at the plate region is given from Eqs. 2.8 and 2.9 as

$$v = -\frac{w_2(S)}{2} \sin 2\theta \tag{2.10}$$

The meridional rotation β (outward rotation is taken to be positive) takes the form

$$\beta = - \frac{\partial w}{\partial S} \tag{2.11}$$

Since the w profile is already prescribed, there is no need to specify β. Also, w is a smooth function of S. Hence, the axial displacement $u(S,\theta)$ will be small in comparison with w, is not a required input, but will be calculated from the analysis.

For an asymmetric loading with n circumferential waves (i.e., cos n θ loading) on the tube, the distance from the shell edge at which the bending stresses decay to about four percent of their edge values is given by asymptotic integration method (2.5) as

$$\delta_n = \pi R \left(\frac{2R[12(1 - \nu^2)]^{\frac{1}{2}}}{n^2(n^2 - 1)t} \right)^{\frac{1}{2}} \tag{2.12}$$

where R is the mean radius of tube, t is the thickness, and ν the Poisson's ratio. For the problem of oval denting (i.e., cos 2 θ loading) of steam generator tubes,

$$\delta_{n=2} = 2.76 \text{ inches} \tag{2.13}$$

Therefore, to eliminate the influence of the top edge boundary condition (taken to be clamped, as shown in Fig. 2.15) on the bending stresses developed at the dented portion of the tube, the tube length above the support plate is taken to be three inches.

The elastic results for a one-mil oval dent obtained using the shell analysis code STAGS is shown in Fig. 2.16. The values are in close agreement with asymptotic expansion solutions. All stresses are the same as shown in Fig. 2.16 but of opposite sign at $\theta = 0^{\circ}$. Maximum stresses in the tube occur at the plate surface. Elastic-plastic analysis results are given in Figs. 2.17 through 2.19. It is seen from Fig. 2.17 that for a particular oval dent size, the tensile circumferential strain exceeds the axial strain. Hence, axial cracks are expected before circumferential cracks. Figure 2.18 shows that the circumferential strain is almost uniform across the plate thickness and remains essentially constant

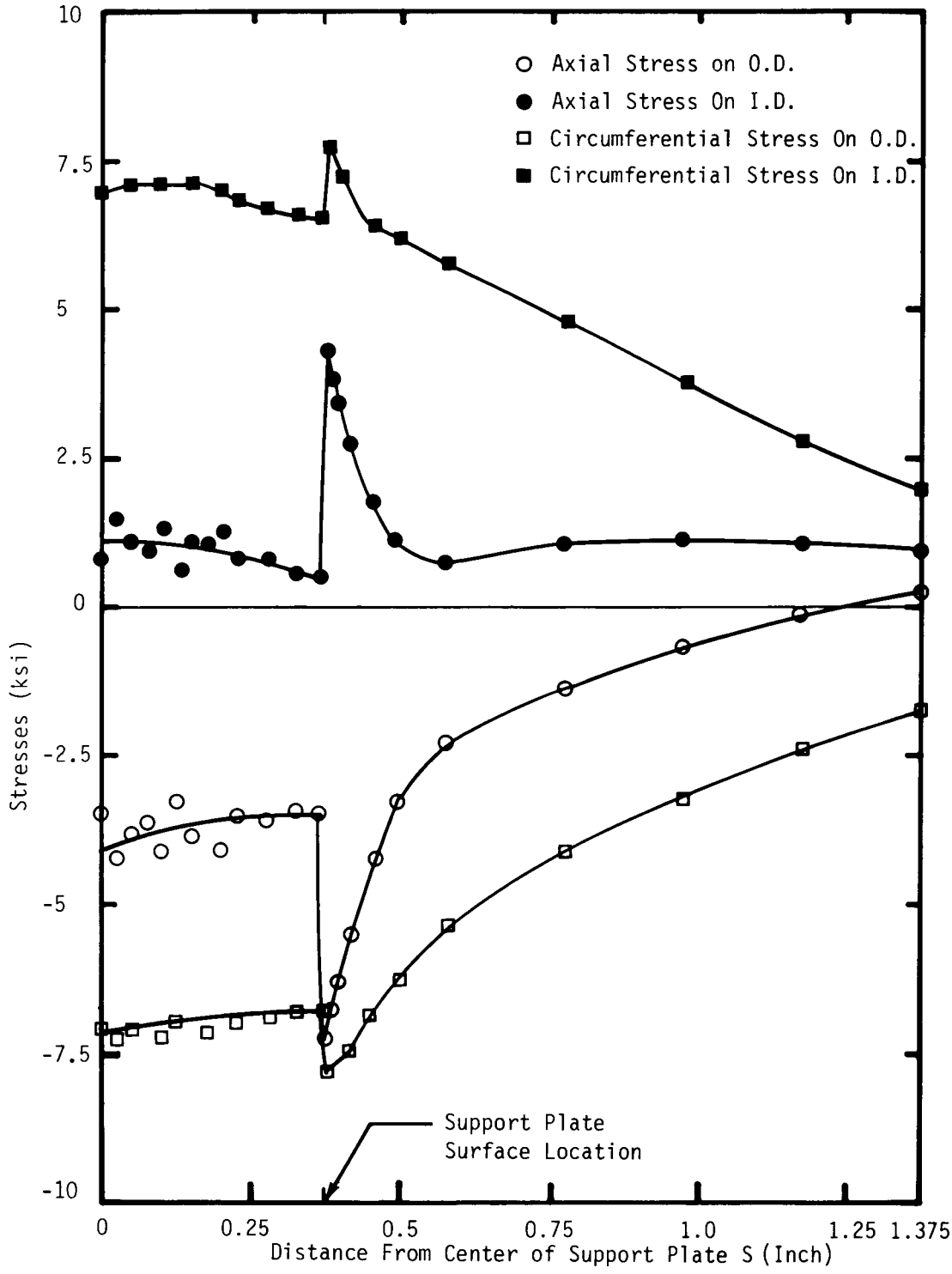

Figure 2.16 - Stresses at Section $\Theta = 90^{O}$ for 1 Mil Oval Dent at Support Plate, Linear Analysis.

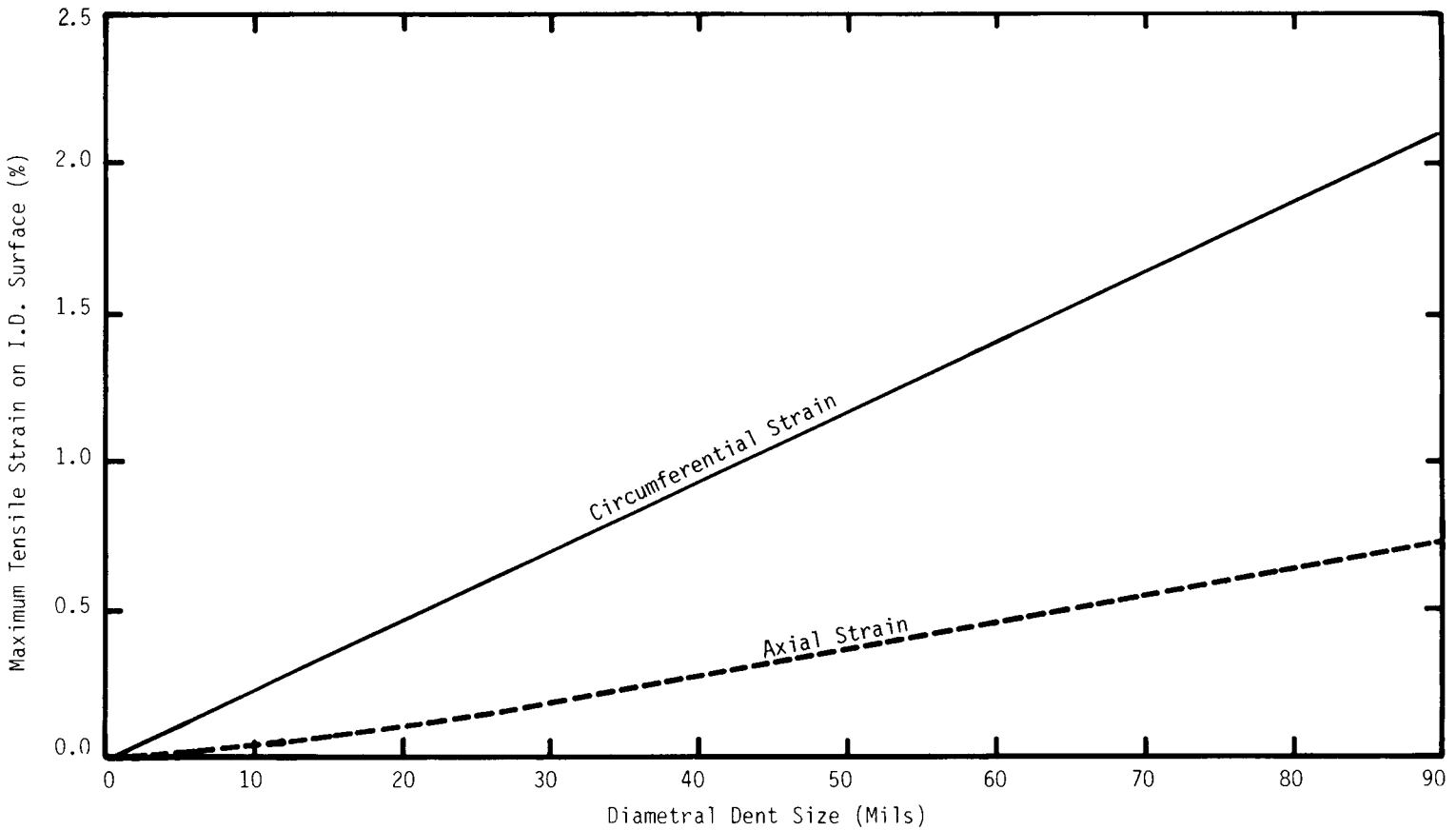

Figure 2.17 - Elastic-Plastic Results for Maximum Tensile Strain on I.D. Surface for Oval Dent.

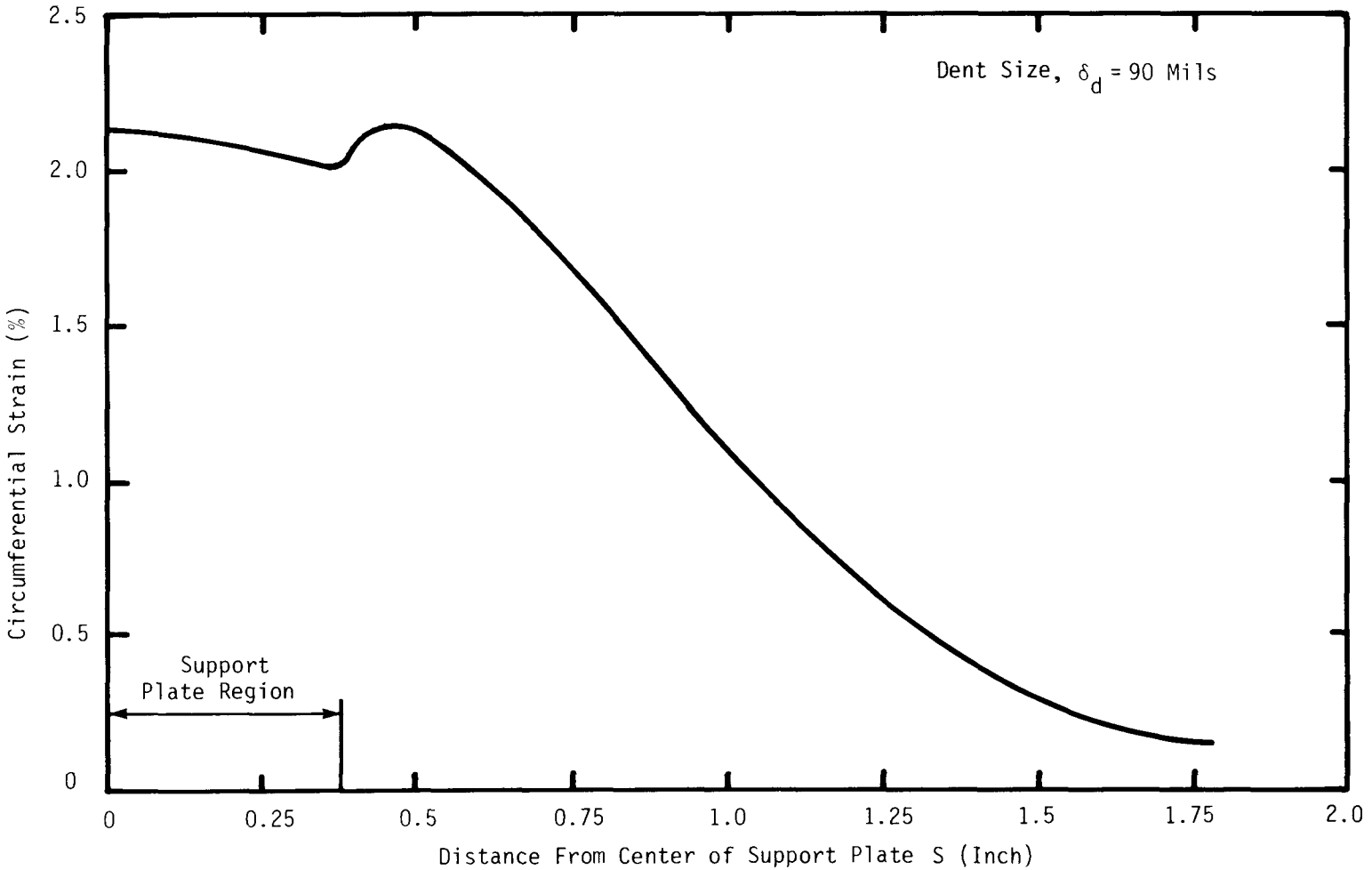

Figure 2.18 - Axial Variation of Elastic-Plastic Circumferential Strain at Inner Surface of Section $\Theta = 90^0$ for Oval Dent.

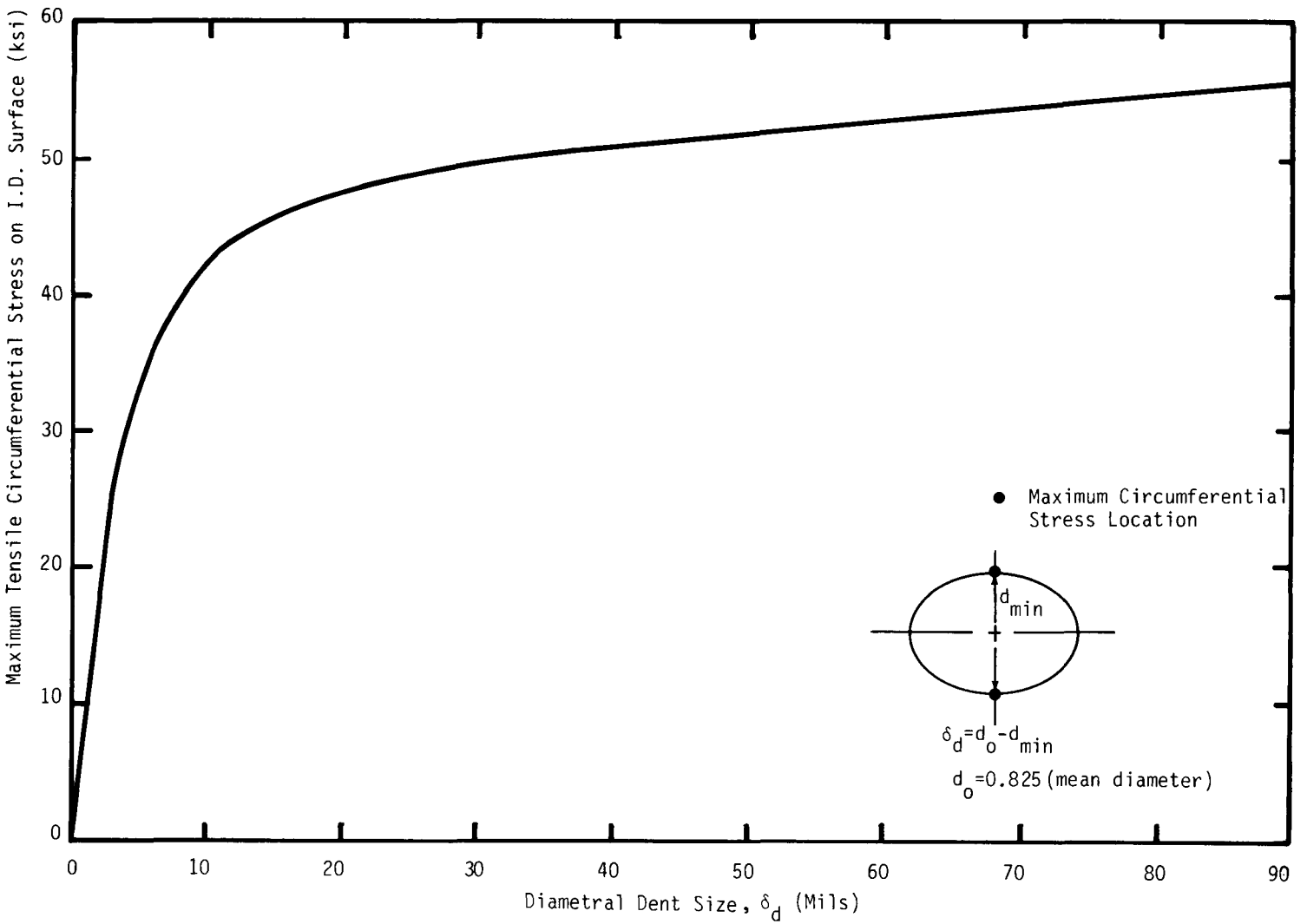

Figure 2.19 - Nonlinear Results for Maximum Tensile Circumferential Stress on I.D. Surface as a Function of Oval Dent Size.

even up to a distance of about 0.25 inch from the plate surface. Thus, longitudinal cracks due to oval denting could occur either within the support plate region or slightly away from the support plate surfaces. Figure 2.19 presents the correlation between the maximum tensile circumferential stress and the dent size. As expected, the problem is linear for small dent depths, but nonlinear analysis treatment is required for all except the smaller dents.

2.8 Analysis of One- and Two-Lobed Dents

A schematic of two typical dented cross-sections that have developed in the field and in which cracks were observed, is shown in Fig. 2.20. The peanut-shaped dent has two approximate planes of symmetry, whereas, the one-lobed dent has only one approximate plane of symmetry. Since only the local behavior near the lobe is desired, by assuming a symmetric lobe on the opposite side of the existing lobe for the localized dent, both shapes in Fig. 2.20 can be treated with the same models. Using the above symmetry assumptions, these two dent shapes were studied by analyzing the two idealized models shown in Fig. 2.21. In Model I, line loads F are applied at sections $\theta = 0^{o}$ and $\theta = 180^{o}$, whereas, in Model II, a normal pressure load is applied over a segment of 45^{o} symmetrically on both sides. The angle 45^{o} is chosen in that it represents the angle subtended by the ligament between two adjacent tube holes. The load magnitude F takes the axial profile shown in Fig. 2.22. The motivation for studying two models is to determine if the corrosion product must be extremely localized to produce the observed shapes (as in Model I) or could it be spread over a larger surface (as in Model II). Since little is known about how such local forces develop in the field, these models must be considered exploratory in nature. It is entirely possible that the dent shapes in Fig. 2.20 are not produced by local corrosion product. Other possibilities are buckling of the tube or local forces on the tube from protrusion of broken support plate ligaments.

The specification of proper boundary conditions will be discussed now. The self-equilibrating line loads can be written in terms of infinite Fourier Cosine Series containing all terms except for the n = 1 term. It was indicated in Sections 2.5 and 2.7 that for axisymmetric loads (i.e., n = 0) and for loads with two circumferential waves (i.e., n = 2), the distances at which the bending stresses decay to about four percent of their edge values are 0.351 inch and 2.76 inches, respectively. For loads with circumferential wave numbers greater than two, such as in the case of Model II where the wave number is eight, the decay distances defined above are lower than the value of 2.76 inches for loads

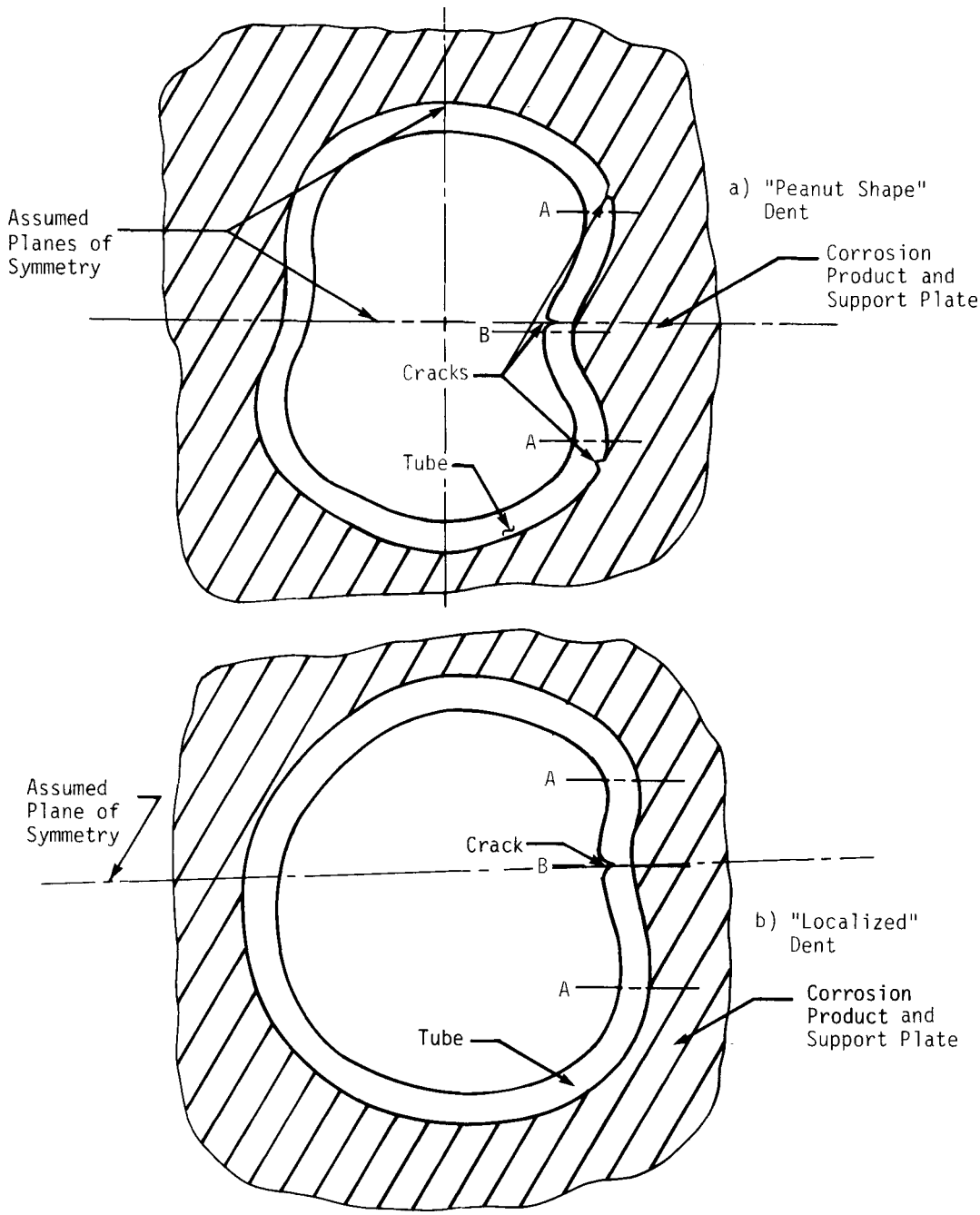

Figure 2.20 - Schematic of Two Tube Dent Shapes, (1) Peanut-Shaped and (b) Localized Dents.

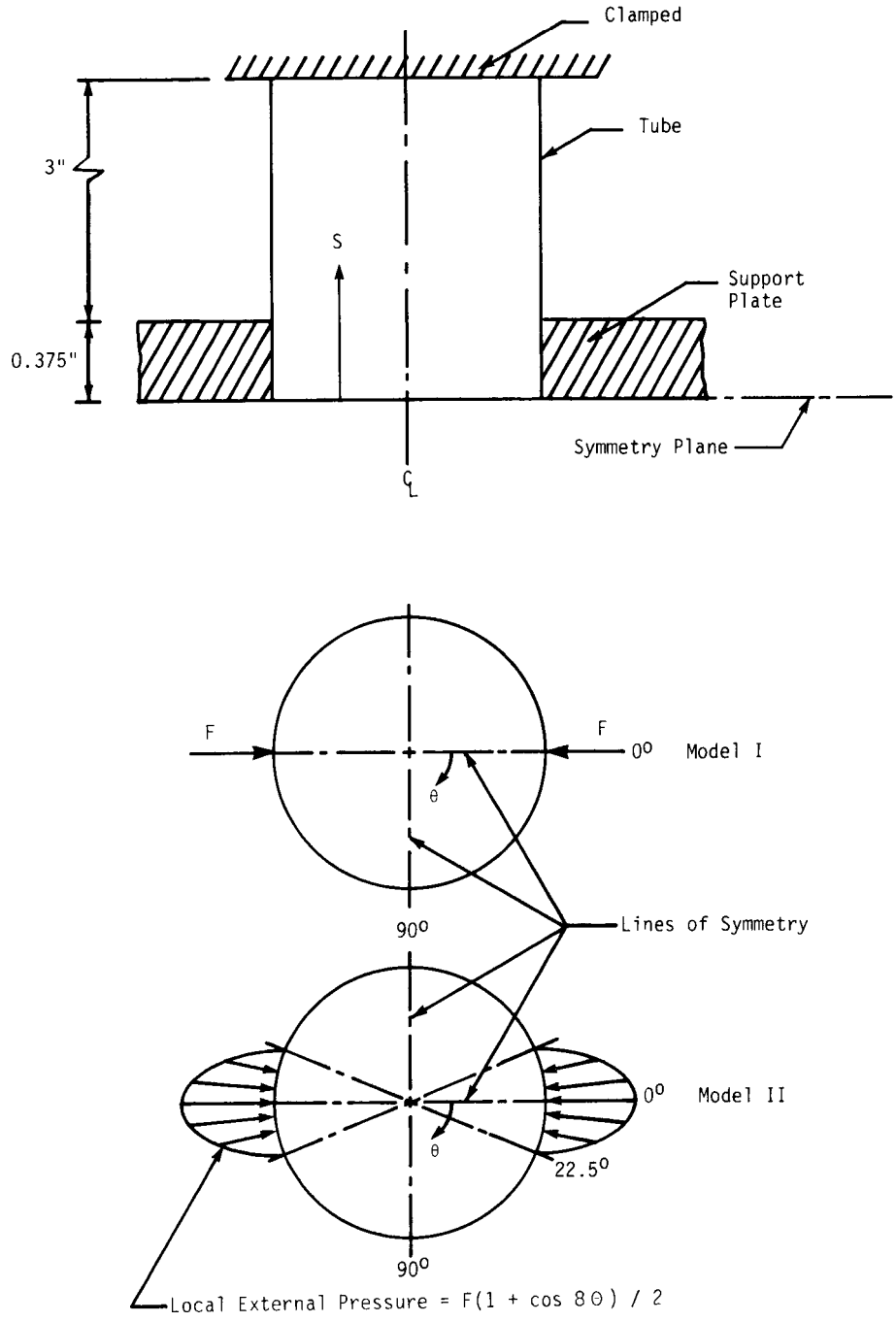

Figure 2.21 - Models Investigated to Simulate Peanut-Shaped and Localized Denting Phenomena Shown in Fig. 2.20.

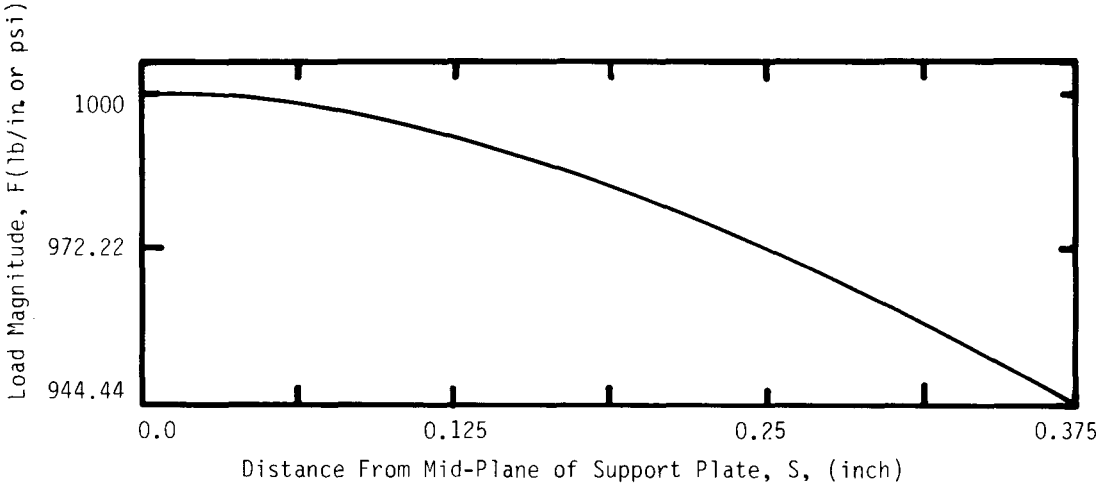

For Model I, F_{yield}^{*} = 103.2 lb/in

For Model II, F_{yield}^{*} = 1713.4 psi

* The value of F at S = 0 when tube begins yielding

Figure 2.22 - Axial Profile of Loading in Models I and II, Shown in Fig. 2.21.

with two circumferential waves. Hence, for both models, the top edge is taken to be three inches from the plate surface so that there is no influence from the top edge boundary condition (clamped, as shown in Fig. 2.21) on the stresses developed at the support plate region. At the symmetry plane edge, four conditions have to be prescribed to form a well-posed problem. This is accomplished by setting the axial displacement u, the meridional rotation β, the normal and tangential shear resultants equal to zero. The applied loads prescribe the normal surface loads acting on the tube. The tangential surface loads in the axial and circumferential directions are zero.

Since the tube is fairly thick (radius to thickness ratio is 8.25) an elastic-plastic analysis is warranted for these two large deflection problems. As a first step, an elastic analysis is carried out for both the models. The results obtained to date are shown in Figs. 2.23 through 2.25. The similarity of displacement shapes for the two models indicates that it would be difficult to determine from deformed tubes taken from operational units whether or not the loading from corrosion products is highly localized. As expected, high tensile circumferential stresses are developed on the I.D. surface under the loading. However, high circumferential stresses developed on the O.D. surface at the ridges (see Section A in Fig. 2.20) cannot be evaluated accurately by the linear elastic analysis.

In reality, this is a large deflection elastic-plastic problem. In both models, from a physical point-of-view, dimples (inverted segments) due to local buckling would be formed under the loads, and they would spread as the load increases. Ridges would develop at Sections A (shown in Fig. 2.20) where high bending stresses and strains occur. Also, at Section B (Fig. 2.20) high bending stresses can develop, depending on how localized the applied loads are.

In the next phase of the program, elastic-plastic analysis of the above-mentioned large deflection problems should be attempted. Caution should be exercised in carrying out an elastic-plastic problem because a longitudinal section, θ = constant, on the tube circumference first loads plastically and then unloads elastically as the dimple spreads with increasing load.

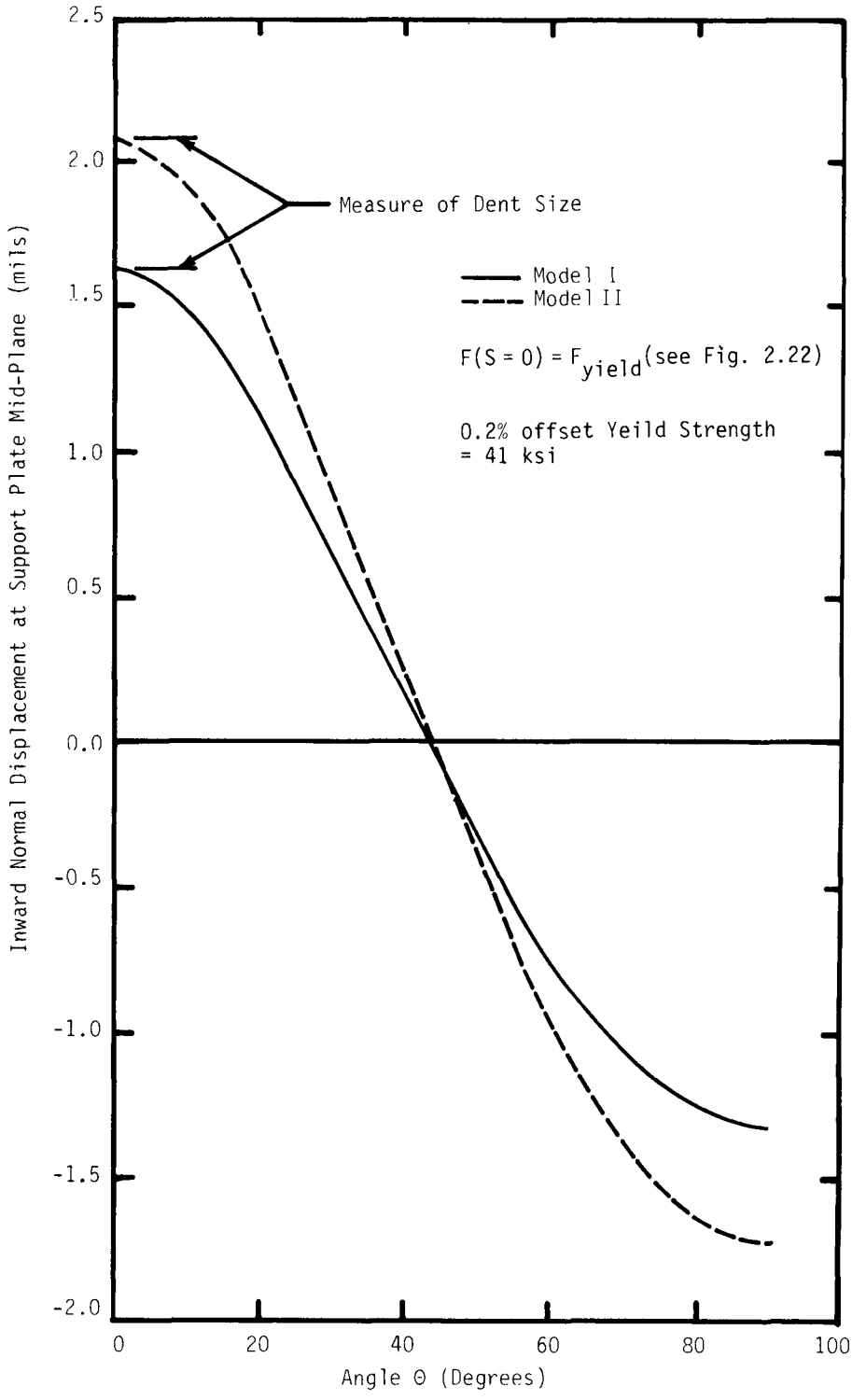

Figure 2.23 - Inward Normal Deflection at Support Plate Mid-Plane in Local Dent Models I and II When Yield Begins.

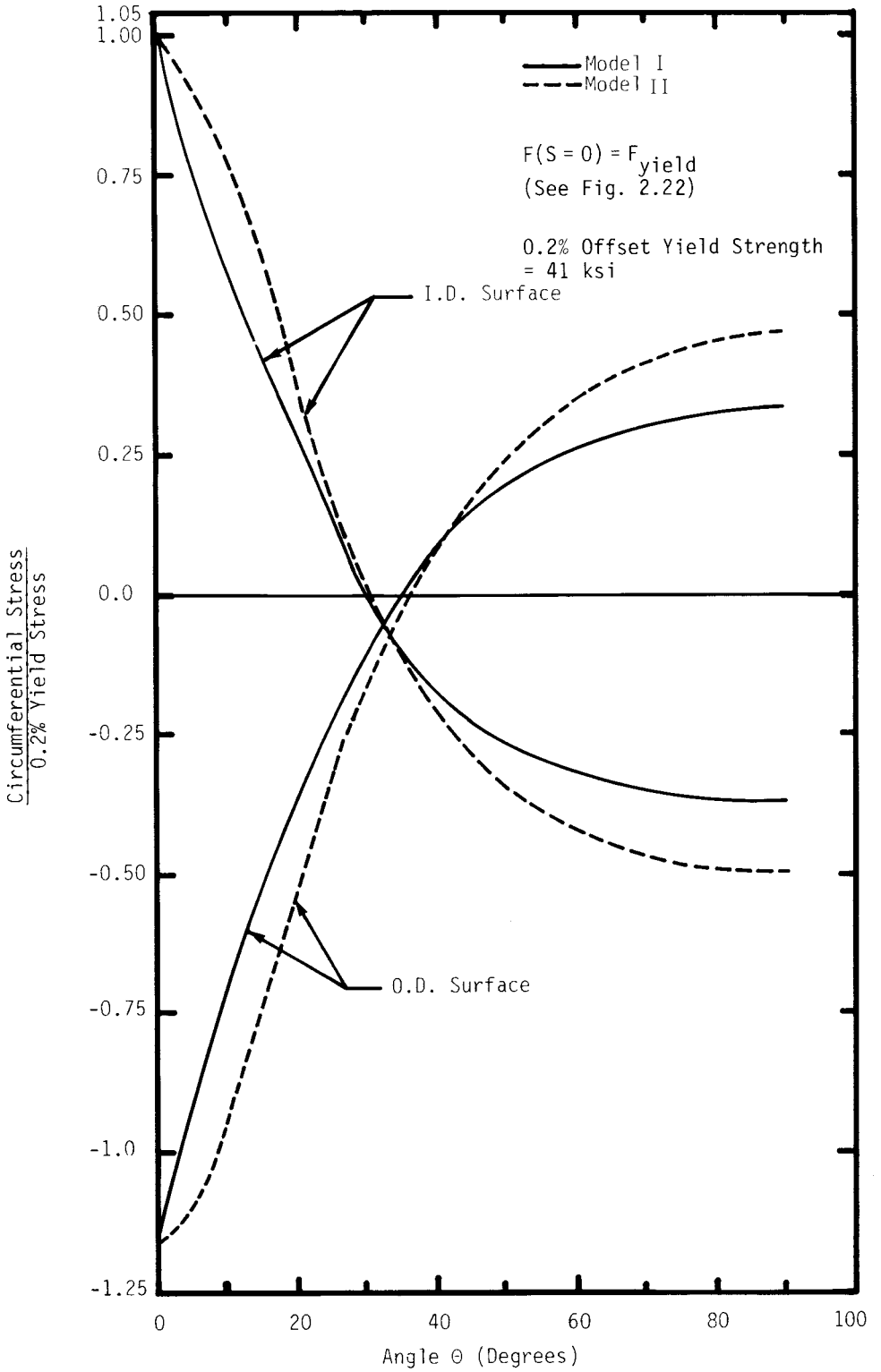

Figure 2.24 - Circumferential Stress Variation at Support Plate Mid-Plane for Models I and II When Tube Begins Yielding.

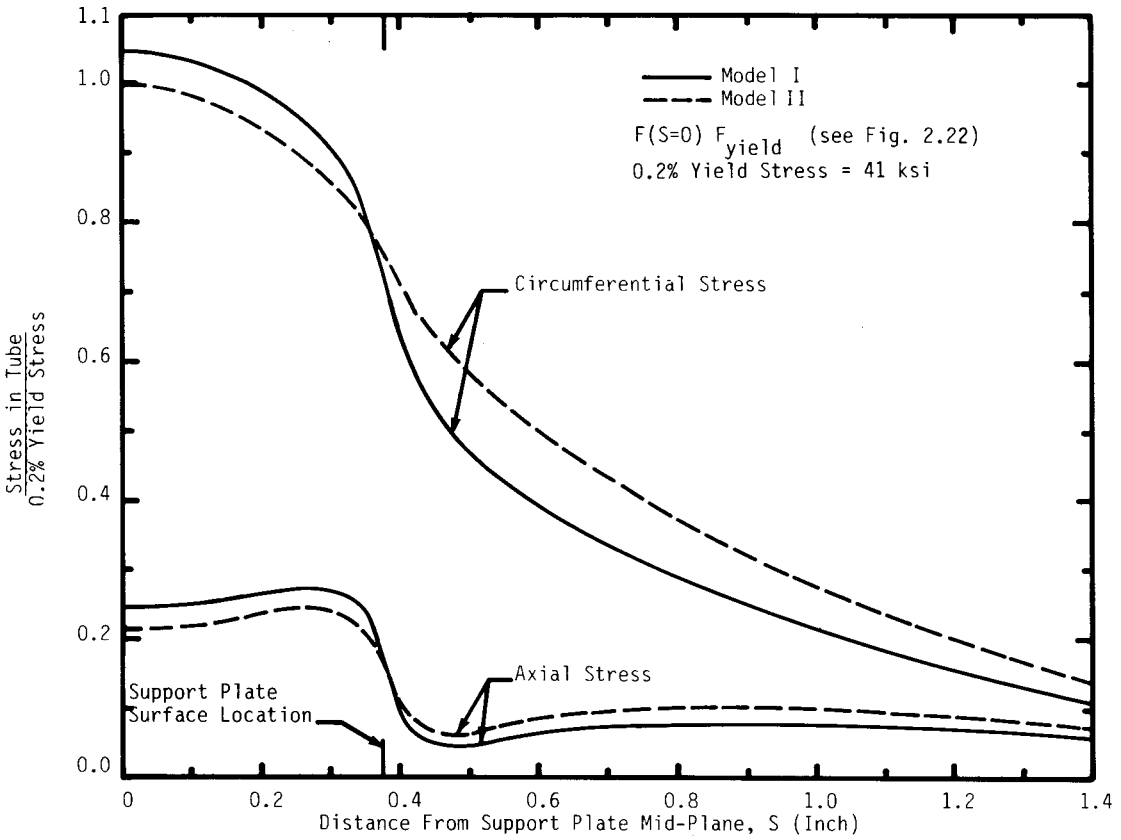

Figure 2.25 - Axial Variation of Tensile Stresses on I.D. Surface at Section $\theta = 0^{o}$ for Local Dent Models I and II, When Tube Reaches Yield.

2.9 Summary

Important results from the tube analyses to date are summarized below. The problems which should be analyzed in the future are also identified here.

1) For an amount of hourglassing at the flow slots that is equivalent to 40 mils of inward movement of each leg of the U-bend section at the first row, the tube is calculated to yield at the apex portion of the bend. For larger amounts of flow slot closure, an elastic-plastic analysis would be required to compute the circumferential strains which may cause axial cracks at the extrados and intrados of the U-bend. To predict these strains accurately, a proper quantification of the residual stress distribution and the initial ovality is required.

2) Maximum stress and strains which develop in a circular tube due to operating pressures are much lower than those which are present when the tube is dented.

3) The axisymmetric component of dents result in high axial tensile stresses and strains on the tube I.D. surface at the elevations of support plate surfaces. These highly localized stresses and strains would indicate a potential for circumferential cracks.

4) Due to perfectly oval dents, the tensile circumferential strain exceeds the axial strain. Hence, axial cracks are more probable than circumferential when ovalization occurs. Also, the longitudinal cracks could occur either within the support plate region or slightly away from the support plate surfaces. Even for an oval dent of diametral depth of 90 mils, the maximum tensile circumferential strains is only 2.5 percent, suggesting that the longitudinal cracks that have been observed in the field might have been formed not by oval dents but by localized denting.

5) Elastic results for the localized dents resulting in one-lobed and two-lobed tube cross-sections show that high circumferential stresses are developed at the apex of the lobe(s). An elastic-plastic large deflection analysis would be required for clear understanding of these problems. Since dimples may be formed by local instability

due to localized oxide growth, an elastic-plastic buckling analysis may also be required. As the tube is free to displace inward and not outward due to the constraint from the corrosion product, this large deflection denting becomes a problem with nonlinear boundary conditions. This is an extremely difficult task, and great care should be taken during such an analysis.

REFERENCES

2.1 "Structural Analysis of General Shells, User Instructions for STAGSC, Vol. 3, Lockheed Palo Alto Research Laboratory, Palo Alto, CA (December 1975).

2.2 White, G. N., Jr., "Application of the Theory of Perflectly Plastic Solids to Stress Analysis of Strain Hardening Solids," Graduate Division of Applied Mathematics, Brown University, Providence, R.I. (August 1950).

2.3 Besseling, J. F., "A Theory of Elastic, Plastic, and Creep Deformation of an Initially Isotropic Material," SUDAER Report No. 78, Department of Aero Engineering, Stanford University, Stanford, CA (1958).

2.4 Ranjan, G. V., "Edge Zone Expansions for Thin Shells With Application to (1) Torispherical Pressure Vessel and (2) Large Deflection of Sphere With Point Load," Ph.D. Dissertation, Stanford University, Stanford, CA (November 1976).

2.5 Steele, C. R., "A Systematic Analysis for Shells of Revolution With Nonsymmetric Loads," Proceedings of the Fourth US National Congress of Applied Mechanics, Berkeley, CA (June 1962), pp. 783-792.

2.6 Steele, C. R., "Shells With Edge Loads of Rapid Variation - II," Journal of Applied Mechanics, Vol. 32, No. 1 (March 1965), pp. 87-98.

2.7 ASME Boiler and Pressure Vessel Code, Section III, Subsection NA, 1977 Edition.

2.8 Clark, R. A. and E. Reissner, "Bending of Curved Tubes," In Advances in Applied Mechanics, Vol. 2, Academic Press, New York, (1951), pp. 93-122.

2.9 Rodabaugh, E. C. and H. H. George, "Effect of Internal Pressure on Flexibility and Stress Intensification Factors of Curved Pipe or Welding Elbows," Trans. ASME, Vol. 79 (1957), pp. 939-948.

2.10 The M. W. Kellog Company, Design of Piping Systems, John Wiley & Sons Company, New York, NY (1956), pp. 52-60.

3.0 ANALYSIS OF SUPPORT PLATE LIGAMENT

3.1 Introduction

The purpose of this Section is to describe the analytical work performed on a support plate. By making use of geometric symmetry and assuming symmetric boundary conditions, a local one-eighth angular segment can represent the ligament behavior between tube and flow holes. The models described herein are mathematical representations of the plate only; the effects of the tube and oxide were considered as boundary conditions in the model. The oxide growth was modelled as a monotonically increasing uniform pressure load on the tube hole surface.

Plate material wastage due to the corrosion process was not considered in that the original plate ligament thickness was not reduced due to oxide formation. This material wastage effect may be negligible in the early stages of denting but would become progressively more important as the corrosion and denting increases. Therefore, the larger the tube hole pressure applied to the model, the less accurate the results will be. The effect of corrosion on the ligament thickness is illustrated in Fig. 3.1 based on the assumption that the corrosion product is magnetite (Fe_3O_4). The development of Fig. 3.1 is given in Appendix B. A tube/oxide/plate model which includes the tube and oxide behavior in the plate model is described in Section 4.0. This model could eventually be used to also account for material wastage.

The objective of the analysis is to determine stresses and strains in the plate ligaments between tube holes and flow holes and to relate these stresses and strains to the degree of denting. Some simple plate ligament boundary conditions were used in this initial study. These results will also identify some of the more important factors controlling plate behavior, which can then be included in more accurate modelling ideas. Two analytical approaches were used. First, an approximate analytical analysis using plasticity theory was performed by hand to bound the general problem of plate ligament yielding. This work was initially conducted to obtain insight concerning the pressures necessary to generate plate yielding. Second, an elastic-plastic model using finite elements was developed.

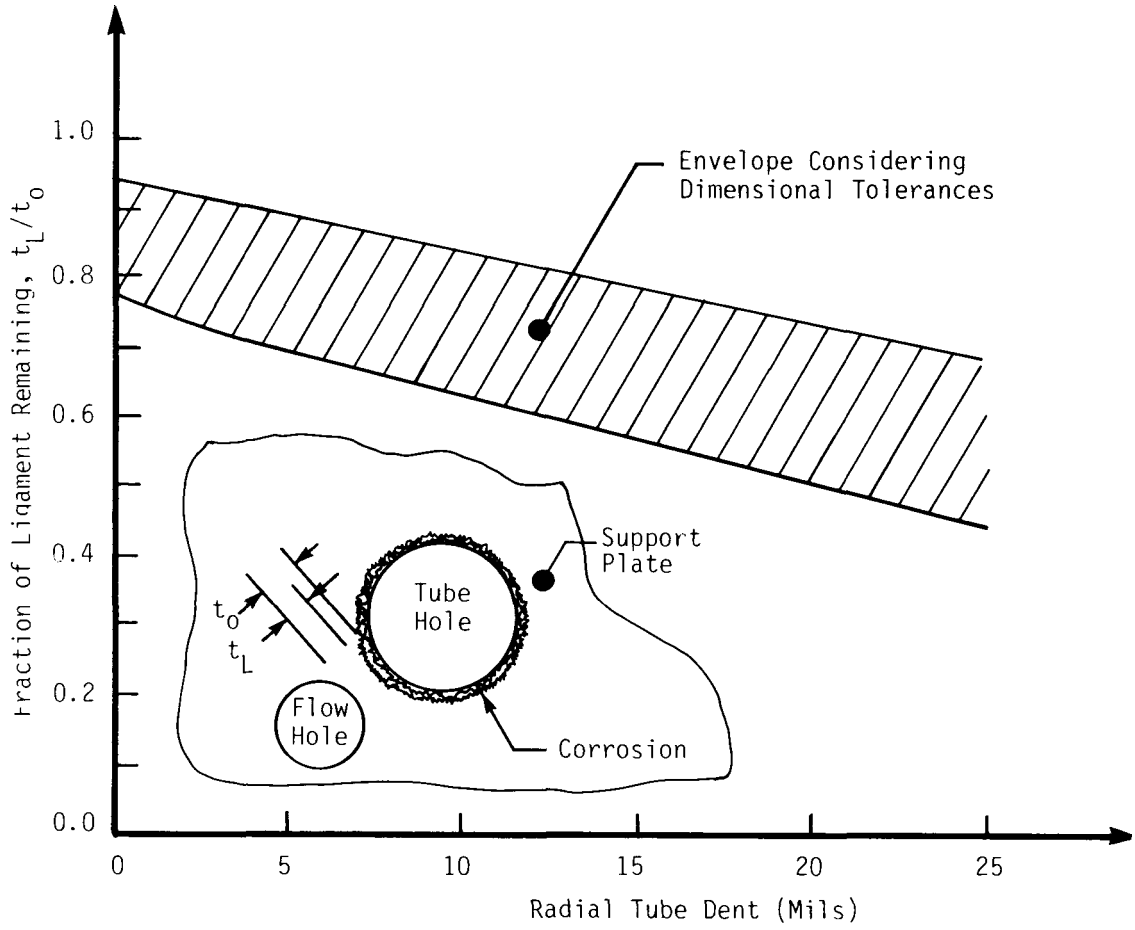

Figure 3.1 - Effect of Corrosion on Support Plate Ligament Thickness.

Two candidate general purpose finite element programs, ANSYS (3.1) and MARC/CDC (3.2), were first applied to a test case problem of a hole in a plate under tension in order to select the best code from the standpoint of accuracy and cost. As a result of this investigation, the MARC code was selected primarily from cost consideration. The details of this study are presented in Appendix I.

3.2 Plate Geometry and Material Properties

3.2.1 Plate Geometry

The majority of steam generator units in service are either Series 44 or 51 designs. A Westinghouse Series 44 support plate geometry was selected for analysis, and results are expected to be applicable to the Series 51 design. The overall plate dimensions and tube hole and flow slot locations are illustrated in Fig. 3.2. The tube hole and flow hole array dimensions supplied by Westinghouse (3.3) are shown in Fig. 3.3. In the analytical models which are described in this Section and in Section 4.0, the average dimensions from the tolerances listed were used for tube hole (A), flow hole (B), and tube hole spacings (C).

3.2.2 Plate Properties

The plate material is a SA-285, Grade C in the hot rolled condition. The engineering stress versus strain behavior at $600^{o}F$ is shown in Fig. 3.4(a) for the longitudinal axis and Fig. 3.4(b) for the transverse axis (3.4). Comparison of the longitudinal and transverse curves show that the effect of rolling direction on stress/strain behavior is negligible up to the 5% strain values used in the analysis. The plate material at $600^{o}F$ exhibits a yield strength, σ_y, equal to 23 ksi and an ultimate strength, σ_{uts}, equal to 70 ksi. ASME Section III Code values (3.4) were used for the elastic properties at $600^{o}F$ which are Young's Modulus, $E = 25.7 \times 10^6$ psi and Poisson's Ratio, $\nu = 0.3$.

3.3 Approximate Bounding Analysis of a Plate Ligament Yielding

3.3.1 Analysis Assumptions

An analysis (3.5) which describes the elastic and fully plastic non-hardening behavior for a pressurized cylinder was used to model initial yielding and the growth and depth of the plastic zone in the ligament region between tube and flow holes (see Fig. 3.6). The tube hole ligament is bounded by the consideration of two separate cylinder models with wall dimensions as shown in Fig. 3.5. A model

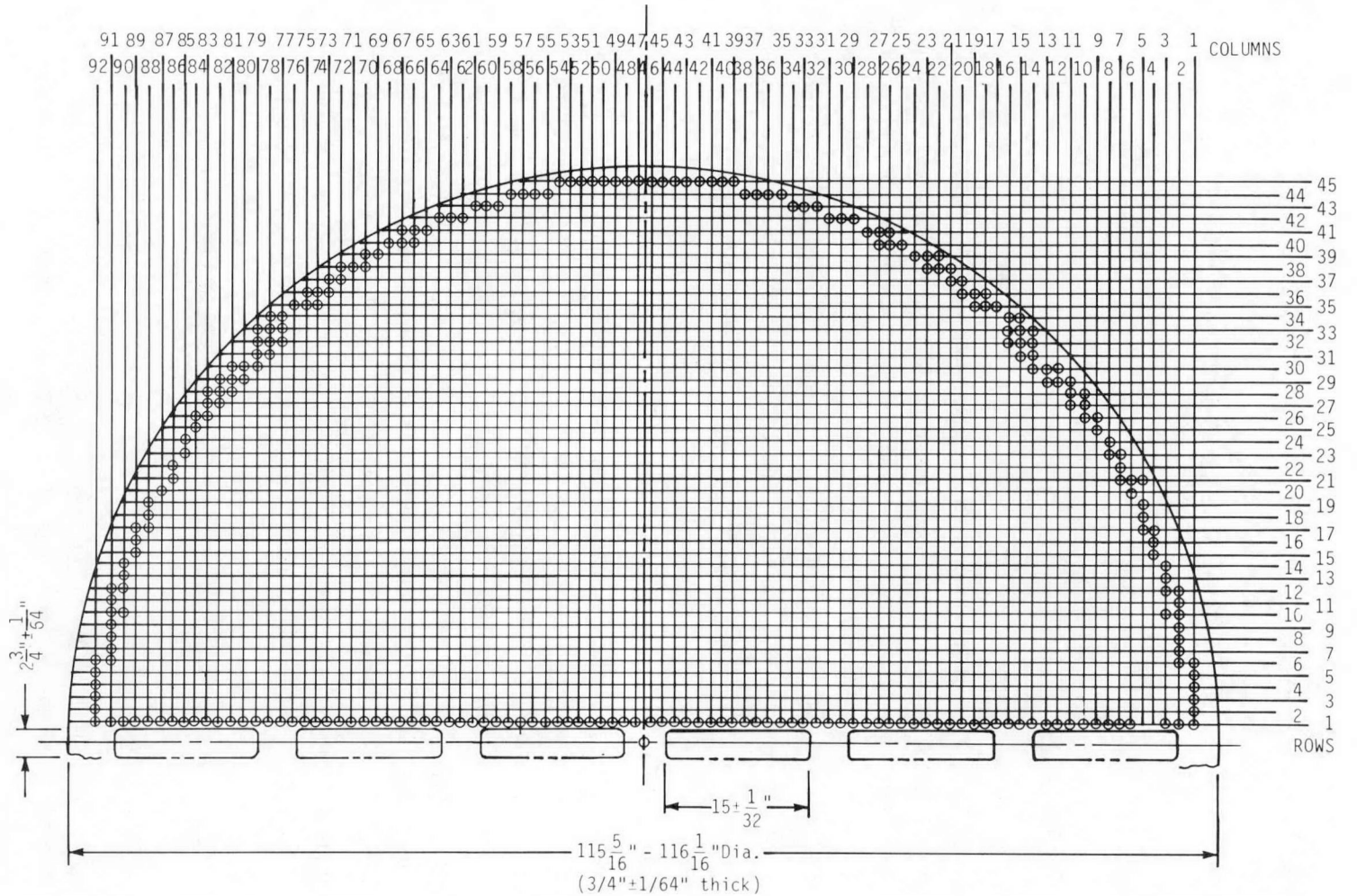

Figure 3.2 - Support Plate Geometry.

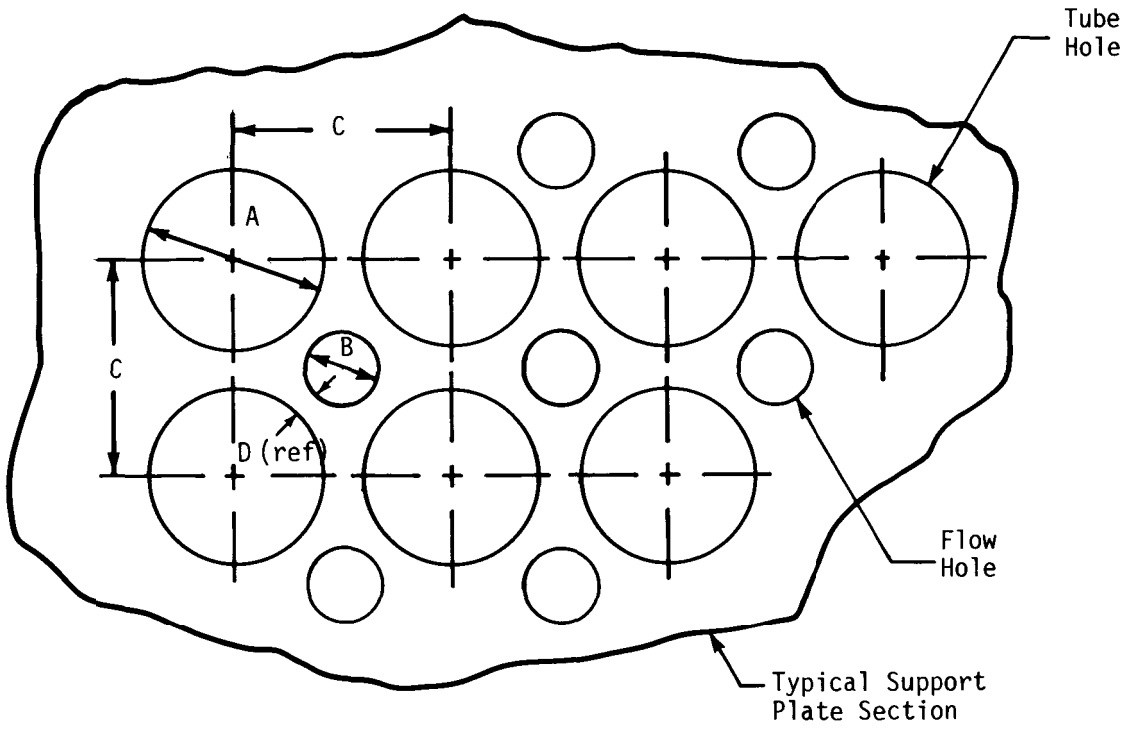

DIMENSION	Minimum	Maximum
A	57/64"	58/64"
B	43/64"	45/64"
C	1.22938"	1.23938"
D	0.0645"	0.0950"

Figure 3.3 - Tube and Flow Hole Array Dimensions for Support Plates.

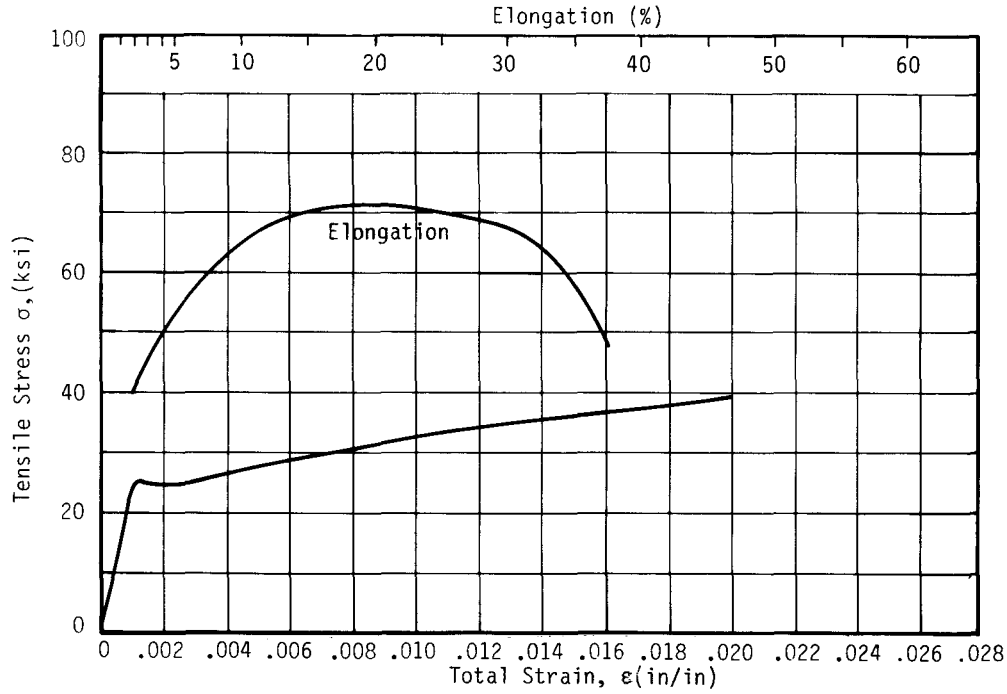

(a) Longitudinal to the Rolling Direction

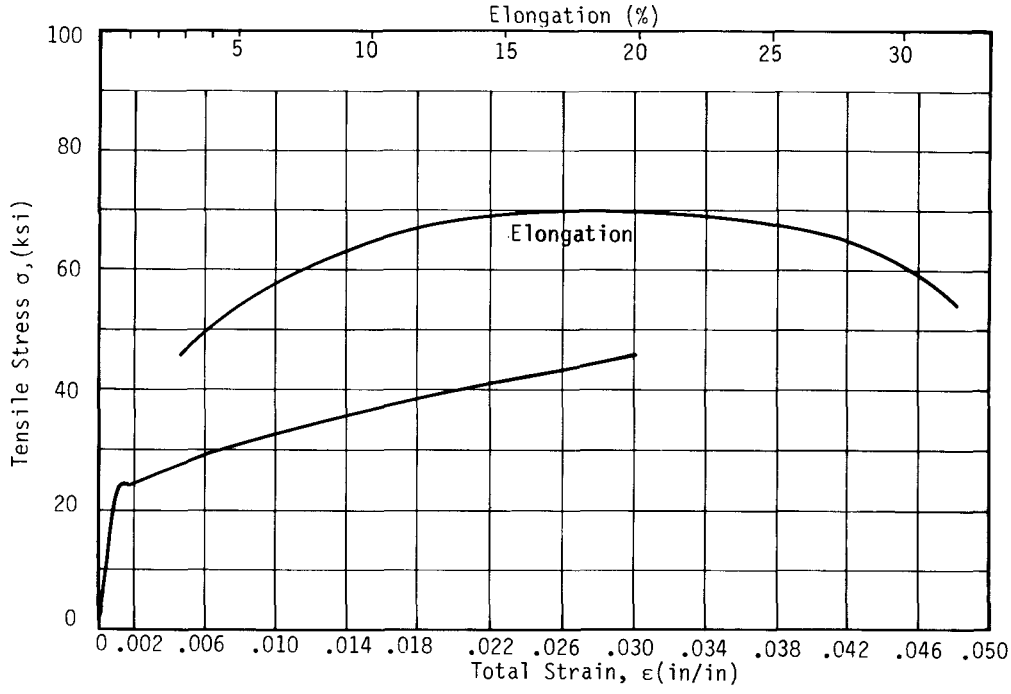

(b) Transverse to the Rolling Direction

Figure 3.4 - Engineering Stress Versus Strain Properties for SA-285, Grade C Hot Rolled Plate at 600°F.

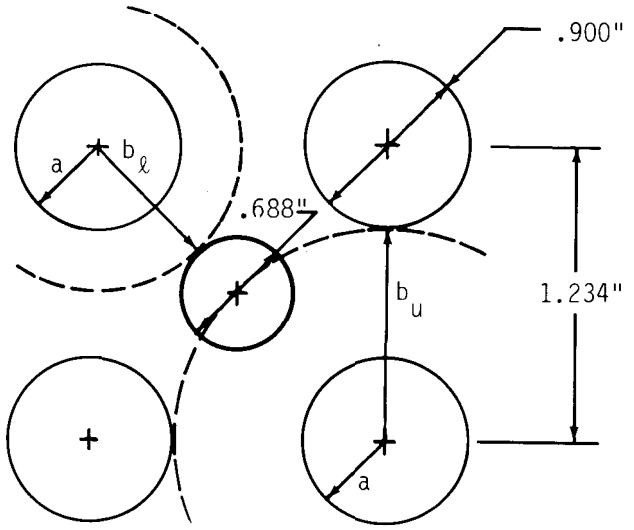

a) Tube/Flow Hole Array

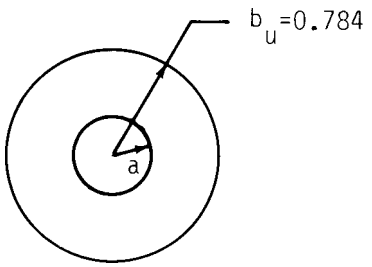

b) Upper Bound Cylinder

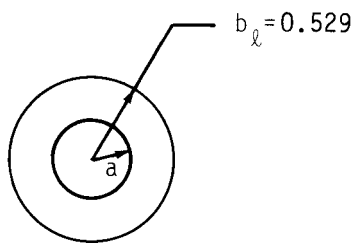

c) Lower Bound Cylinder

Figure 3.5 - Cylinder Geometries for Bounding Analysis of Support Plate Ligament.

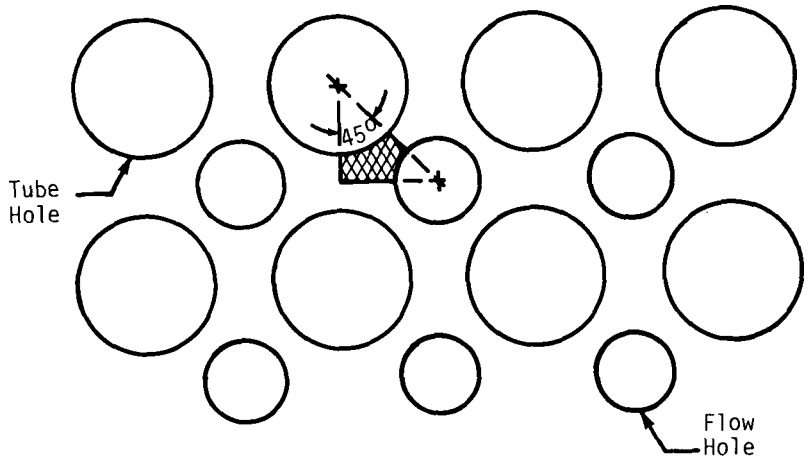

a) Support Plate Ligament Local Model (Enlarged Below)

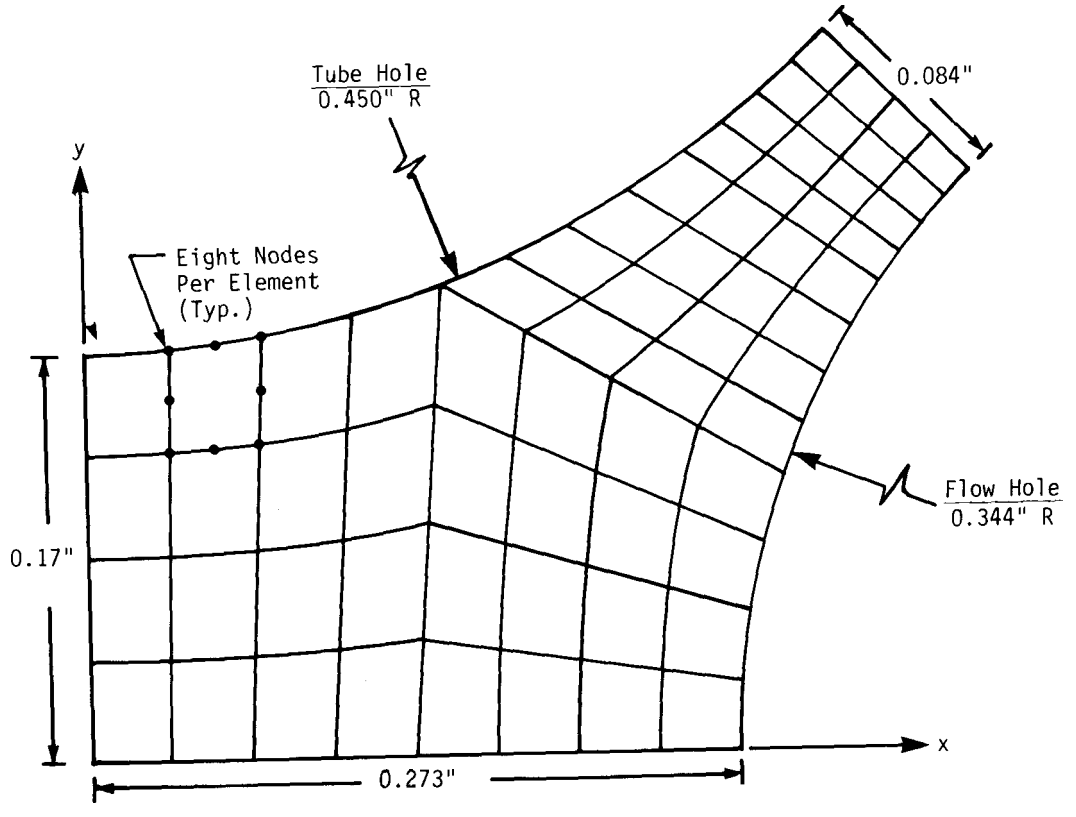

b) Finite Element Model of the Ligament Region

Figure 3.6 - Finite Element Model Geometry of a Plate Ligament.

for computing an upper bound to the plate ligament yielding is shown in Fig. 3.5(b) where the cylinder thickness is taken to be equal to the metal thickness between tube holes. The predictions from this model would be reasonable if the initial and subsequent yielding is predominantly in the thicker portion (between tube holes) of the ligament. In the original work, the upper bound calculations were performed for an infinitely thick cylinder; however, after more detailed models were developed, it was evident that the computed pressures were too large. In contrast to the upper bound approach, the lower bound yield model, which is shown in Fig. 3.5(c), should be a good approach if the yielding occurs in the minimum ligament section between the tube and flow holes. The calculation of the initial yield pressures using these two approaches is presented next.

3.3.2 Calculation of Initial Yield Pressures and Tube Dent Depths

The elastic stresses for a cylinder under internal pressure for plane stress ($\sigma_{zz} = 0$) at the point of maximum stress ($r = a$) are

$$\sigma_{rr} = -p \tag{3.1a}$$

$$\sigma_{\theta\theta} = -(1 + b^2/a^2)p/(1 - b^2/a^2) \tag{3.1b}$$

where $a/b = 0.57$ and 0.84 for upper and lower bound models, respectively. The initial yield pressure using a von Mises yield criterion is determined from

$$p_y = (\sigma_y/\sqrt{3})(1 - a^2/b^2)/(1 + a^4/3b^4)^{\frac{1}{2}} \tag{3.2}$$

For the upper and lower bound model dimensions and $\sigma_y = 23$ ksi, the range in p_y is

$$3.4 \text{ ksi} \leq p_y \leq 8.8 \text{ ksi} \tag{3.3}$$

The axisymmetric tube dent depth as a function of applied pressure has been both analytically approximated and numerical computed in Section 2.6. The elastic tube wall diametral deflection is shown in Fig. 2.14. From Fig. 2.14, the tube dent depth for the lower bound p_y is 1.12 mils, using the results from the uniform pressure STAGS model. Since the upper bound pressure will cause the tube to yield before the plate, the elastic-plastic results of δ versus p given in Fig. 2.13 show that $\delta_d > 160$ mils for p equal to the upper bound value. Because of the wide range between the upper and lower bounds of dent depths, it cannot be

determined from these simple models whether plate yielding begins at small or large dent depths. More accurate models such as those in Sections 3.4 and 3.5 are required.

3.3.3 Plastic Ligament Analysis

The relationship between plastic zone depth and applied internal pressure using an approximation to the von Mises yield criterion is presented in (3.5) and

$$p = (2\sigma_y/\sqrt{3}) \left[\ell n(c/a) + \tfrac{1}{2}(1 - c^2/b^2) \right] \tag{3.4}$$

where c is the depth of the plastic zone so that $a \leq c \leq b$. The errors associated with this approximation will decrease as c approaches b. The pressure to cause the cylinder to become fully plastic is determined from Eq. (3.4) by setting $c = b$

$$p = (2\sigma_y/\sqrt{3})\, n(b/a) \tag{3.5}$$

and the upper and lower bound pressures are computed to be 14.9 ksi and 4.3 ksi, respectively. Referring again to Fig. 2.14, the tube dent depth for the lower bound p is

$$\delta_d > 1.0 \text{ mils} \tag{3.6}$$

and the tube would experience large deformations for the upper bound. The lower bound result indicates the possibility of fully plastic ligaments even though the tube is still elastic, but again the upper bound result is too large to state this as a conclusion. These bounding calculations will later be compared to numerical results presented in Section 3.5.

3.4 Finite Element Representation and Boundary Conditions

3.4.1 Finite Element Model

The tube hole and flow hole array pattern for a Westinghouse support plate is shown in Fig. 3.6(a). The smallest repeatable region between tube holes and flow holes is bounded by the intersections of three radial lines which pass through the tube hole and flow hole centers and form an isosceles right triangle. This ligament region, which will be referred to as the plate ligament model, is shown

as the cross-hatched area in Fig. 3.6(a). Original dimensions are used in the analysis, without accounting for metal loss due to corrosion. The effect of this simplification is that the model becomes progressively less representative as the denting increases. Higher stresses under the same loads would result if this simplification had not been made. This also affects results where plate deflections are compared with tube deflections. In these cases, the plate relative stiffness would be smaller than indicated by the comparisons herein.

An enlarged view of the plate ligament model showing the finite element mesh used in the analysis is shown in Fig. 3.6(b). The model is a two-dimensional, elastic-plastic, plane stress model using eight-noded isoparametric elements provided in the MARC/CDC program. The eight nodes are positioned at each corner and on each side. The element is a distorted quadrilateral type in that the boundaries can be curved. The strains, stresses, and yield condition requirements are computed at nine integration points located within each element from the eight nodal displacements by a quadratic shape function. This interpolation function is such that each edge has a parabolic displacement variation. The corresponding strain variation in any direction is approximately linear.

The yield criteria is based on von Mises, and the strain hardening behavior is isotropic. A monotonically increasing loading was assumed since the build-up of corrosion products is expected to be non-decreasing. The plastic strain rate behavior used in the MARC program is determined from the Prandt-Reuss equations.

3.4.2 Boundary Conditions

The growth of corrosion products in the crevice between the tube and support plate as illustrated in Fig. 2.1 causes a radial outward pressure on each tube hole. This tends to make each tube hole larger, resulting in a tendency for the entire support plate to expand in its plane.

An illustration of how the tube support plate is constrained in its plane is shown in Fig. 3.7. At six points around the plate periphery, it is constrained against radial growth by wedges and channels that span the annular gap between the support plate and the steam generator external shell. These local restraints result in a support plate boundary that is neither free to expand nor completely restrained from expansion. Therefore, no one set of boundary conditions (applied to the ligament model described in Section 3.4.1) is representative of all locations in the support plate.

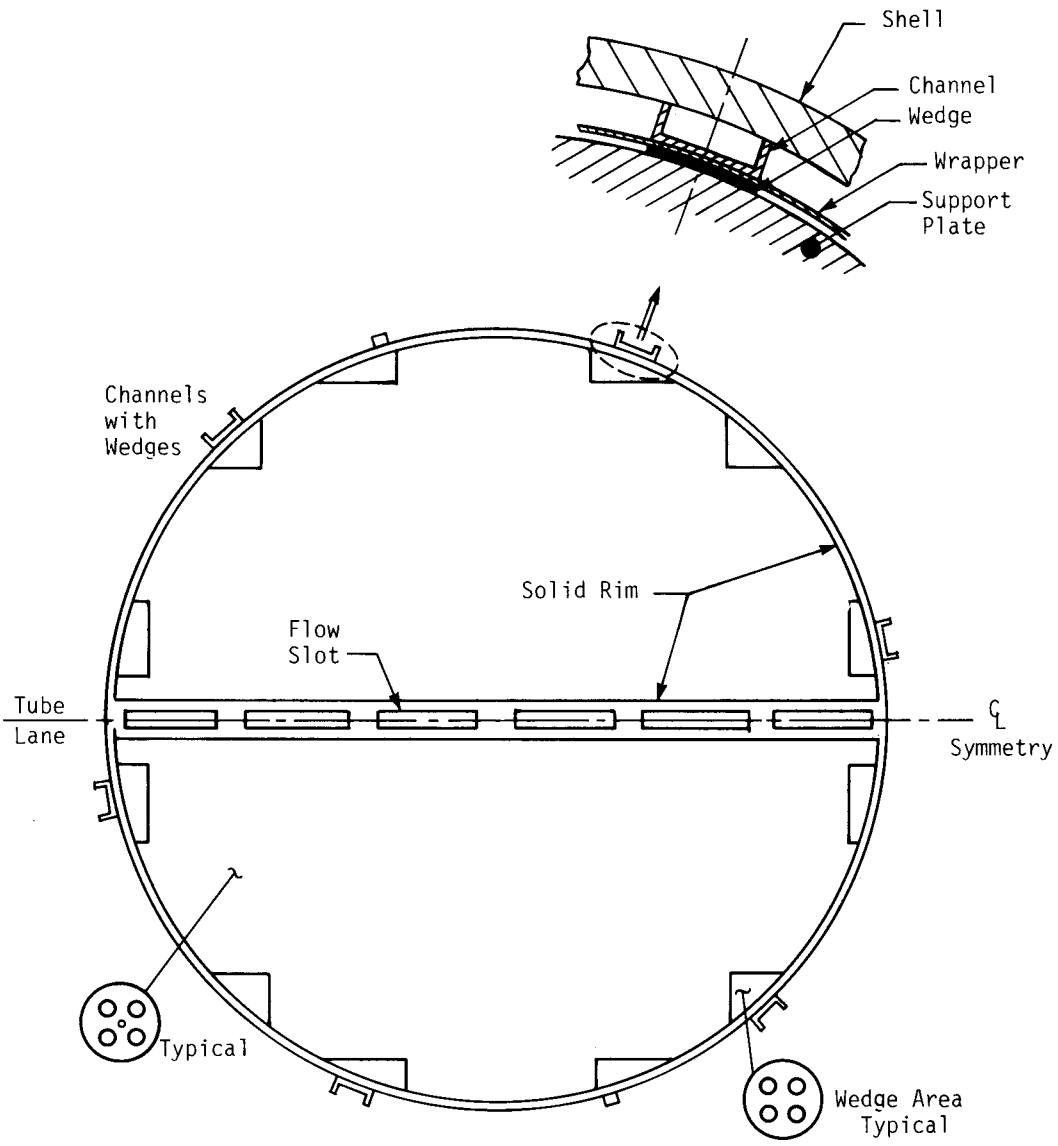

Figure 3.7 - Tube Support Plate In-Plane Constraints.

The ligament model is a local model, and the conditions which must be applied to the boundaries of the model will depend on the location of this local model within the global plate geometry. Ideally, a global plate analysis of the entire support plate would be performed initially using a rather coarse grid followed by a refined analysis of a smaller region, such as the ligament model described in Section 3.4.1, using as boundary conditions the solution results from the global analysis. Presently, two different idealized sets of boundary behavior were formulated.

For the first condition (Fig. 3.8a), the ligament is considered fully constrained (no global plate expansion), and symmetry boundary conditions are used where both the normal displacement (u_n) and shear traction (t_s) are zero. In the second condition (Fig. 3.8b), the symmetry boundary between tube holes is allowed to expand freely but under the condition that normal displacement is equal to some constant value which is independent of x and satisfies the condition

$$\int_0^{x_0} t_n(x,0)dx = 0 \tag{3.7}$$

The physical meaning of Eq. (3.7) is that the resultant force applied to the boundary at y = 0 is zero. In both the fully constrained and expansion models, the tube hole has a uniform pressure p exerted on its surface and zero shear traction, and the flow hole is stress free.

Puristically, the fully constrained model represents a plate with the outer edge completely constrained from expansion with no cut-outs or protuberances such as flow slots. The expansion boundary condition model represents the same idealized plate with the outer edges completely free to expand. Practically, the fully constrained model represents areas of the plate that are near solid portions of the plate or points of restraint. Since the plate is basically constrained in the steam generator by the six channels and wedges, this model is probably also representative of the middle region of the half-plate away from free boundaries. The compromise with reality in this latter representation has not been determined. The expansion boundary condition model provides a realistic representation of behavior perpendicular to free surfaces such as flow slots and the outside boundary away from attachments and solid areas.

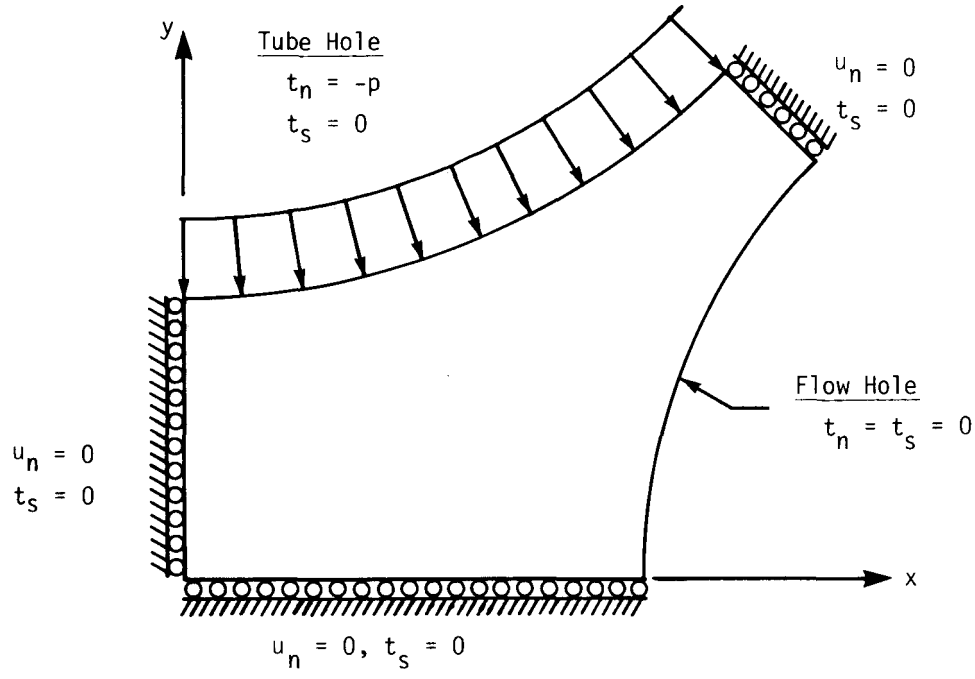

a) Fully Constrained Boundary Conditions

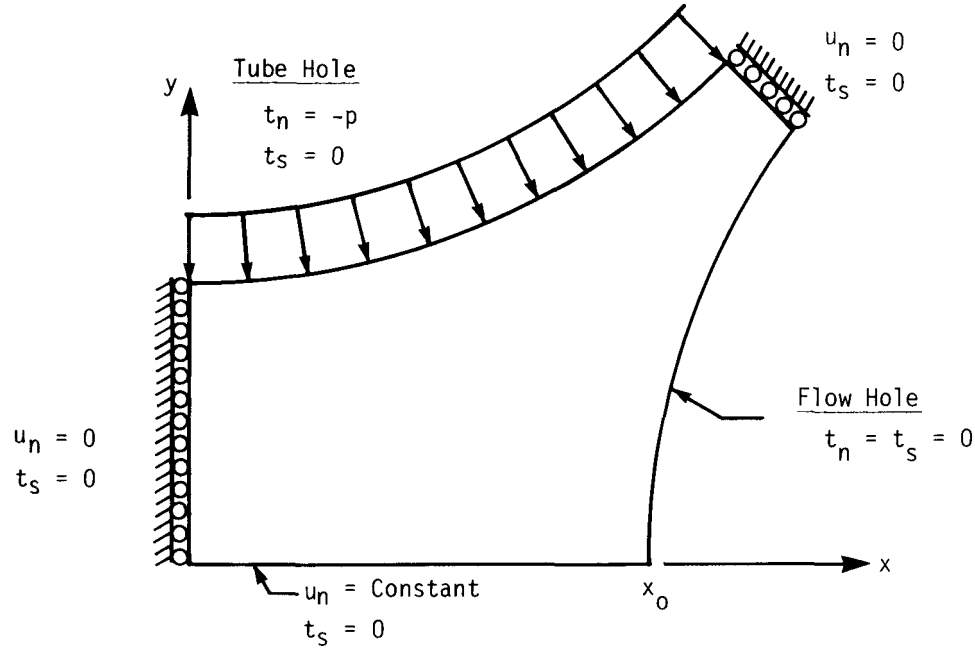

b) Expansion Boundary Conditions

Figure 3.8 - Plate Ligament Boundary Conditions.

3.5 Numerical Results

3.5.1 Elastic Results at Initial Yield

The von Mises equivalent stress contours, $\bar{\sigma}$, at initial plate yield for the fully constrained ligament are shown in Fig. 3.9. Initial yielding occurs at the flow hole surface at y = 0 when the internal tube hole pressure is 6250 psi. The corresponding tube dent depth for this pressure applied axisymmetrically to a tube was determined in Section 2.0 to be 24 mils from Fig. 2.14. This result shows that significant tube dents are required to cause plate yielding in highly constrained regions of the support plate as near rigid supports. The element displacement plot at initial yield pressure is shown in Fig. 3.10.

When the plate expansion boundary conditions are applied, the resulting variation of von Mises stress is computed to be as shown in Fig. 3.11. The point of initial yield is again on the flow hole side but occurring at the minimum ligament thickness region. The pressure to cause initial yield in the expansion case is 2550 psi which is 41% of the initial yield pressure for the fully constrained model. This result is in reasonable agreement with the lower bound analytical result of 3400 psi given by Eq. (3.3), and this pressure represents a tube dent depth of only 0.62 mils. At this pressure level, the tube is still elastic. This shows that support plate yielding occurs for very shallow tube dents in unconstrained regions of the support plate such as near flow slots. The resulting displaced element plot for the expansion case is shown in Fig. 3.12.

A comparison of the hoop stress $\sigma_{\theta\theta}$ which is nondimensionalized to the yield strength σ_y = 23 ksi as a function of the distance across the minimum ligament section, z/t, for the two boundary cases is given in Fig. 3.13. Also shown in Fig. 3.11 is the ratio of hoop strain to yield strain ($\sigma_{\theta\theta}/\varepsilon_y$). From this comparison, $\sigma_{\theta\theta}$ for the constrained case is almost a pure bending stress field, whereas, in the expansion case, the ligament sustains a positive tensile stress due to the relaxed conditions on the normal displacements on the boundary y = 0 as compared to the fully constrained case which allows the ligament to stretch.

The radial deflection of the tube hole is shown in Fig. 3.14. The radial deflection at the minimum ligament section ($\theta = 45^{o}$) is greatest for the constrained model for the initial yield pressures indicated. A similar deflection plot for the flow hole surface is given in Fig. 3.15.

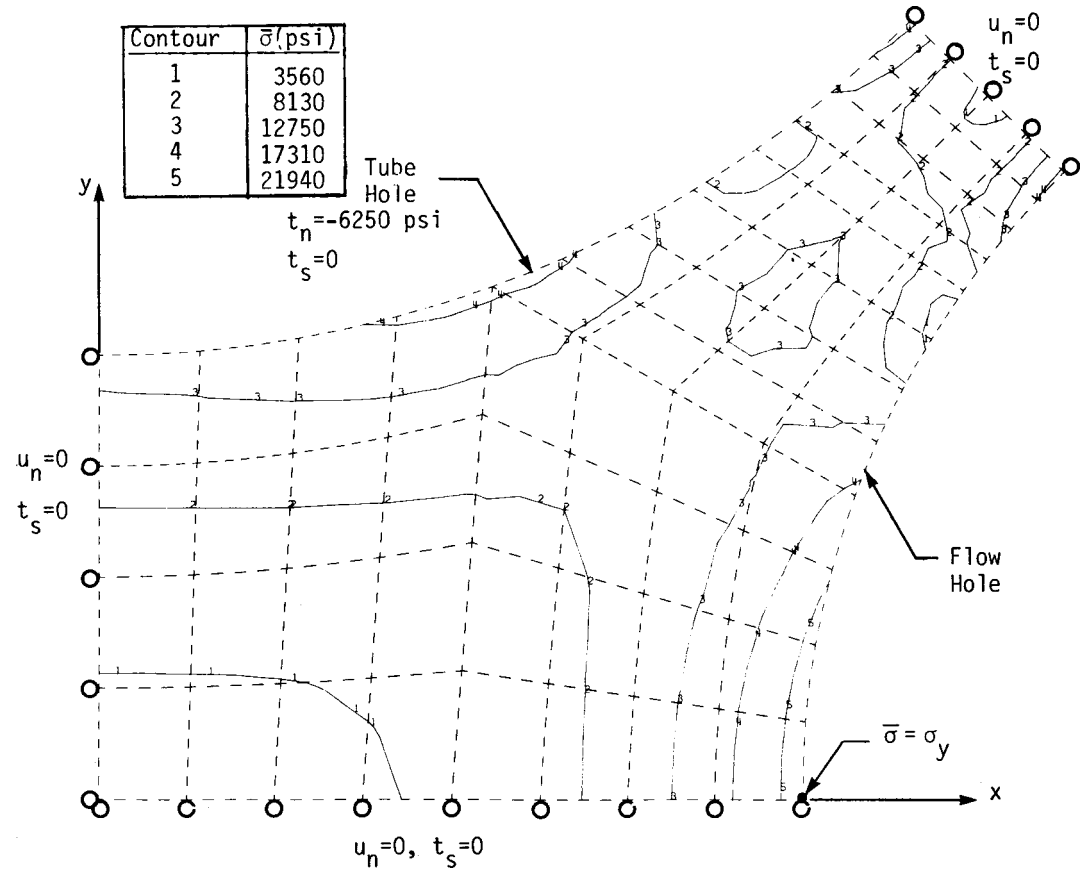

Figure 3.9 - Equivalent von Mises' Stress Contour at Initial Yield for Fully Constrained Case.

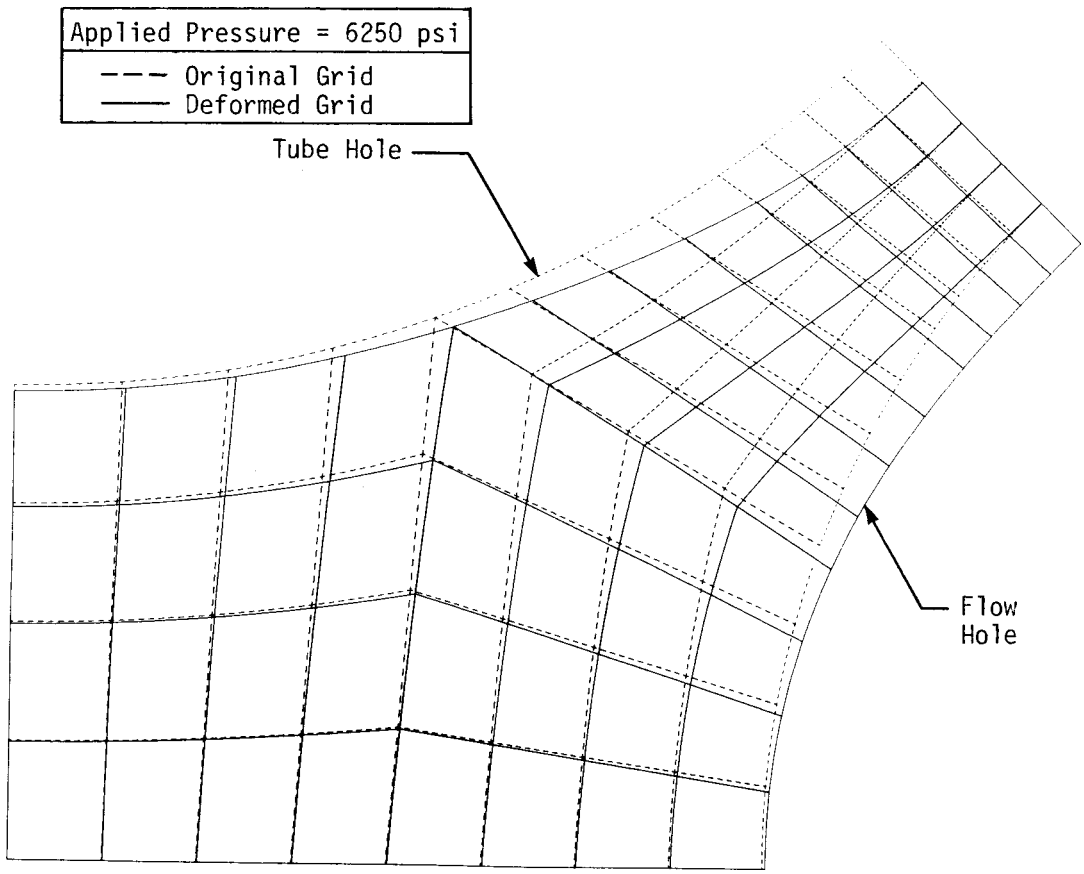

Figure 3.10 - Displacement Plot at Initial Yield for Fully Constrained Case. (Stress contours of Fig. 3.9 apply).

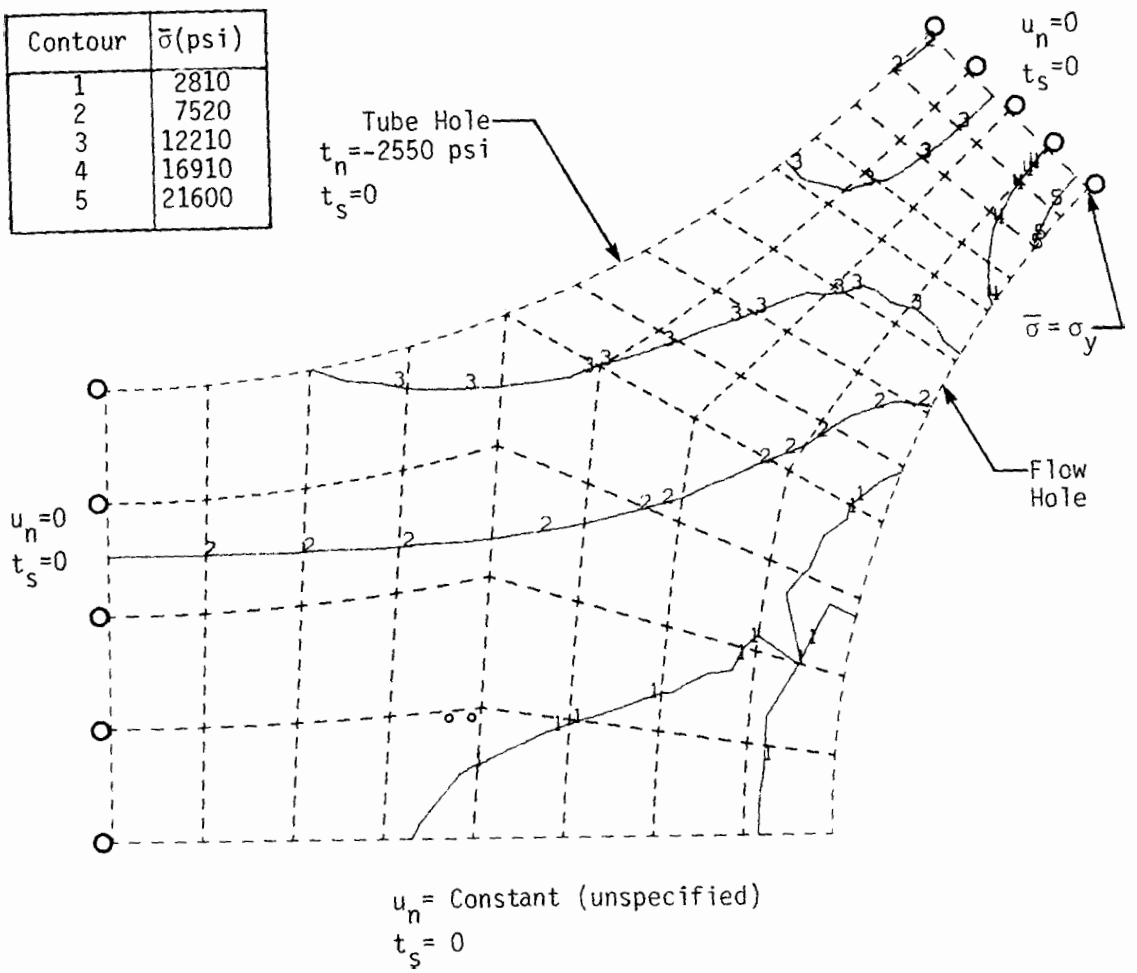

Figure 3.11 - Equivalent Von Mises' Stress Contours at Initial Yield for the Plate Expansion Case.

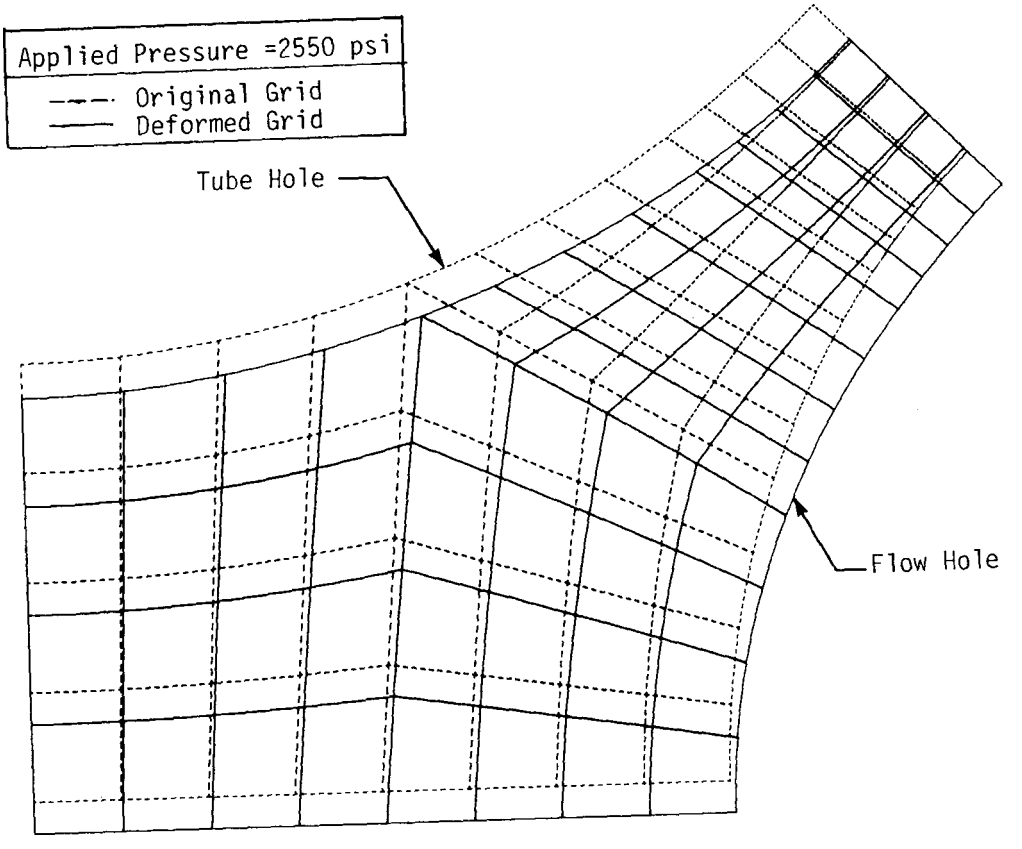

Figure 3.12 - Displacement Plot at Initial Yield for Plate Expansion Case. (Stress contours of Fig. 3.11 apply).

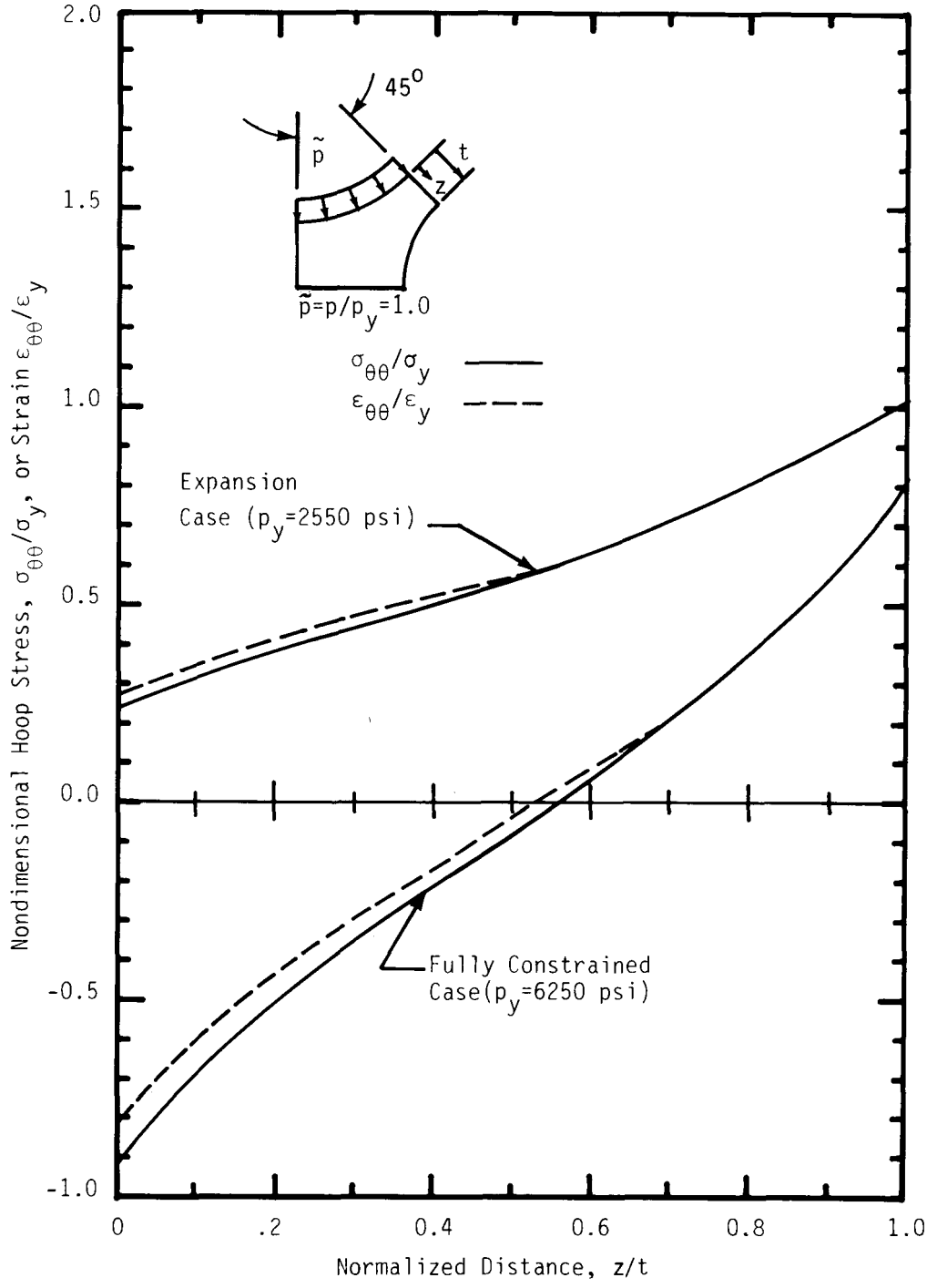

Figure 3.13 - Nondimensional Hoop Stress and Strain Versus Distance Across the Minimum Ligament Section for p/p_y=1.0 (Initial Yield).

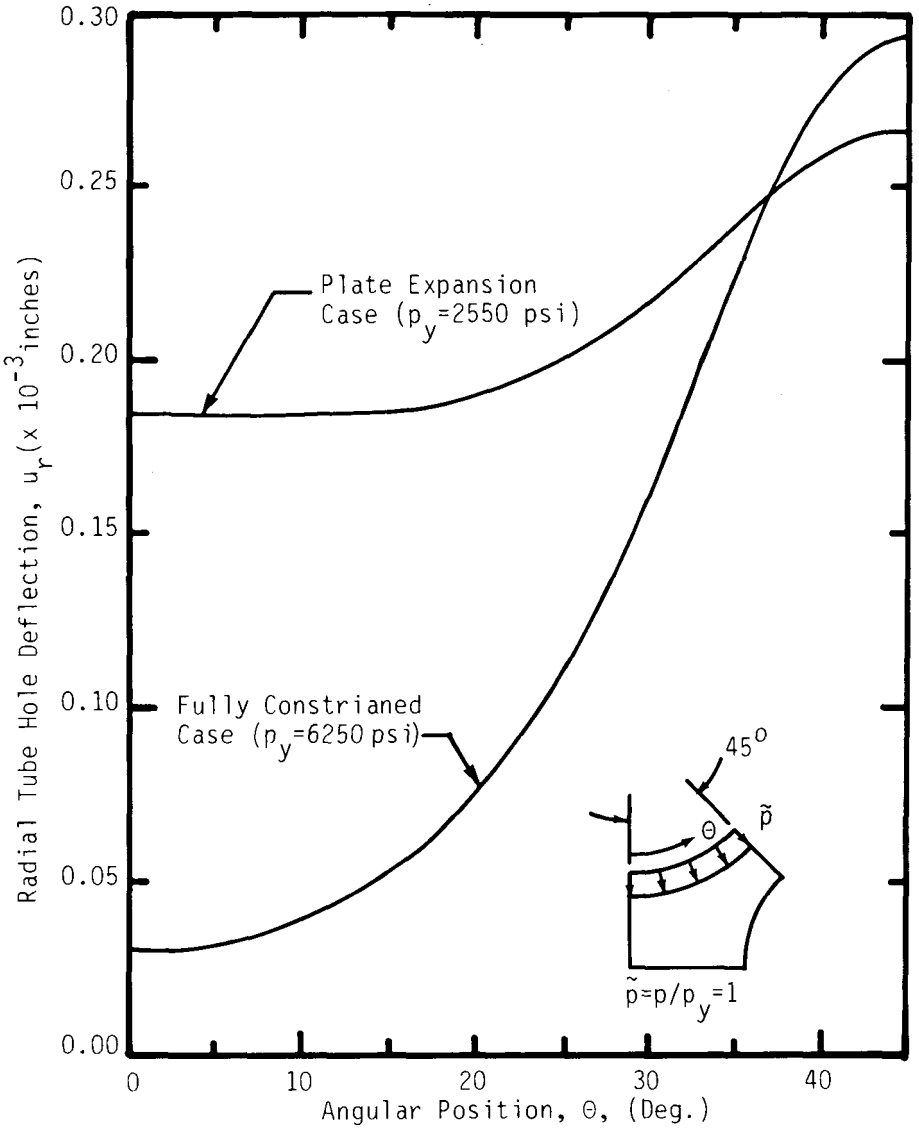

Figure 3.14 - Radial Deflection of the Tube Hole Surface as a Function of Angular Position at Initial Yield (p/p_y=1).

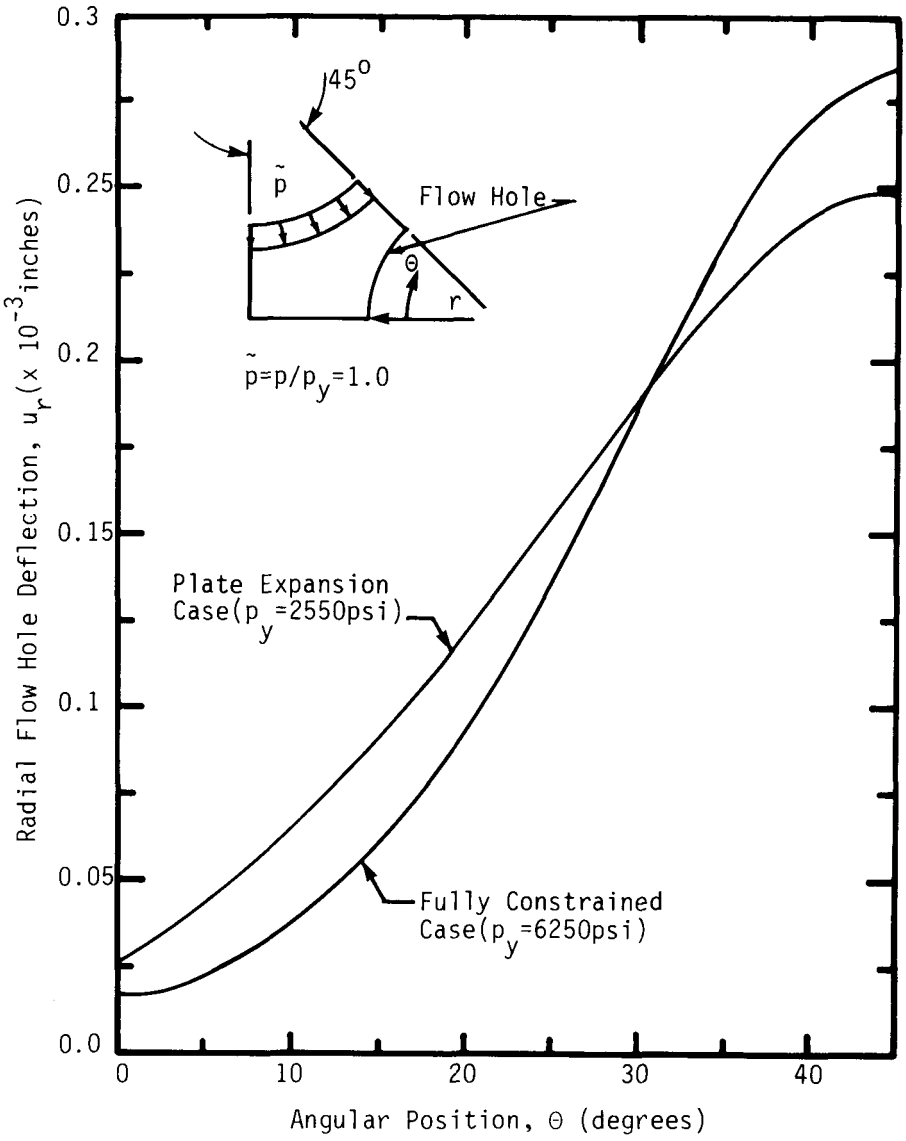

Figure 3.15 - Radial Flow Hole Deflection as a Function of Angular Position Around the Hole for $p/p_y=1.0$ (Initial Yield).

3.5.2 Elastic-Plastic Results

In the elastic-plastic analysis, the internal tube hole pressure was increased in monotonic increments, with maximum incremental pressures of 0.1 p_y for the respective models. The resulting hoop stress across the minimum ligament section for values of p equal to 1.5, 2, and 3 times the initial yield pressure is shown in Fig. 3.16. The corresponding hoop strain for p/p_y = 2 and 3 is given in Fig. 3.17.

The plastic zones within the ligament for p/p_y equal to 1.5, 2 and 3 are shown in Fig. 3.18 for the fully constrained case and Fig. 3.19 for the plate expansion case. The unshaded portions are the elastic regions, whereas, the shaded areas are the regions that are being plastically loaded. The cross-hatched area in Fig. 3.18 for p/p_y = 3 is a local region which is unloading elastically. The pressure at which the minimum ligament section ($\theta = 45^o$) is fully plastic is 16,200 psi for the fully constrained case and only 5620 psi for the expansion case. Based on these model results, the ligaments near the free boundaries of the plate would be fully plastic across the minimum sections (at 5620 psi) before the ligaments in constrained regions experience initial yielding (at 6250 psi). From Fig. 2.15, it is evident that the entire plate ligament yields near free boundaries for small dent depths, but in constrained regions large tube deformations are expected to precede yielding of the entire ligament.

The maximum tensile hoop stress and strain at the minimum ligament section as a function of tube hole pressure or tube dent depth is given in Fig. 3.20. The tube dent depth is based on the results from Section 2.6.1 for the axisymmetric tube model. For the fully constrained conditions, the minimum ligament section ($\theta = 45^o$) may never become fully plastic because the tube would experience large deformation first. A dent of only 9.5 mils is required for a fully plastic ligament for the expansion conditions. The foregoing observations are summarized in Table 3.1.

The radial deflection of the tube hole for the fully constrained conditions is shown in Fig. 3.21. The computed deformations indicate the change in the shape of the hole is square-like with the length at each side approximately equal to the original diameter of the tube hole. A similar plot for the expansion model (Fig. 3.22) indicates the same square-like shape except that the hole diameter is also dilating. A comparision of the maximum radial deflection for each model, which occurs at the minimum ligament thickness ($\theta = 45^o$), is given in Fig. 3.23.

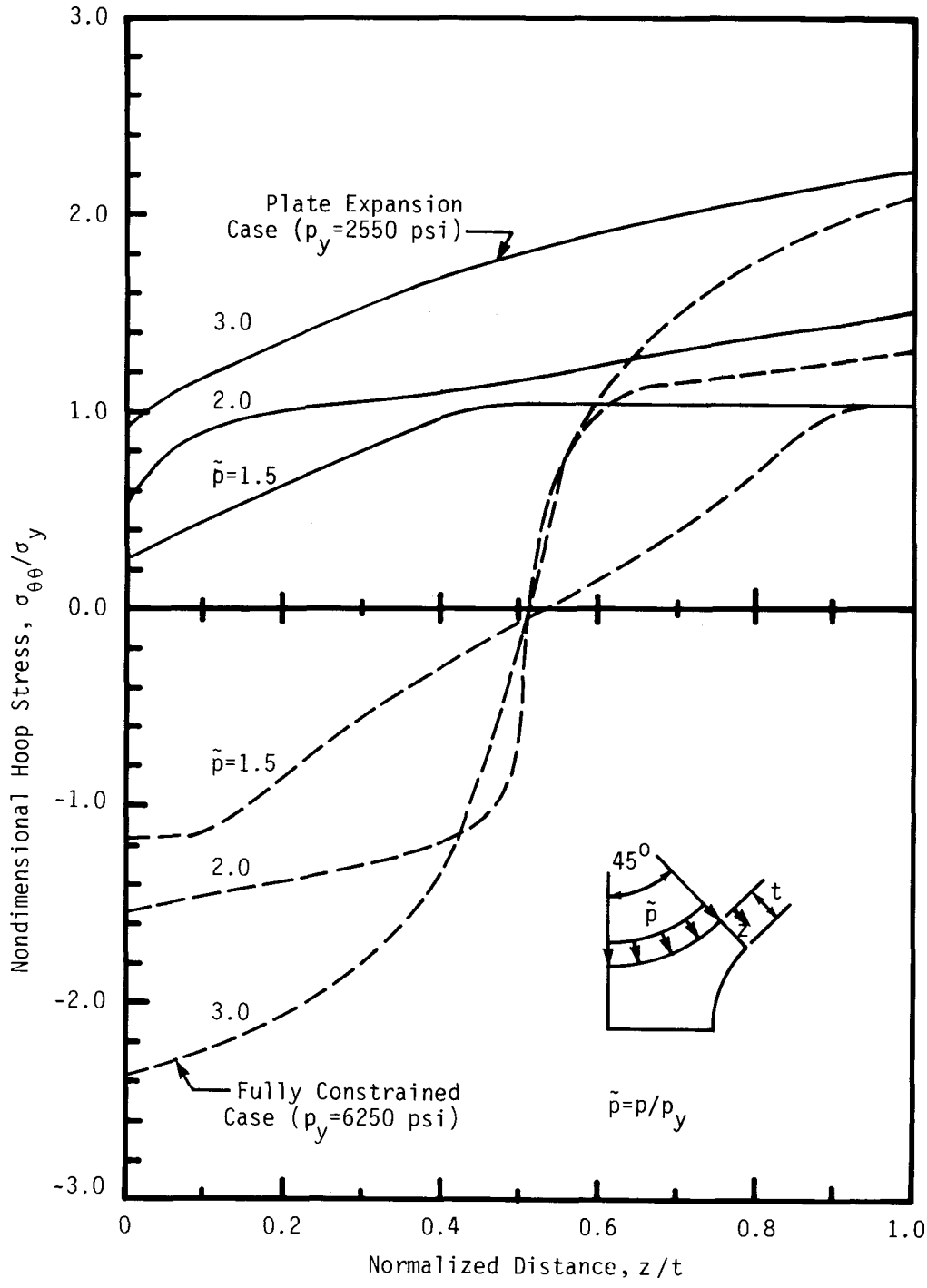

Figure 3.16 - Nondimensional Hoop Stress Versus Distance Across Minimum Ligament Section (p/p_y = 1.5, 2.0, 3.0).

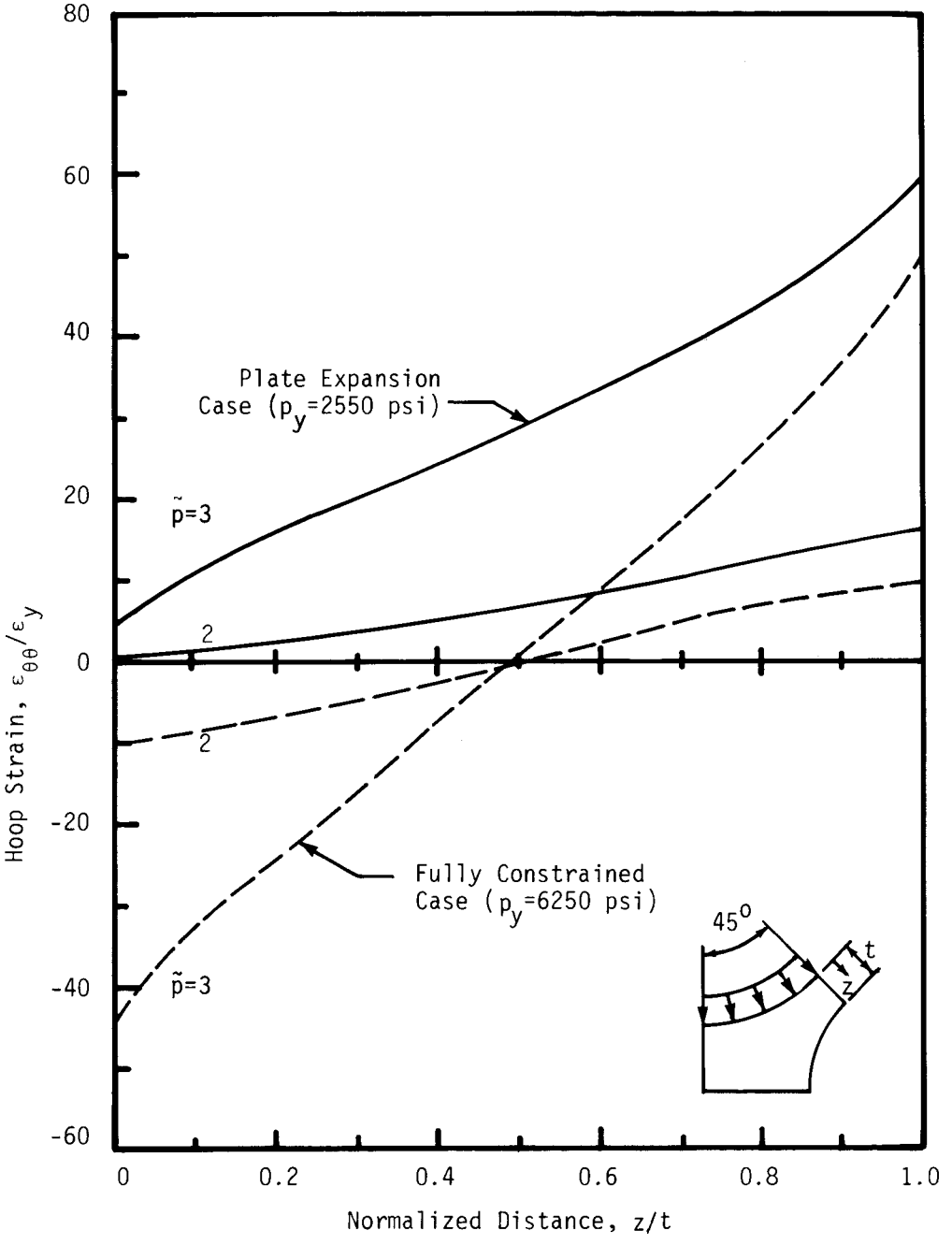

Figure 3.17 - Ligament Hoop Strain Versus Distance Across Minimum Ligament Section for p/p_y = 2.3.

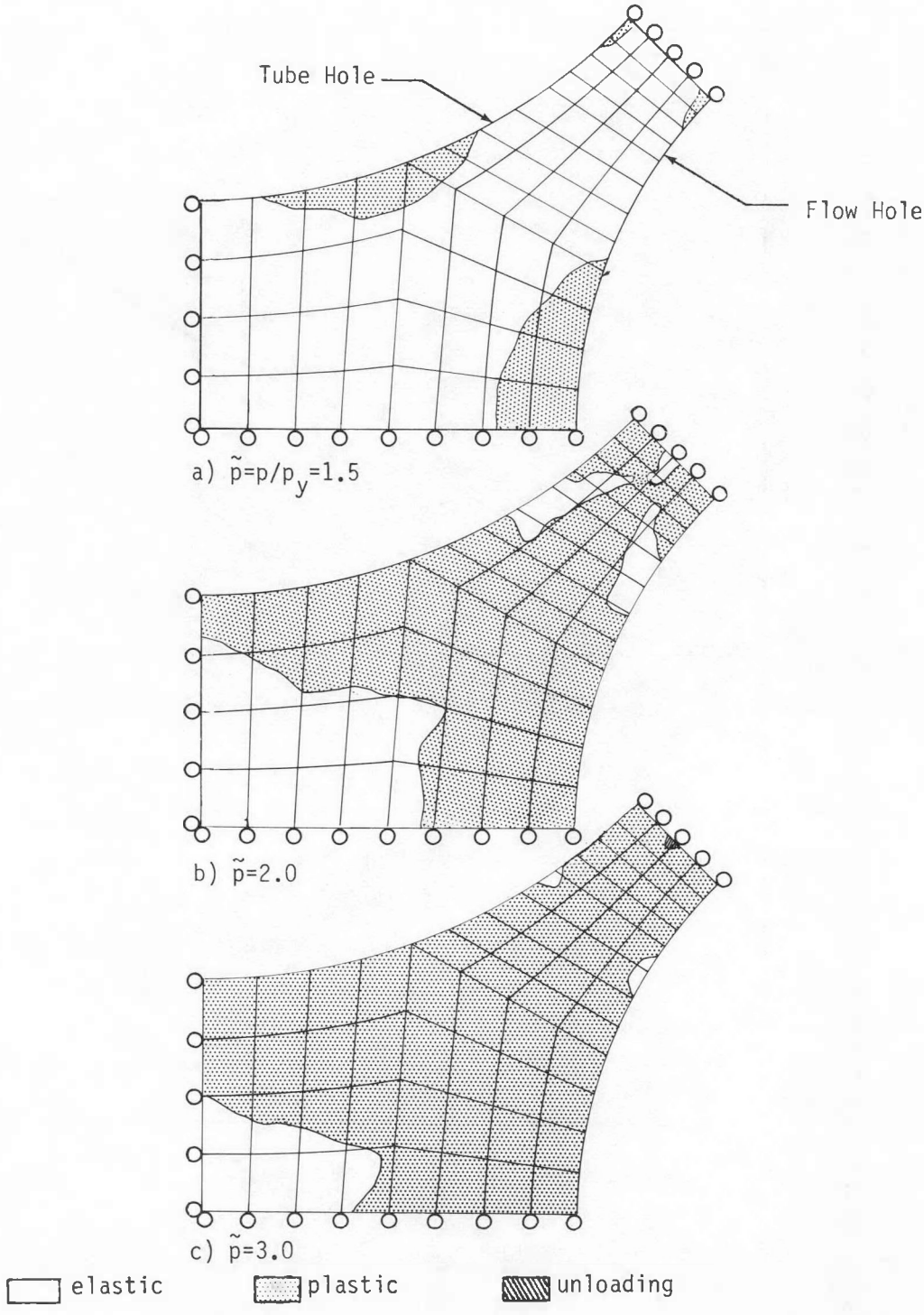

Figure 3.18 - Plastic Zone Shape and Growth as a Function of Applied Pressure For the Fully Constrained Conditions.

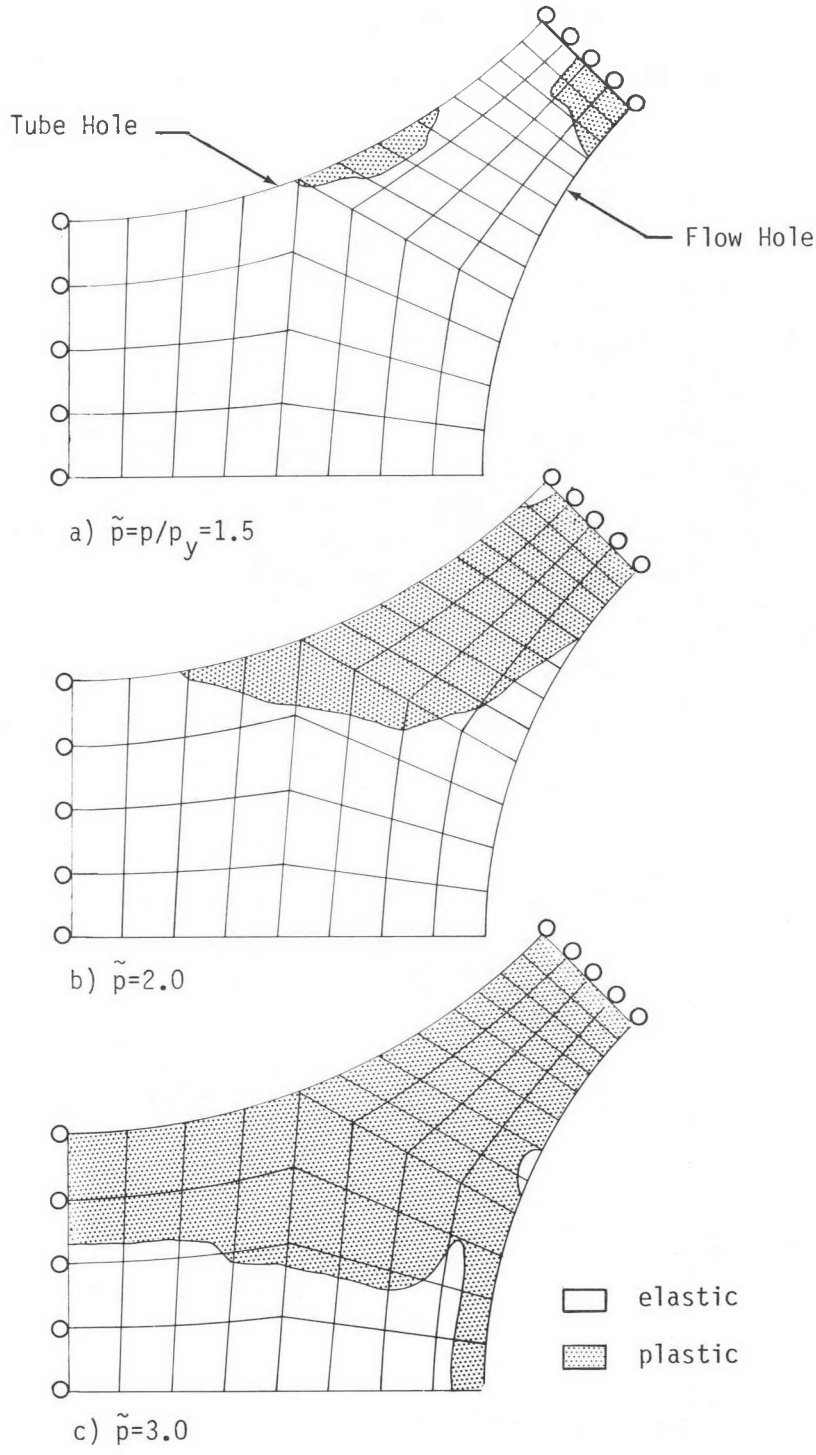

Figure 3.19- Plastic Zone Shape and Growth as a Function of Applied Pressure for Expansion Conditions.

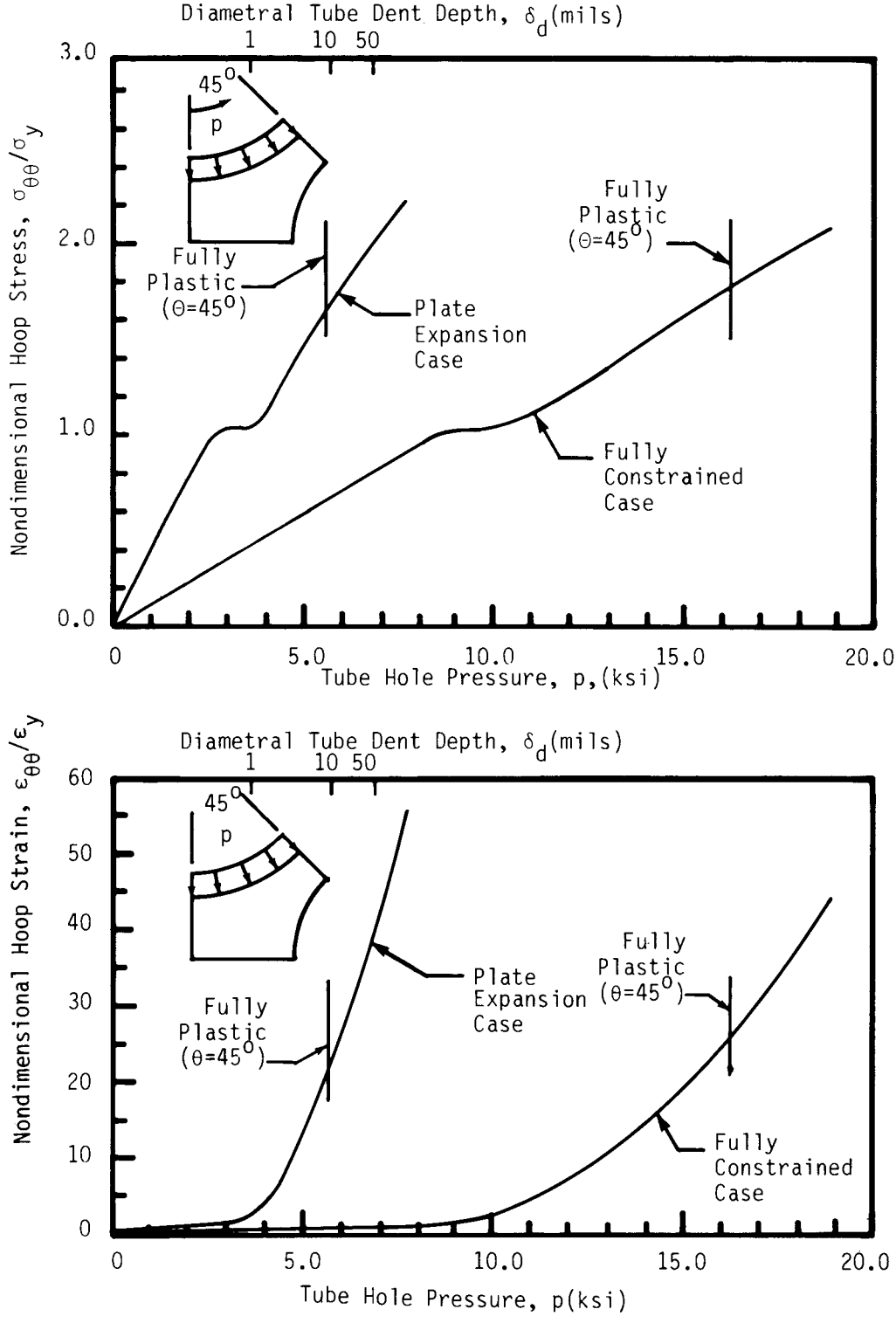

Figure 3.20 - Maximum Hoop Stress and Strain at the Minimum Ligament Section as a Function of Tube Hole Pressure or Tube Dent Depth.

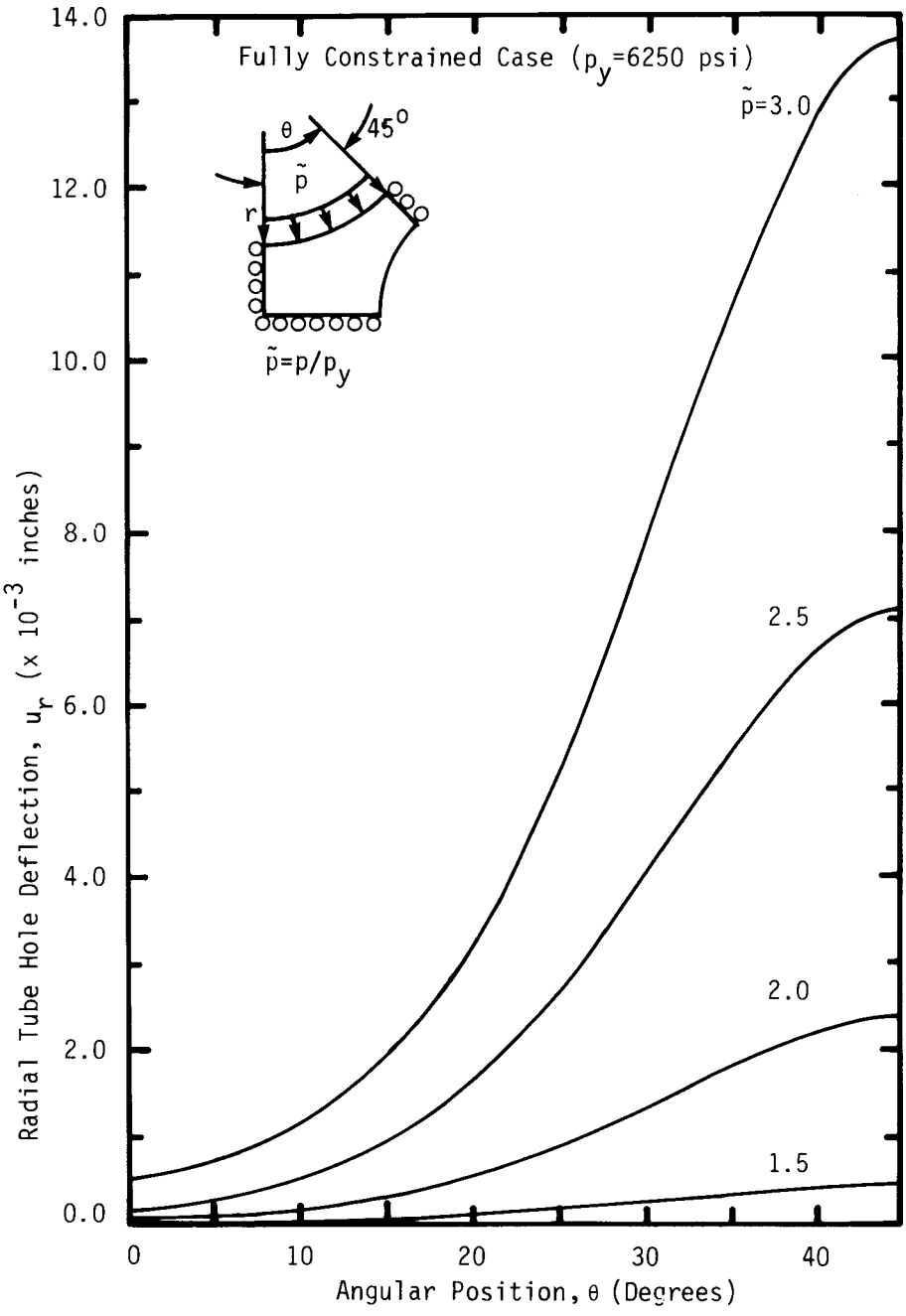

Fig. 3.21 - Elastic-Plastic Radial Tube Hole Deflection As a Function of Angular Position for the Fully Constrained Conditions.

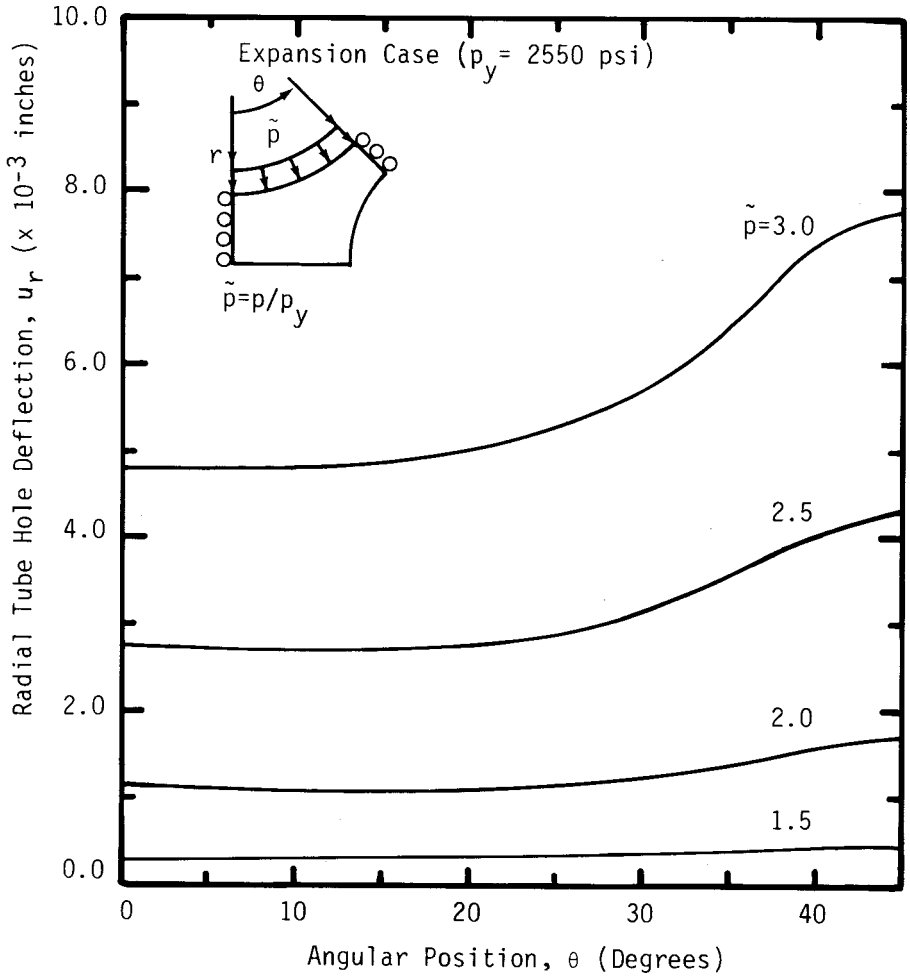

Figure 3.22 - Elastic-Plastic Radial Tube Hole Deflection as a Function of Angular Position for the Plate Expansion Conditions.

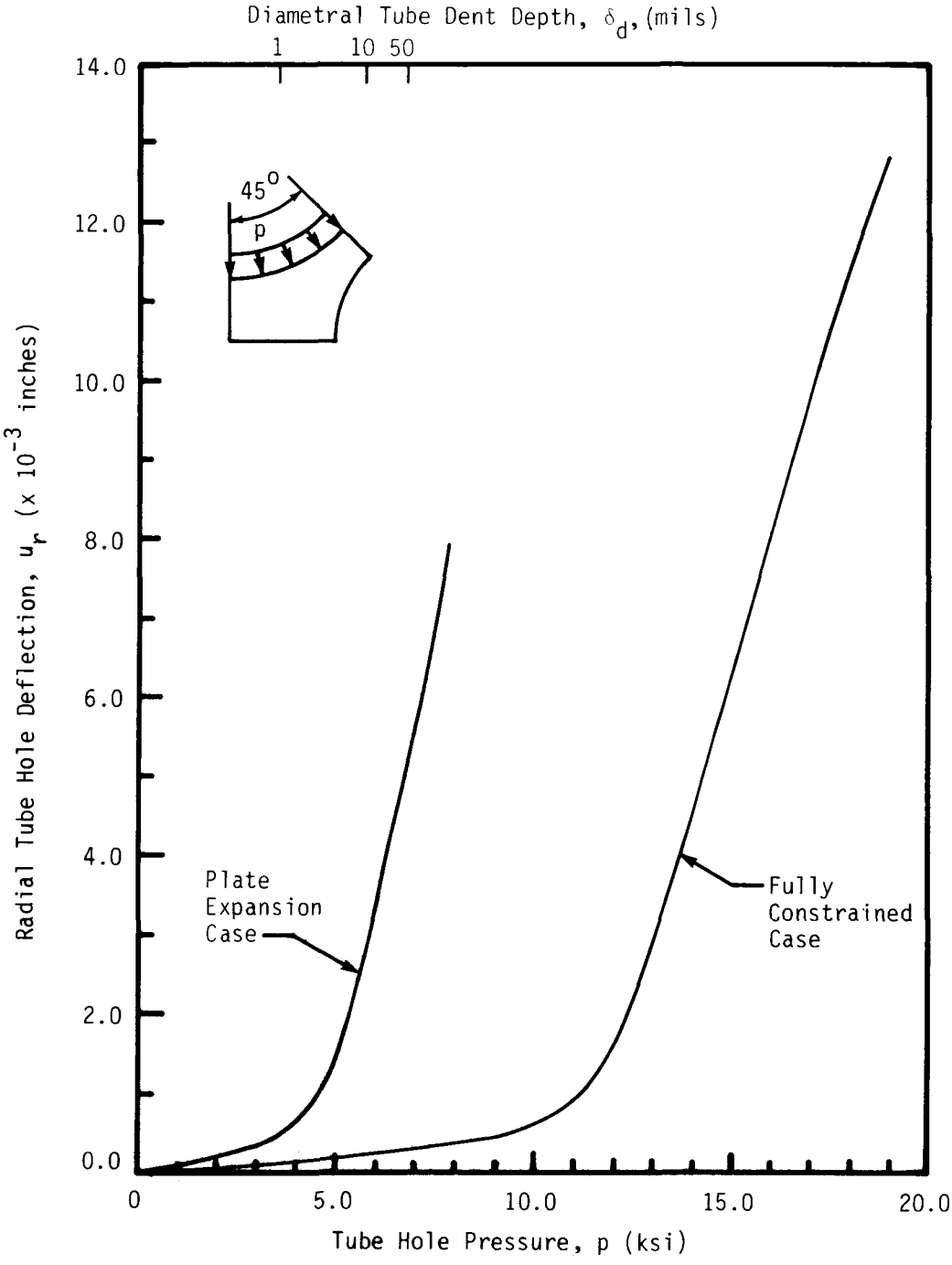

Fig. 3.23 - Maximum Tube Hole Radial Deflection as a Function of Tube Hole Pressure or Tube Dent Depth.

TABLE 3.1

SUMMARY OF RELATIONSHIP BETWEEN SUPPORT PLATE YIELDING AND TUBE DENT DEPTH

SUPPORT PLATE REGION	TUBE DIAMETRAL DENT DEPTHS (mils)	
	At Initial Yield of Support Plate Ligament	At Complete Yield of Minimum Ligament Section
Near Free Boundaries	0.62	9.5
Constrained Regions	24	Large Tube Deformation

3.5.3 Approximate Elastic-Plastic Extrapolation for Quarter Symmetry

Some interesting results regarding tube hole deformation can be obtained by combining the analysis of the fully constrained model with the expansion case. Model geometries of the two cases are combined to form a one-quarter ligament where the solution for u_r for $0^o < \theta < 45^o$ is determined from the expansion model behavior, and u_r for $45^o < \theta < 90^o$ is formulated from the fully constrained results. Physically, the resulting model applies to any position in the support plate where expansion can occur in one direction, but the plate is constrained in the orthogonal direction. This is approximately true near flow slots.

To solve this quarter model exactly, compatibility in $u_r(r)$ between the models at $\theta = 45^o$ for all values of r would have to be satisfied. Since $\theta = 45^o$ is no longer a line of symmetry, the quarter model cannot be exactly determined from the one-eighth models. What is attempted herein is to present an approximate analysis where only compatibility in u_r at the tube hole surface ($r = 0.45"$, $\theta = 45^o$) is enforced in order that some additional insight into tube hole and tube deformations can be obtained. The motivation for this work will be demonstrated next in that the "peanut" shape tube denting observed in the field is strongly suggested for these approximate quarter model results.

With compatibility in u_r at the hole surface at $\theta = 45^o$, the elastic radial tube hole deflection result is as shown in Fig. 3.23. Figure 3.24(b) is a 360^o polar representation of the elastic deformation. The "peanut" shape of tube is suggested from the plate model results in that a change in curvature is observed at the $\theta = \pi n/2$ quarter points. Tube local denting is further suggested in the approximate elastic-plastic results shown in Fig. 3.25. It is important to note that in satisfying compatibility at one point, in general, a discontinuous applied pressure ($\tilde{p}_1$ vs. $\tilde{p}_2$) exists at $\theta = 45^o$. A plot of $\tilde{p}_2/\tilde{p}_1$ versus $\tilde{p}_1$ is given in Fig. 3.26 where it is shown that the average ratio between $\tilde{p}_2$ and $\tilde{p}_1$ is about 2.2.

3.6 Summary of Results

1) An elastic-plastic finite element analysis for two different conditions was conducted which models regions both near rigid supports and free boundaries (fully constrained case and plate expansion case, respectively).

2) Both models were analyzed to a stress level of approximately 2.2 times the yield stress or to approximately 5% total strain.

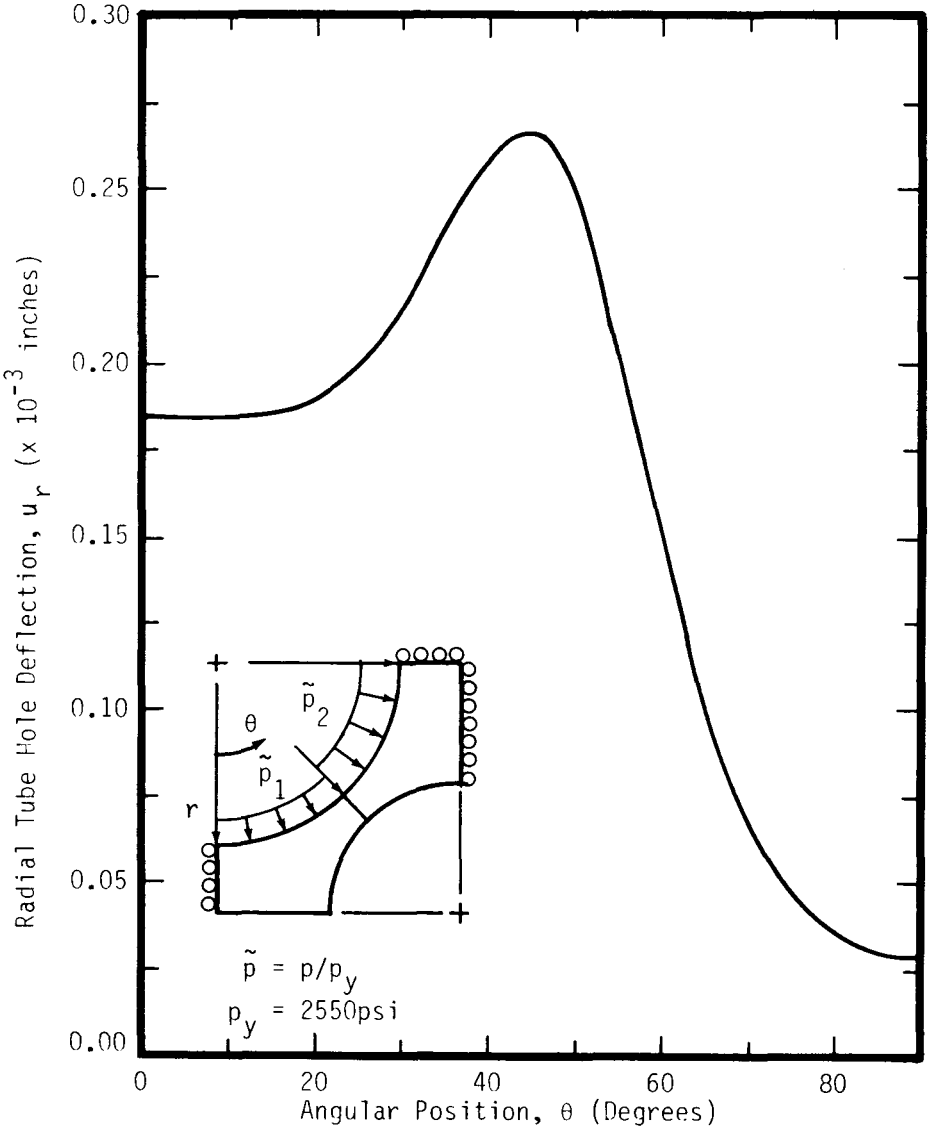

Figure 3.24a - Approximate Radial Tube Hole Deflection for One-Quarter Ligament Representation as a Function of Angular Position at Initial Yield ($\tilde{p}_1 = 1$).

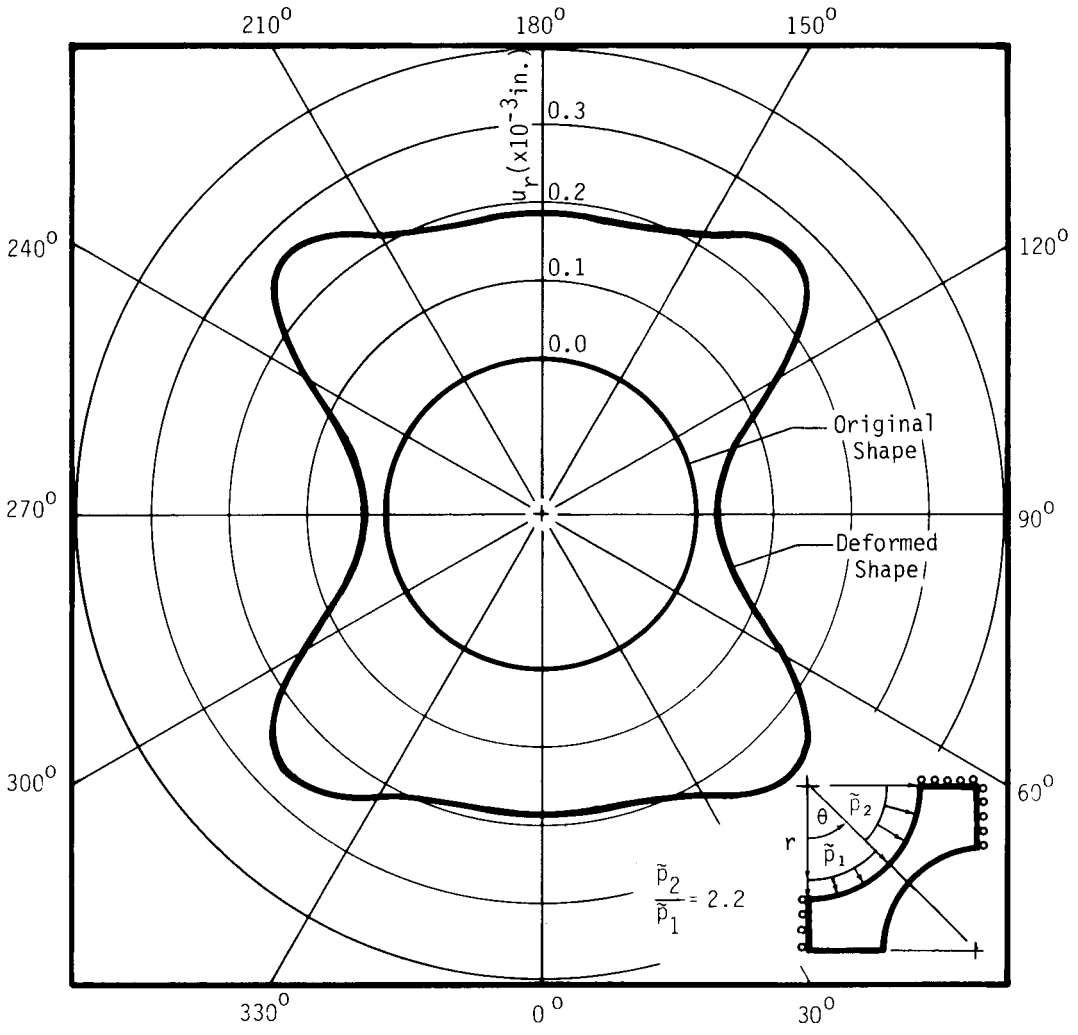

Figure 3.24b - Polar Representation.

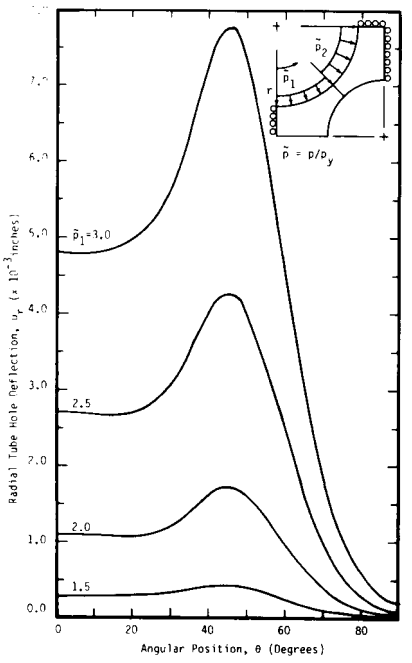

a) Radial Displacement Results

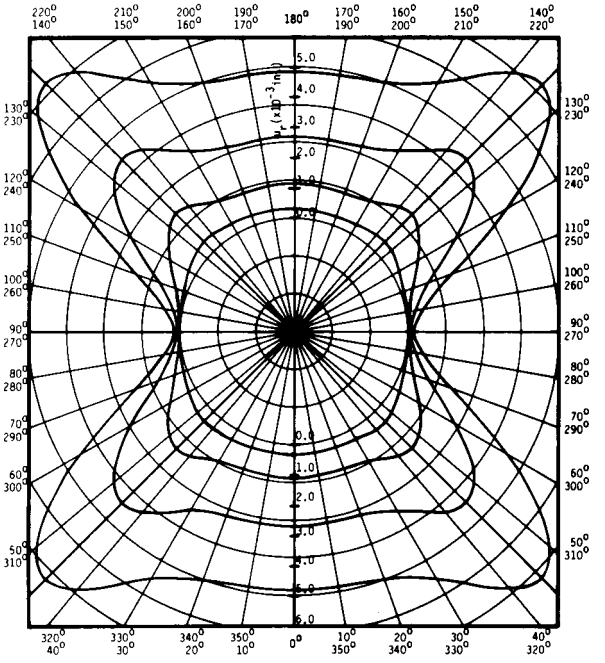

b) Polar Representation

Figure 3.25 - Approximate Elastic-Plastic Tube Hole Deflections for a One-Quarter Ligament Representation as a Function of Angular Position.

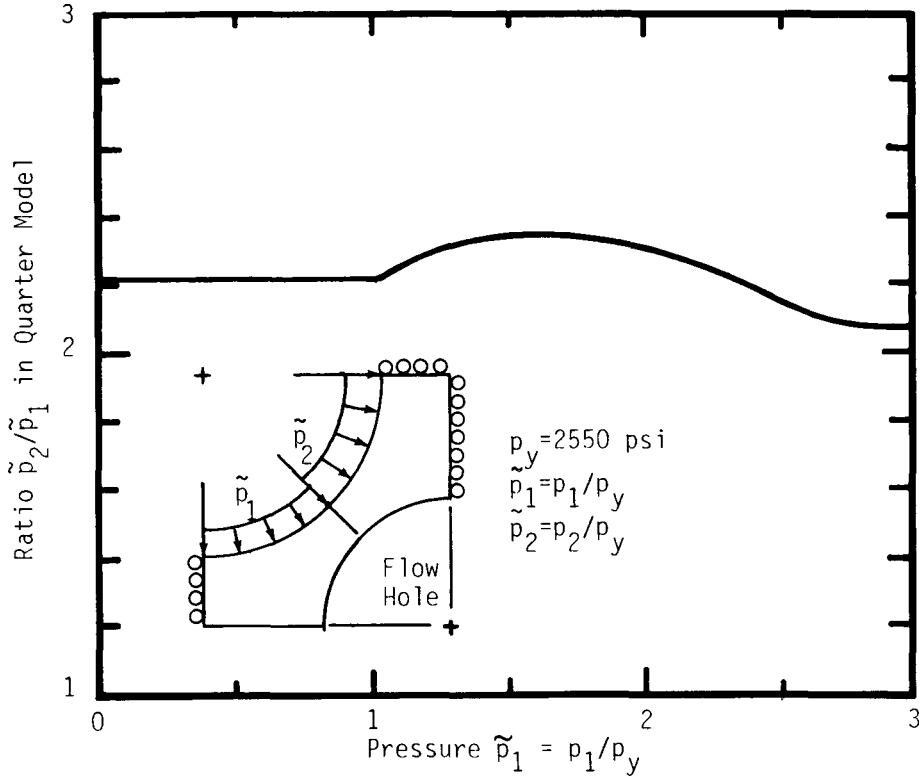

Figure 3.26 - Ratio $\tilde{p}_2/\tilde{p}_1$ Versus $\tilde{p}_1$, in Approximate Quarter Model Analysis.

3) The results for initial yield condition indicate first yielding in the plate occurs in the ligaments near the free boundaries (i.e., flow slots or plate O.D.) at a small tube dent dpeth of only 0.62 mils while the tube is still elastic. Larger tube dents in the plastic range are necessary for yielding to initiate near rigid supports.

4) Tube dent depths of about 10 mils are required to cause fully plastic plate ligaments near flow slots and free boundaries. Tubes experience large deformations before ligaments become fully plastic in constrained regions.

5) Approximate analysis, based on combining results of two one-eighth symmetry models to give a one-quarter deformation pattern for the tube holes near flow slots, strongly suggest the "peanut" shape tube deformations similar to those observed in the field.

REFERENCES

3.1 DiSalvo, G. J. and J. A. Swanson, "ANSYS: Engineering Analysis System User's Manual," Second Edition (March 1, 1975).

3.2 MARC-CDC, Nonlinear Finite Element Analysis Program, Version G (1975).

3.3 Data supplied by Westinghouse; letter dated May 6, 1977.

3.4 ASME Boiler and Pressure Vessel Code, Section III, Subsection NA, 1977 Edition.

3.5 Hill, R., Mathematical Theory of Plasticity, Oxford Press (1950).

4.0 COMBINED PLATE/TUBE/OXIDE MODEL

4.1 Introduction

The plate analysis described in this Section extends the plate ligament models presented in Section 3.0 to include the tube and the oxide which forms in the annulus between the tube and support plate. The combined plate/tube/oxide model was solved only for the elastic case for the plate expansion boundary conditions described in Section 3.4.2. These results are presented and compared to the elastic results for the uniform pressure model given in Section 3.5.1 for the same set of boundary conditions.

The objectives of the model are the same as those discussed for the uniform pressure case; however, this combined model provides two important improvements. First, with the tube also contained in the model, a direct correlation between dent depth and stresses and strains in the tube and plate can be obtained through one model. Second, the effect of a growing oxide was included in the model. The oxide growth is analytically achieved by applying an isothermal radial expansion of the oxide annulus between the tube and plate. The result will be a compatible set of interface conditions between the tube, plate, and oxide involving the normal displacements and tractions which will be computed internally based on the relative local stiffness of the model rather than some assumed distribution as was done in Section 3.0. Plate material wastage due to the corrosion process was again not considered in the model so that the model would be progressively less representative of the actual performance as denting increases. Additional details regarding the combined model are discussed next.

4.2 Combined Finite Element Representation

The mathematical model discussed in this Section is a finite element representation which combines the plate ligament with the tube and the oxide. This combined plate/oxide/tube finite element model is shown in Fig. 4.1. The finite elements are the same eight-noded curved isoparametric quadrilaterals used for the uniform pressure model, and the element behavior is as described in Section 3.4. The model is a plane stress model; however, the height (z axis) of the tube element

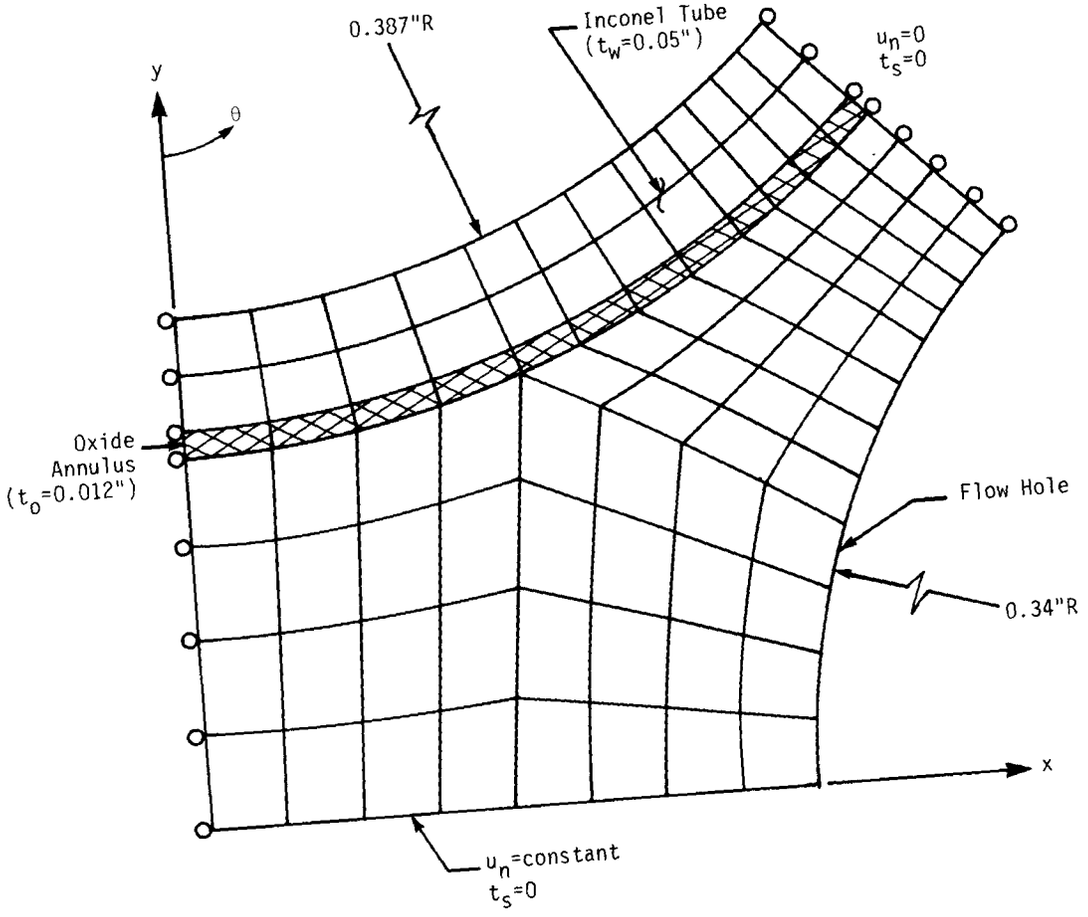

Figure 4.1 - Finite Element Model and Expansion Boundary Conditions for the Plate Ligament/Oxide/Tube Geometry.

was made 33% greater than the plate thickness to approximate the three-dimensional stiffness effects of the long tube. This height approximation was based on the elastic-plastic tube results for the axisymmetric uniform pressure case presented in Section 2.7.

The plate material behavior is the same as the uniform pressure model which is given in Fig. 3.3. The tube material is Inconel 600 (see Section 2.3), and the elastic properties at $600^{o}F$ are elastic moduls, $E = 29.2 \times 10^{6}$psi, Poisson's ratio $\nu = 0.3$, and yield strength $\sigma_y = 41$ ksi. The oxide material is assumed to initially fill the gap between tube and plate and to be bonded to both the plate and the tube. This assumption is justified as long as the oxide remains only in compression as it did in this elastic analysis. As mentioned earlier, the oxide growth is simulated by a radial thermal expansion of the oxide annulus. This was accomplished by setting the coefficient of thermal expansion in the circumferential direction to be zero. A preliminary literature search for oxide properties produced only thermal expansion data (4.1) from which the coefficient of thermal expansion $\alpha = 0.6 \times 10^{-5}$ in/in/^{o}F. For the purpose of performing an initial elastic model checkout, the elastic properties for the oxide were assumed to be modulus of elasticity $E = 38.6 \times 10^{6}$ psi which is 1.5 times the plate modulus, and Poisson's ratio $\nu = 0.3$. The properties could have a significant effect on the results and should be quantified before any elastic-plastic analysis is conducted.

4.3 Numerical Results

4.3.1 Plate Ligament Results

The von Mises equivalent stress contours at initial yield for the plate expansion boundary conditions are shown in Fig. 4.2. Although the stress levels in the plate and tube are approximately at the same level at the minimum ligament section, the plate yields first since σ_y is only about half σ_y of the tube. The maximum tube dent depth at initial plate yield computed from this model is 0.56 mils. A displaced mesh plot showing the original geometry is given in Fig. 4.3.

A comparison of the hoop stress and strain for the combined model with that of the uniform pressure results from Fig. 3.12 at the minimum ligament section is shown in Fig. 4.4. Both models indicate initial yielding occurs at the flow hole side of the plate ligament at the minimum section ($z/t = 1$); however, the overall level of $\sigma_{\theta\theta}$ and $\varepsilon_{\theta\theta}$ is higher for the combined model indicating more direct

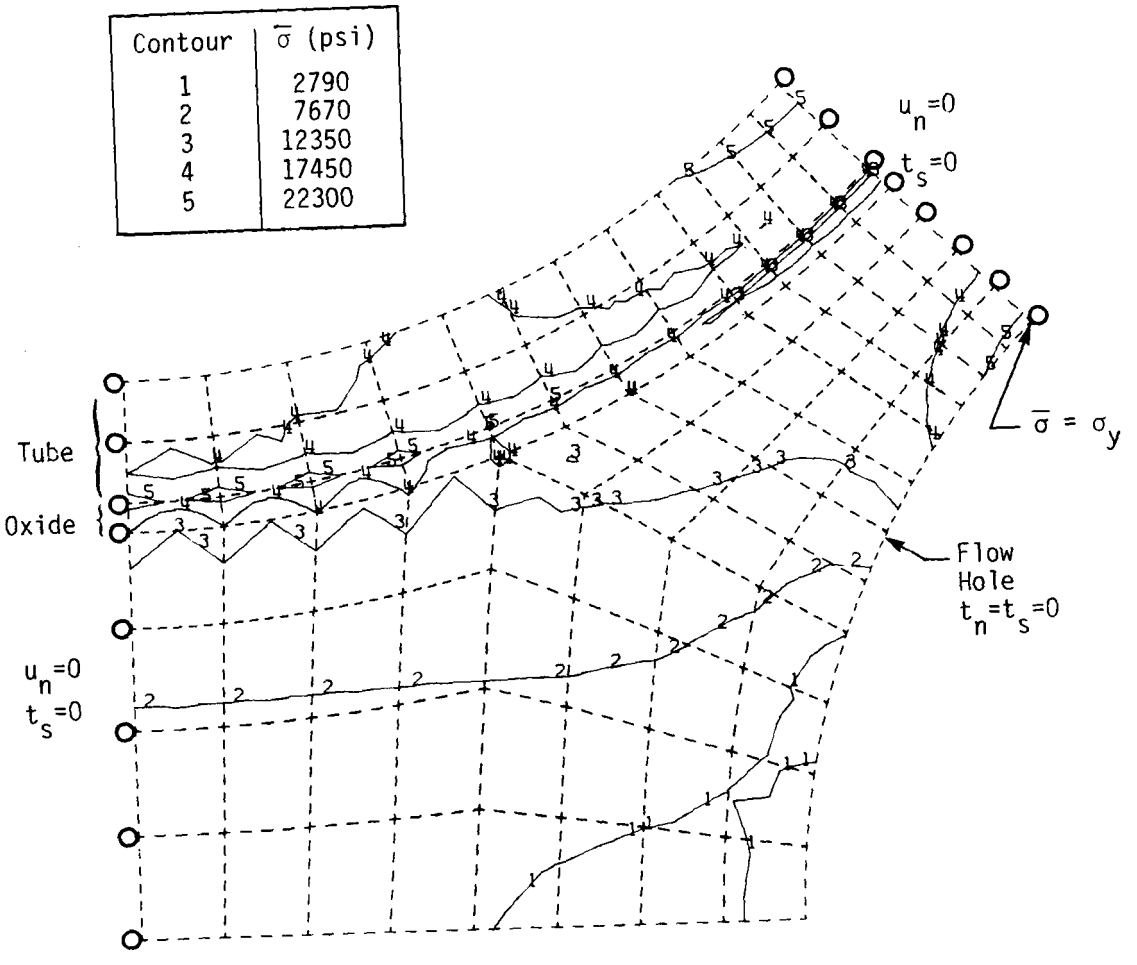

Figure 4.2 - Equivalent von Mises' Stress Contours at Initial Plate Yield for the Expansion Case.

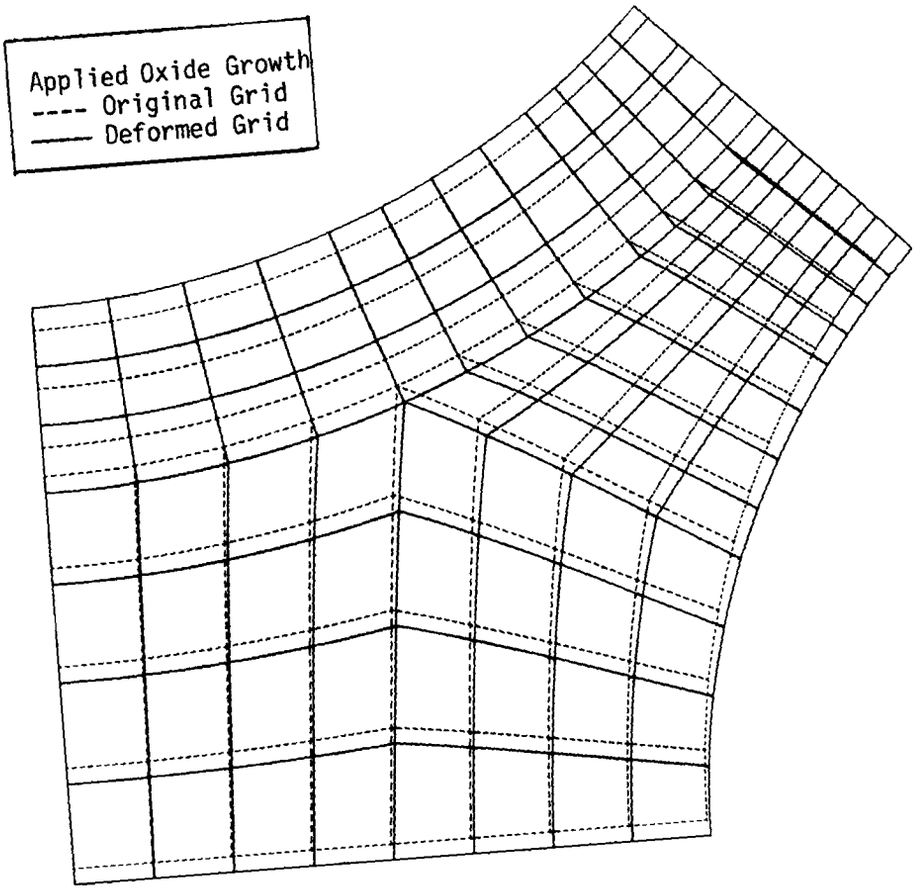

Figure 4.3 - Displacement Plot at Initial Yield for Expansion Conditions, (Stress Contours of Fig. 4.2 Apply).

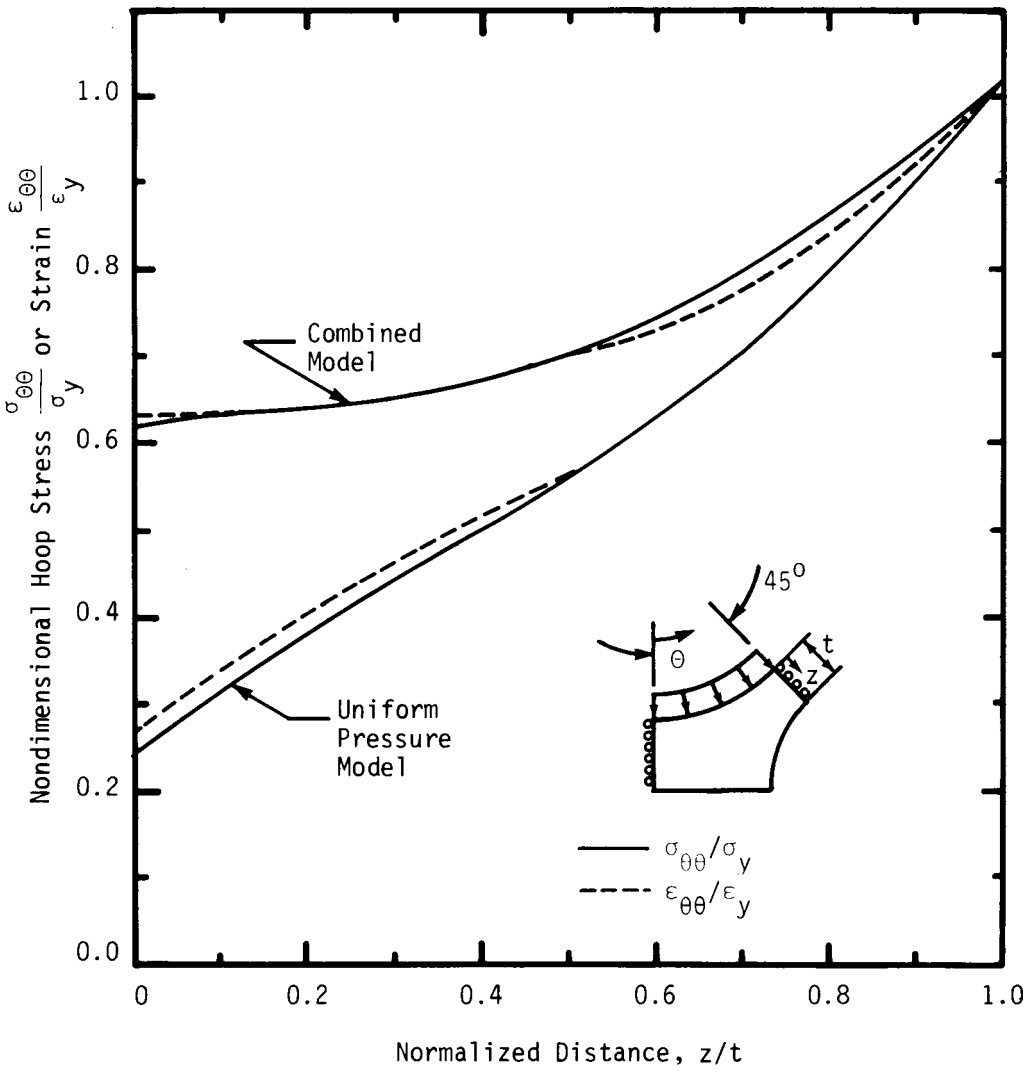

Figure 4.4 - Nondimensional Ligament Hoop Stress or Strain Versus Distance Across Minimum Ligament Section for $p/p_y=1$ (Initial Yield).

tension and less bending than predicted by the uniform pressure model. The radial pressure (Fig. 4.5) generated for initial yield by the oxide expansion varies significantly as a function of angular position and everywhere exceeds the uniform pressure case value. The radial pressure levels reach a maximum where the ligament is the thickest radially and approaches the uniform pressure case value at the minimum ligament section ($\theta = 45^{o}$). This is consistent with the fact that yielding occurs first at this section, and the stresses there should be most influenced by pressure applied directly to the ligament. For simple comparison, the radial stress in the tube near the O.D. is also shown in Fig. 4.5. These stress levels fall below the uniform pressure case. This indicates a significant radial stress gradient exists between the plate, oxide, and tube, which reveals a deficiency in the models of Sections 2.0 and 3.0. However, the magnitude of the radial stress gradient is dependent on the oxide elastic properties, which were estimated.

A comparison of the radial tube hole and flow hole deflections for both models is given in Figs. 4.6 and 4.7, respectively. In Fig. 4.6, the plate/tube/oxide model indicates larger radial tube hole displacements than the uniform pressure case; however, more variation in u_r is observed when the pressure is uniform. The flow hole displacement results presented in Fig. 4.7 show a similar behavior for u_r for both models with the combined model values being everywhere larger than the uniform pressure case.

4.3.2 Tube Results

The hoop stress and strain in the tube as a function of distance through the tube wall at initial plate yield is shown in Fig. 4.8 for three different angular positions. All values are compressive and nearly constant in magnitude except as θ approaches the minimum ligament section ($\theta = 43.8^{o}$) where some bending is observed. The variation in hoop stress and strain as a function of angular position for the inside and outside diameters of the tube is shown in Fig. 4.9. Since the O.D. surface of the tube is in contact with the oxide, some local variations in the hoop values are noted for θ between 15^{o} and 35^{o}. It is within this region where the radial pressures were also observed to vary (see Fig. 4.5). In contrast, the I.D. variation is smooth and continuous with the maximum compressive hoop stress and strain values occurring at the minimum ligament section. Also shown in Fig. 4.9 are the inside and outside hoop stresses which are computed for a uniform outside pressure of 2550 psi which was determined in Section 3.0 to be the yield pressure for the ligament for uniform pressure conditions. These stresses fall

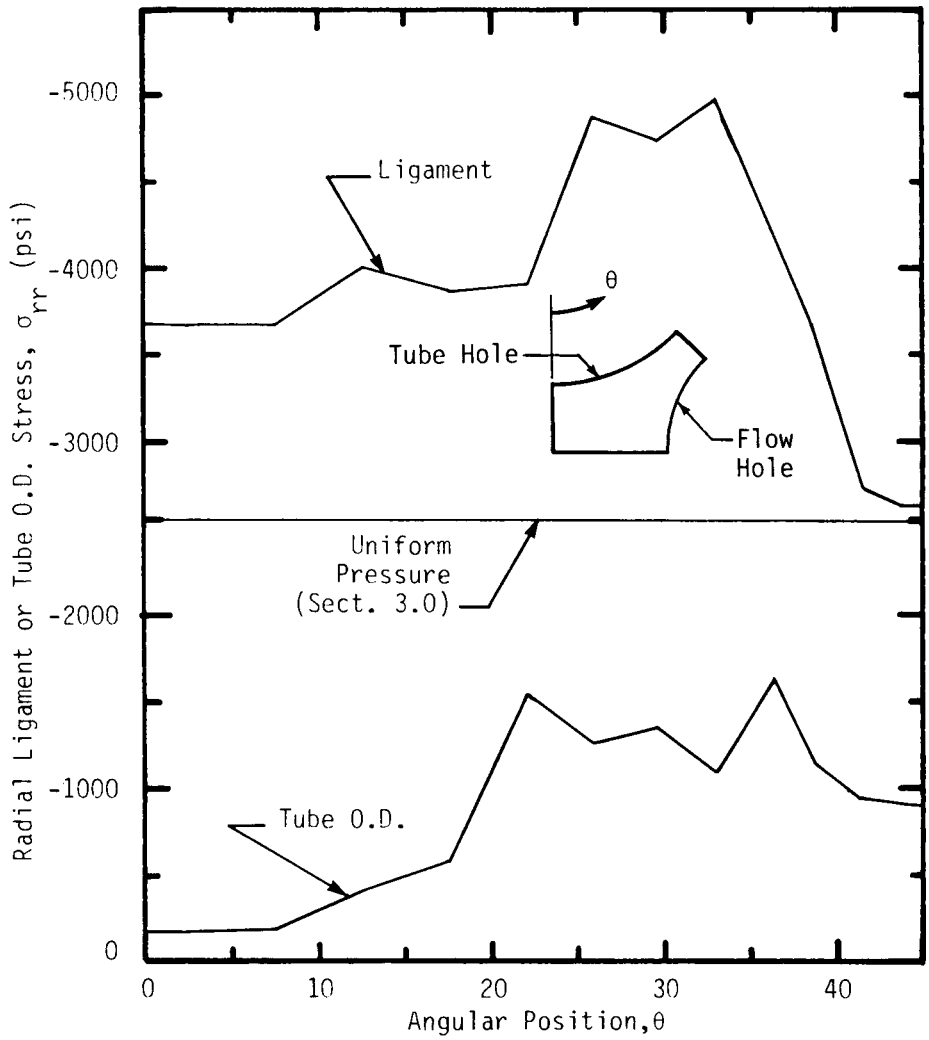

Figure 4.5 - Radial Ligament and Tube O.D. Stress as a Function of Angular Position at Initial Yield.

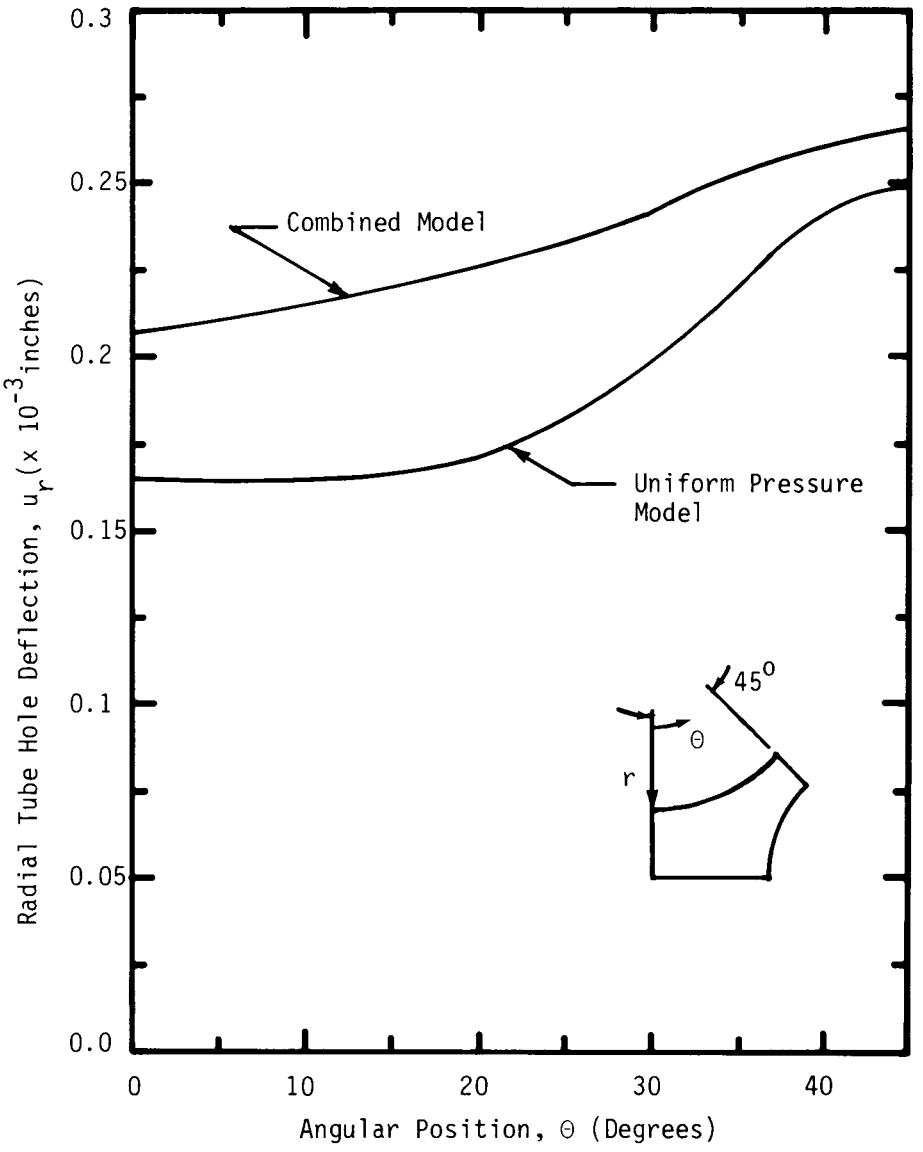

Figure 4.6 - Radial Tube Hole Deflection as a Function of Angular Position at Initial Yield for Plate Expansion Conditions.

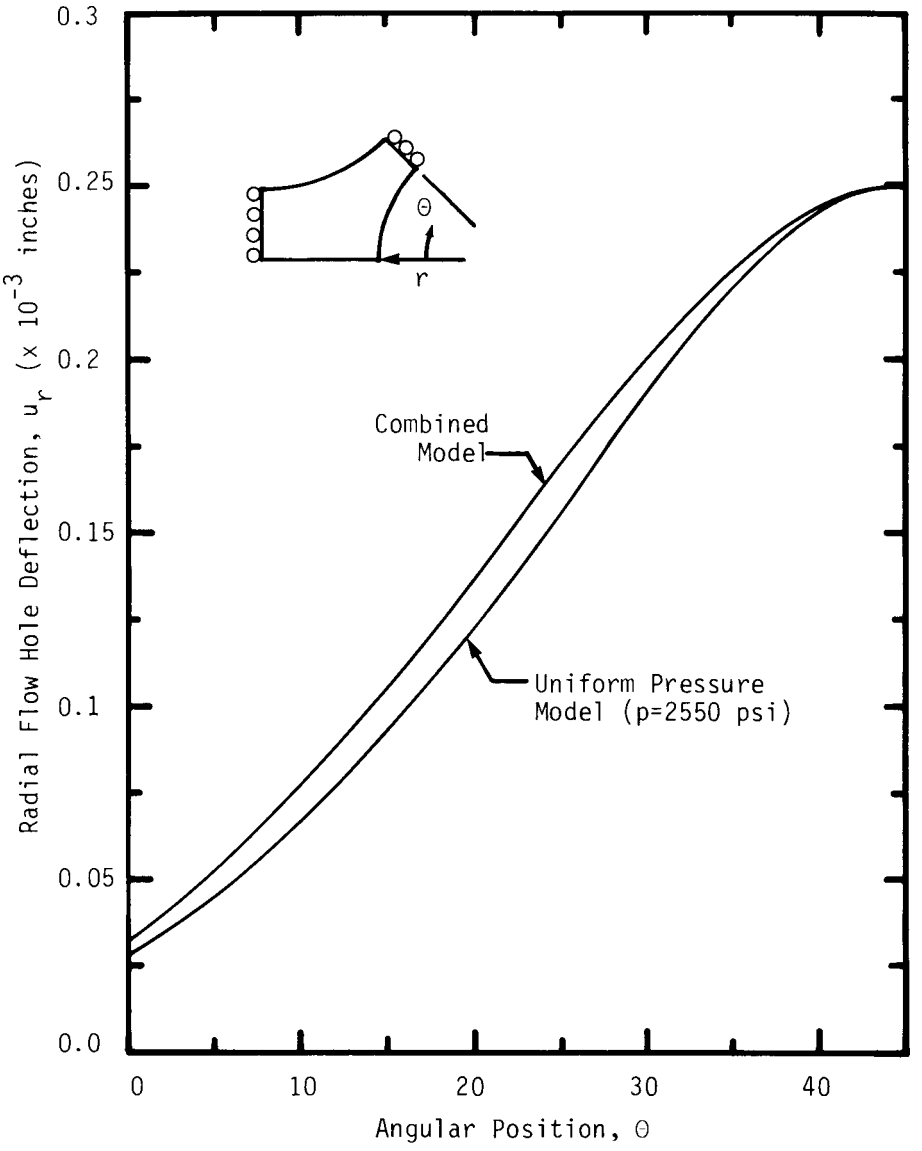

Figure 4.7 - Comparison of Radial Flow Hole Deflection at Initial Plate Yield as a Function of Angular Position.

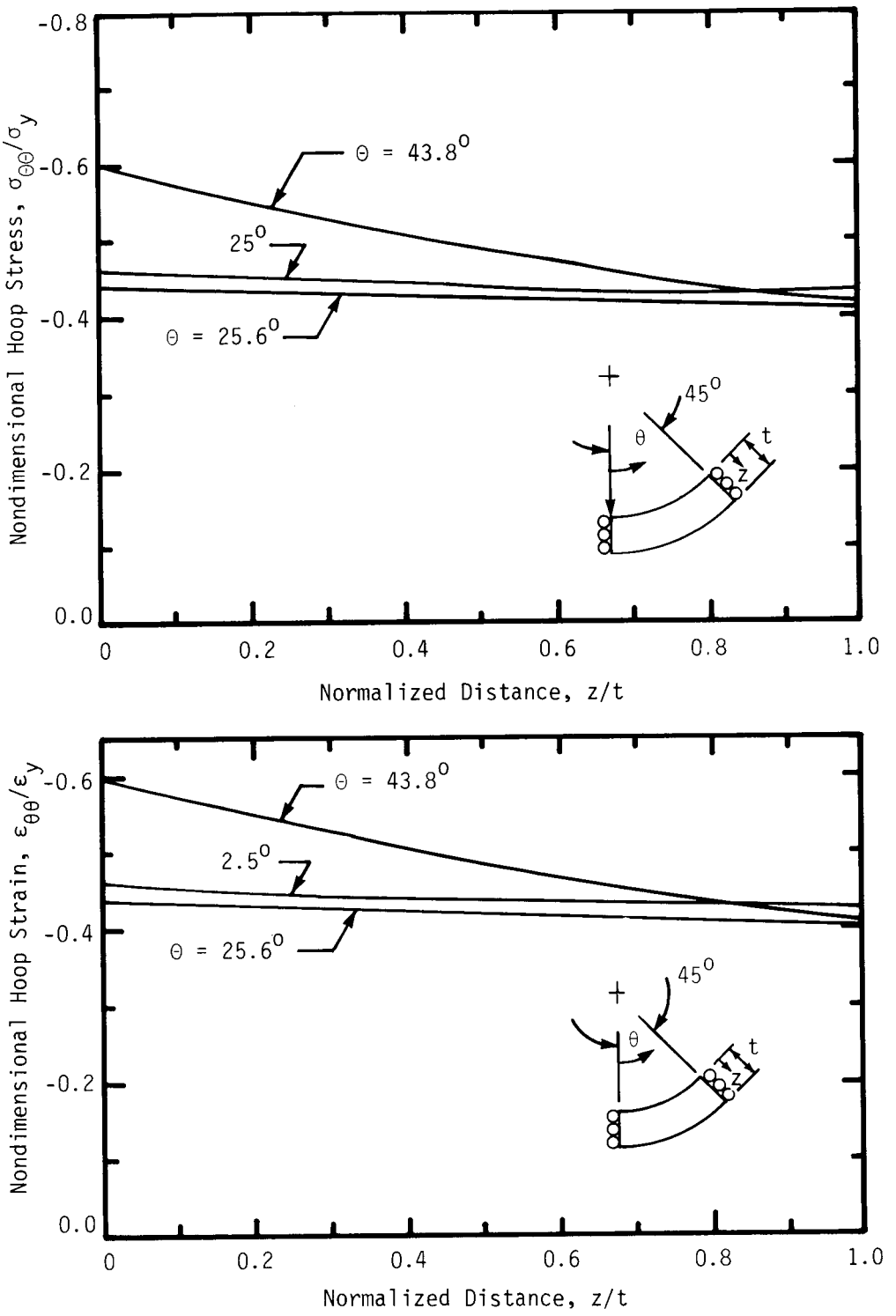

Figure 4.8 - Tube Hoop Stress and Hoop Strain as a Function of Thickness at Initial Plate Yield.

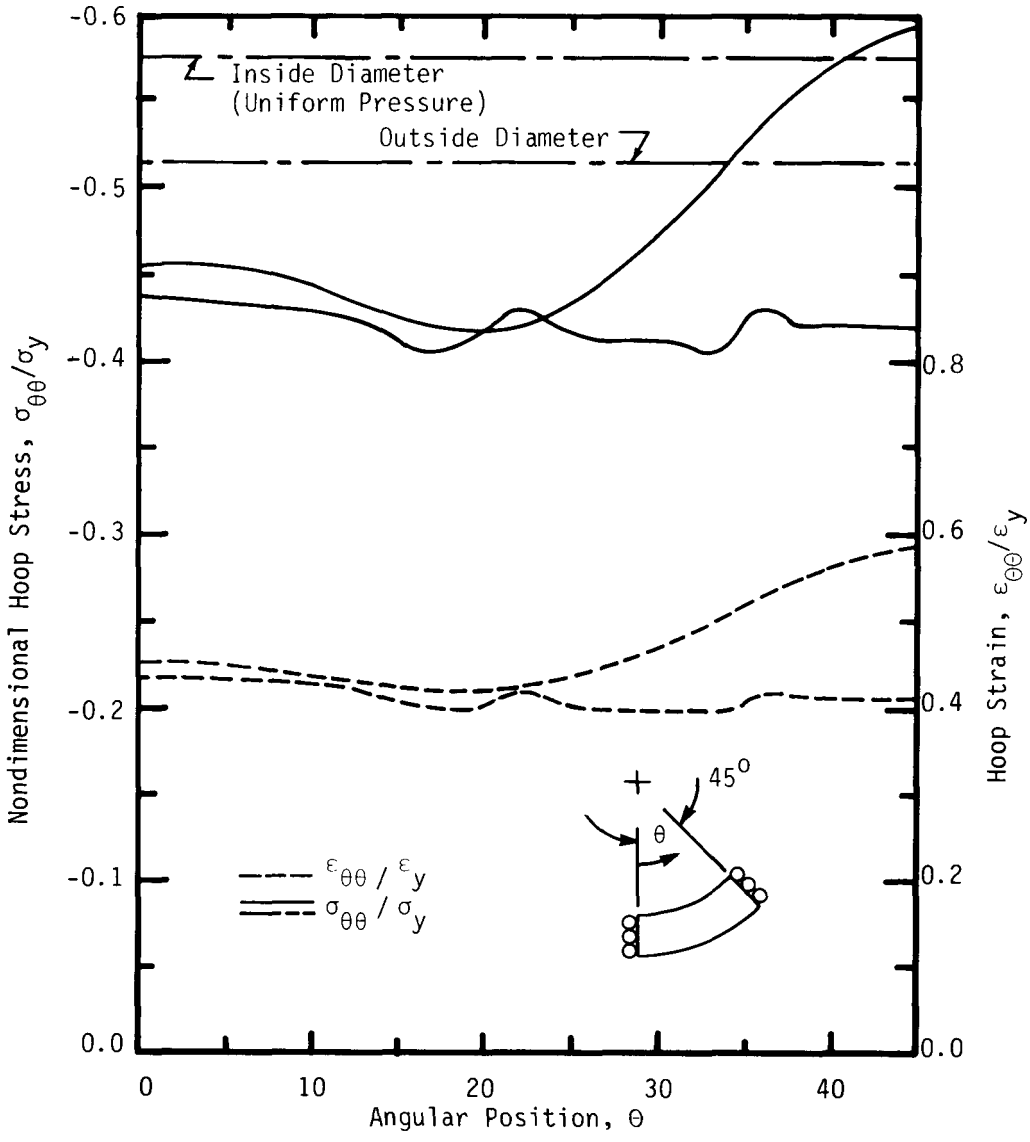

Figure 4.9 - Tube Hoop Stress and Strain for the Inside and Outside Diameters as a Function of Angular Position at Initial Plate Yield.

above the numerical results because of the lower radial stress effects on the tube as illustrated in Fig. 4.5.

The tube dent depth, δ_d, versus angular position computed for the tube at initial plate yield is shown in Fig. 4.10. The maximum dent depth which occurs at $\theta = 0^o$ is 0.56 mils. The dent depth for the uniform pressure model (p = 2550 psi) is also indicated in Fig. 4.10 from the axisymmetric tube model results from Section 2.7.

4.4 Summary of Results

1) The elastic results were obtained for a ligament model which includes the tube and oxide behavior for the case of plate expansion boundary conditions using assumed oxide properties.

2) Initial yielding first occurs in the plate at the flow hole surface at the minimum ligament, as is also predicted by the uniform pressure model of Section 3.0.

3) The hoop stresses in the tube were everywhere compressive and the maximum stress occurs at the inner diameter at the minimum ligament section. The stress magnitude in the tube at plate yield was approximately 60% of the yield.

4) The tube dent depth at initial plate yield is small and varies as a function of angular position around the tube hole with the maximum value (0.56 mils) occurring at the thicker portion of the ligament ($\theta = 0^o$).

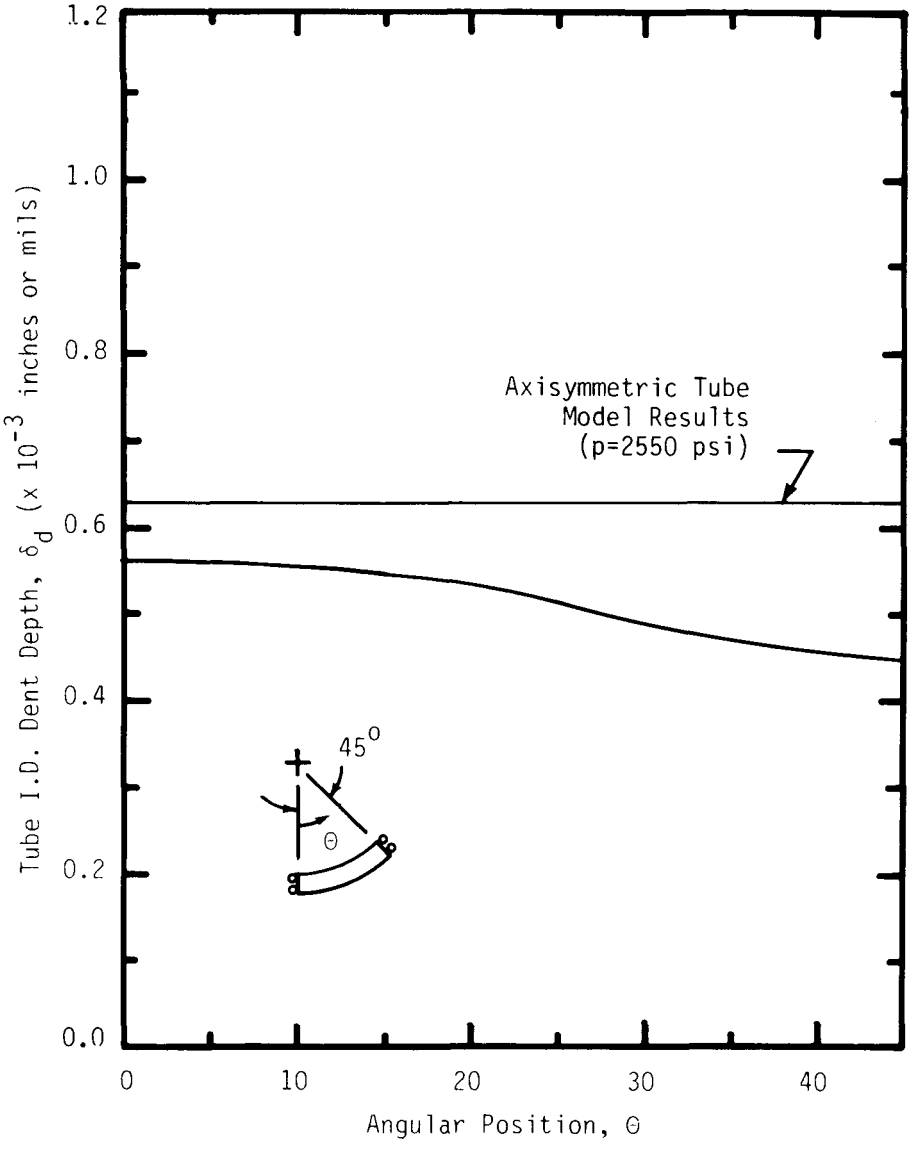

Figure 4.10 - Comparison of Tube Dent Depths at Initial Plate Yield as a Function of Angular Position.

REFERENCES

4.1 Sharma, S. S., "Thermal Expansion of Crystals," Proceedings of the Indian Academy of Sciences (A), 31 (1950), Pp. 261.

5.0 CONCLUSIONS

Mechanical aspects of the steam generator tube denting phenomena have been studied using analytical and numerical stress analysis models. The results of this preliminary study are:

1) Yielding of tube U-bends begins with only about 40 mils of support plate flow slot deformation, compared to observed deformations of more than 800 mils.

2) Ovalization of the tube cross-section at U-bends causes circumferential bending stresses consistent with stress corrosion cracking which has been observed at this location.

3) The maximum stress in the tubes due to operational pressure is approximately 21,000 psi compared to a 0.2% yield strength of 41,000 psi for Inconel 600 at 600^{o}F.

4) For axisymmetric dents, yielding in the tube begins with a 1.12 mil diametral dent depth. The maximum tensile stress is longitudinal.

5) For oval dents of the shape analyzed, gross yielding of the tube occurs at a diametral dent depth of about 10 mils. The maximum tensile stress is circumferential.

6) Yielding in plate ligaments near free edges such as flow slots begins when the tube diametral dent depths are approximately 0.60 mils, and the tube is at 60% of yield. Neglecting support plate wastage due to corrosion, tube diametral dent depths of about 24 mils are required to begin yielding plate ligaments near rigid support points or plate interior regions.

7) Yielding entirely across plate ligaments occurs near free edges at tube dent depths of about 9.5 mils. Yielding entirely across plate

ligaments may never occur near rigid support points because the tube experiences large deformations first. The latter conclusion may not hold for more refined models where plate metal loss due to corrosion is included.

8) Tube hole shapes qualitatively approximating the shape of deformed tubes from operating steam generators can be reproduced analytically.

6.0 RECOMMENDATIONS

Using the results of these preliminary analytical studies, the following recommendations are made, with the intent of acquiring future data to improve the knowledge of the denting phenomena and, therefore, the ability to suggest corrective actions from analytical results.

1) Any tubes pulled from steam generators for examination should be examined for circumferential as well as longitudinal cracks at support plate locations.

2) An inspection system that can measure tube profiles at dents should be used to greatly enlarge the data base for comparison with future analysis results from the combined tube/plate/oxide model.

3) At any time a steam generator is inspected, as much information as feasible should be recorded about the specific condition of support plates, such as location of cracked ligaments, degree of ligament corrosion, and mapping of the extent of plate corrosion with respect to tube hole row and column position.

4) The combined tube/plate/oxide models presented in Section 4.0 of this report should be extended to the plastic range and modified to account for plate metal loss due to corrosion. This local model should be interfaced with a global model to obtain boundary conditions for various plate locations.

5) A combined tube/plate/oxide model should be developed for the Combustion Engineering design.

6) Failure criteria for the tube and plate should be developed from the available lab and field data (including U-bends). The failure criteria should be interfaced with analytical models to provide a predictive capability.

7) The possible side effects of tube denting on the remainder of the steam generator system should be examined, and the most important ones analyzed quantitatively.

8) The analytical models developed should be used to study the effect of plant operational changes and proposed design corrections.

APPENDIX A

SELECTION OF ELASTIC-PLASTIC FINITE ELEMENT CODE FOR PLATE ANALYSIS

A.1 INTRODUCTION

As part of the plate analysis, an initial phase of the work was to select a finite element code which could be used to solve the plate models. A test case which involved a hole in a finite width plate under tension was designed. Originally three programs were selected as likely candidates, ANSYS (3.1), MARC/CDC (3.2), and a large strain finite element code currently under development at Stanford University. The primary purpose of the latter program was to provide a three-way check on the more common ANSYS and MARC codes. However, if this code showed superior qualities, it would have been used to perform the plate analyses. Actually, difficulties arose in attempting to execute the program, and it was dropped from consideration. The final selection was made between ANSYS and MARC based on cost since the two programs gave similar results.

A.2 TEST CASE DESCRIPTION

A hole in a plate under uniaxially applied uniform displacement was selected as the test case problem. The plate width to hole diameter was three-to-one with a uniform plate thickness of 0.3 inches. The analysis was conducted under large deflection, plane stress conditions.

The plate geometry showing the finite element mesh is given in Fig. A.1. The elements are eight-noded isoparametric quadrilaterals. The same finite element grids, element type, boundary conditions, material properties displacement increments were used in both ANSYS and MARC analyses. The strains, stresses, and yield condition requirements are computed at nine integration points located within each element.

The yield criterion is based on von Mises, and the strain hardening behavior is isotropic. The plastic stress-strain behavior is determined from Prandtl-Reuss Theory. The stress-strain behavior of the material is given in Fig. A.2.

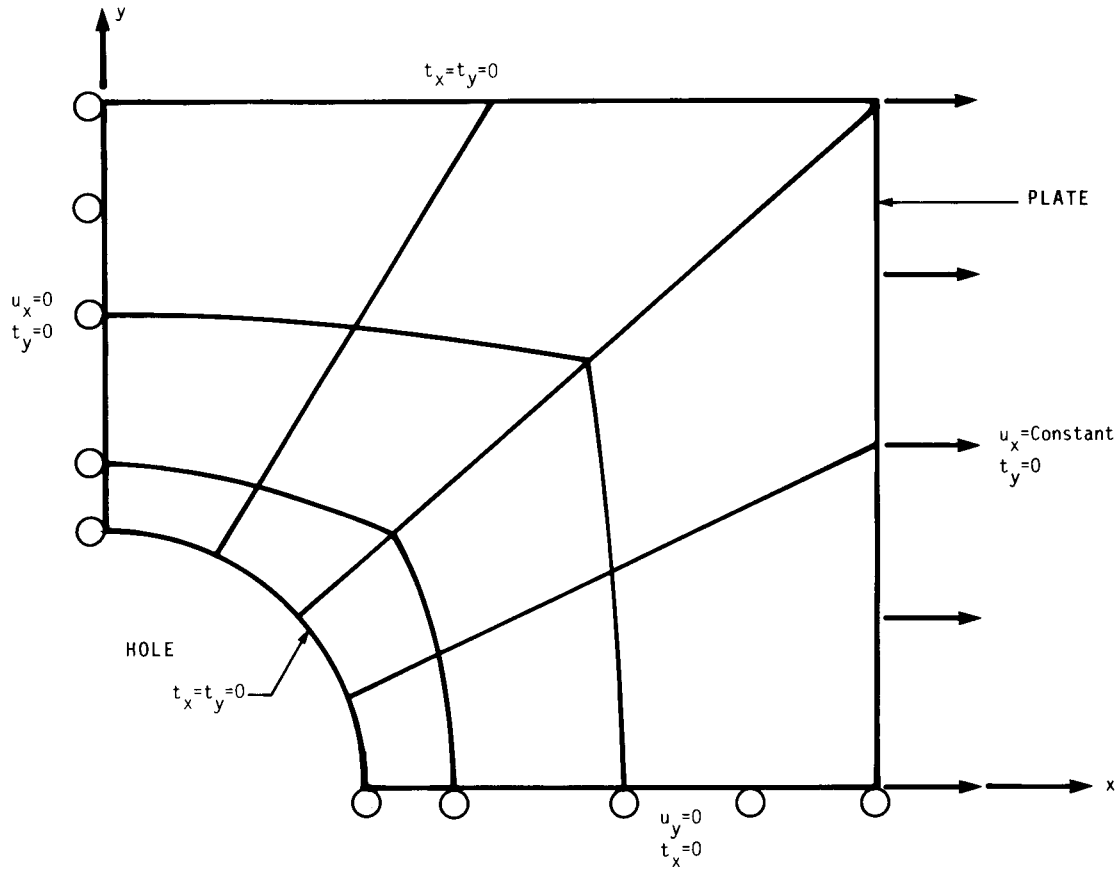

Figure A.1 - Finite Element Geometry for Test Case Problems.

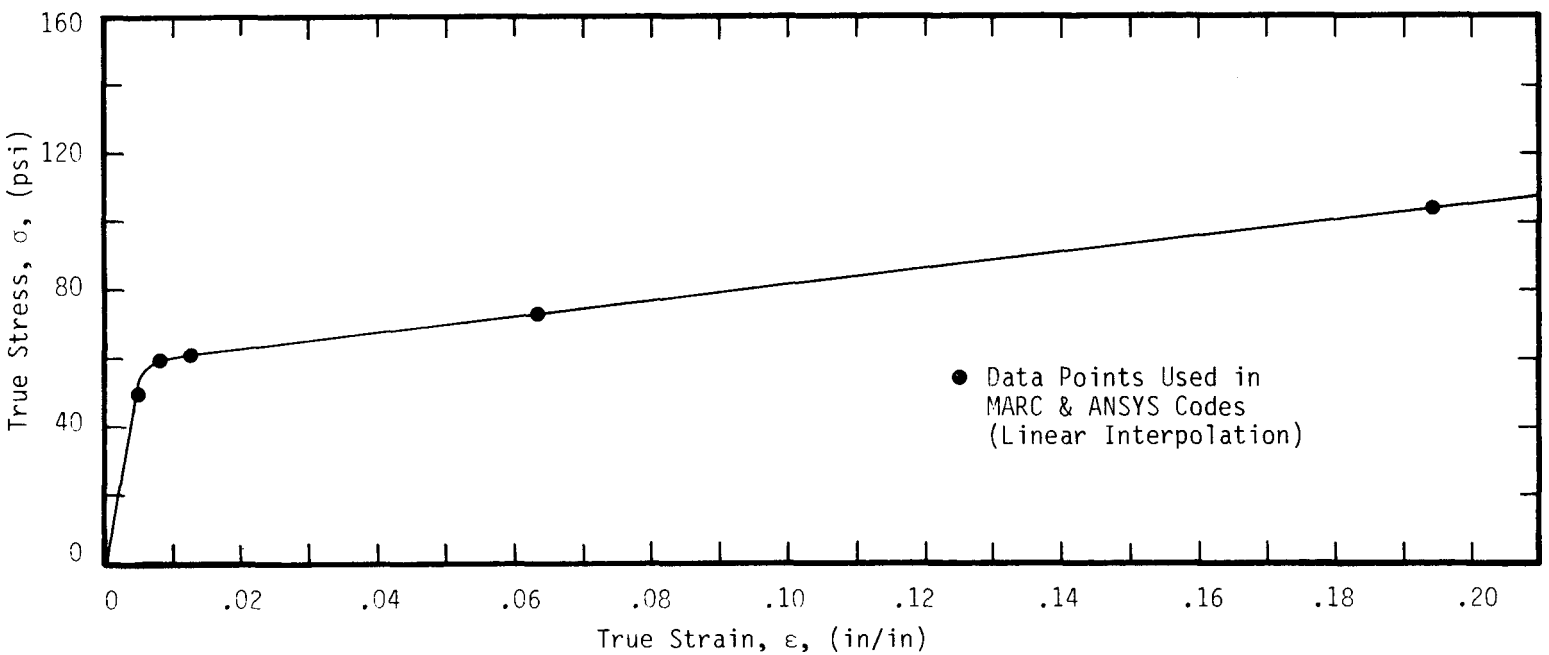

Figure A.2 - Stress-Strain Behavior for Test Case Material.

The modulus of elasticity was 10×10^6 psi and Poisson's ratio was 1/3. The yield strength, σ_y, was 49.8 ksi.

A.3 NUMERICAL RESULTS

A comparison of the elastic results gave exact agreement between both codes. Elastic-plastic stress comparisons were excellent. A comparison of the force-deflection behavior between the two codes is given in Fig. A.3. For a global plate strain of 4.3% (which is of the same order as steam generator support plate global strains), the difference in total force computed between ANSYS and MARC is less than 4%. Since both of these codes are widely used and give essentially the same results for this example problem typical of steam generator support plate problems, either code was presumed to be technically acceptable. However, since the example problem did not have a known exact solution, the example problem provides only an indirect indication of technical correctness. Agreement within 4% of the two computer codes does not mean that the models in this report represent the physical problem within 4%.

A.4 COST COMPARISONS

For the initial elastic step, the ANSYS cost was about 12% less expensive than the MARC cost. For the complete analysis, however, MARC was considerably cheaper with the cost approximately 43% of the ANSYS cost. Since both programs are made available through CDC on a cost plus basis, it is not known how much of this difference is due to code efficiency versus individual code royalty charges.

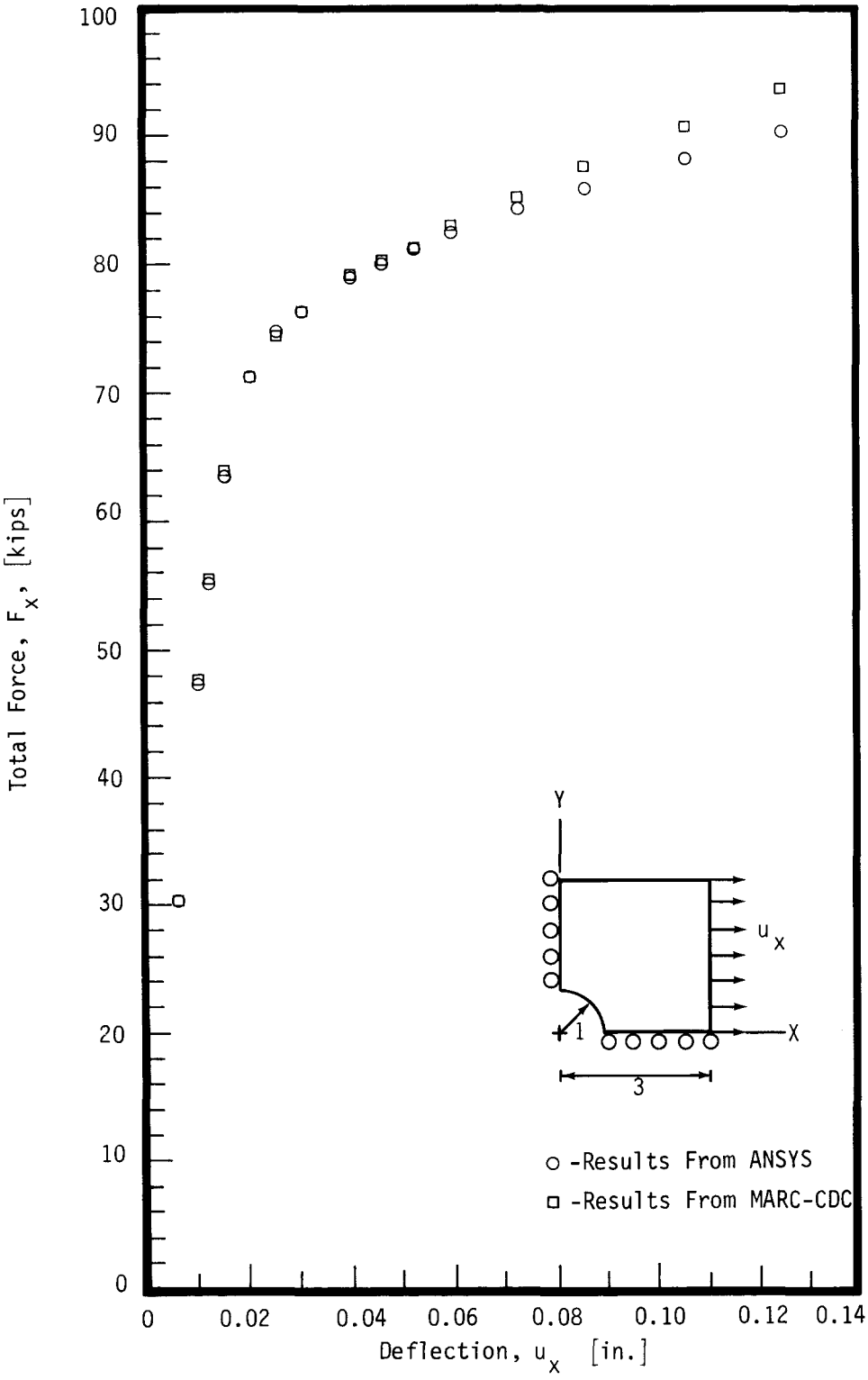

Figure A.3 - Comparison of the Force-Deflection Results of Two Finite Element Codes (ANSYS & MARC) For a Hole in a Plate Under Tension

APPENDIX B
EFFECT OF CORROSION ON SUPPORT PLATE LIGAMENT THICKNESS

In the present analysis oxide growth was modelled as a monotonically increasing uniform pressure load on the tube hole surface. Material wastage due to corrosion was not considered. At each loading step, some of the plate material is converted into a corrosion product which is most commonly found to be magnitite (Fe_3O_4). Thus, plate corrosion reduces the thickness of the ligament between the tube holes and flow holes.

For moderate tube dents, the loss of plate metal can be neglected without significantly affecting the analysis results for the support plate. This assumption enormously simplifies the computing task. For large tube dents, it becomes necessary to consider the reduction of the plate ligament thickness. In those severely dented cases, a complete coupled analysis should be performed whereby at every loading step, the plate ligament thickness is reduced to properly account for the oxide formation. A quantitative assessment described next shows how the ligament thickness decreases as tube denting progresses.

The gap that the corrosion product fills is given by:

$$g = a + \frac{\delta_T}{2} + \delta_p + t_o - t_L \qquad (B.1)$$

where

a = Original gap between the plate and tube

δ_T = Diametral tube dent depth

δ_p = Plate displacement

t_o = Initial ligament thickness at minimum cross-section

t_L = Remaining ligament thickness

The conversion factor for metal to corrodent volume is a constant given by:

$$k = \frac{g}{t_o - t_L} \tag{B.2}$$

For magnetite (Fe_3O_4), the value of k is about 2.1. Combining the above equations, an expression for the fraction of remaining plate ligament is obtained.

$$\frac{t_L}{t_o} = 1 - \frac{1}{t_o(k - 1)} \left(a + \frac{\delta_T}{2} + \delta_p \right) \tag{B.3}$$

Figures B.1 and B.2 plot (t_L/t_o) as a function of tube dent depth for the expansion and constrained boundary conditions described in Section 3.4.2. The plate displacement, δ_p, depends on the boundary conditions. Due to variations in the tube and tube hole diameter dimensions (see tolerances in Fig. 3.3), upper and lower bound curves for the minimum and maximum initial gap cases are plotted in Fig. B.1.

The effect of the ligament thickness reduction has not been directly related to the accuracy of the analysis. Note that there is a significant dependence on the dimensional tolerances and on the volume conversion factor, k. For some suspected corrosion products, the value of k is much larger than 2.1 (i.e., > 9) resulting in much less ligament thickness loss than is shown in Fig. B.1 for a given tube dent depth.

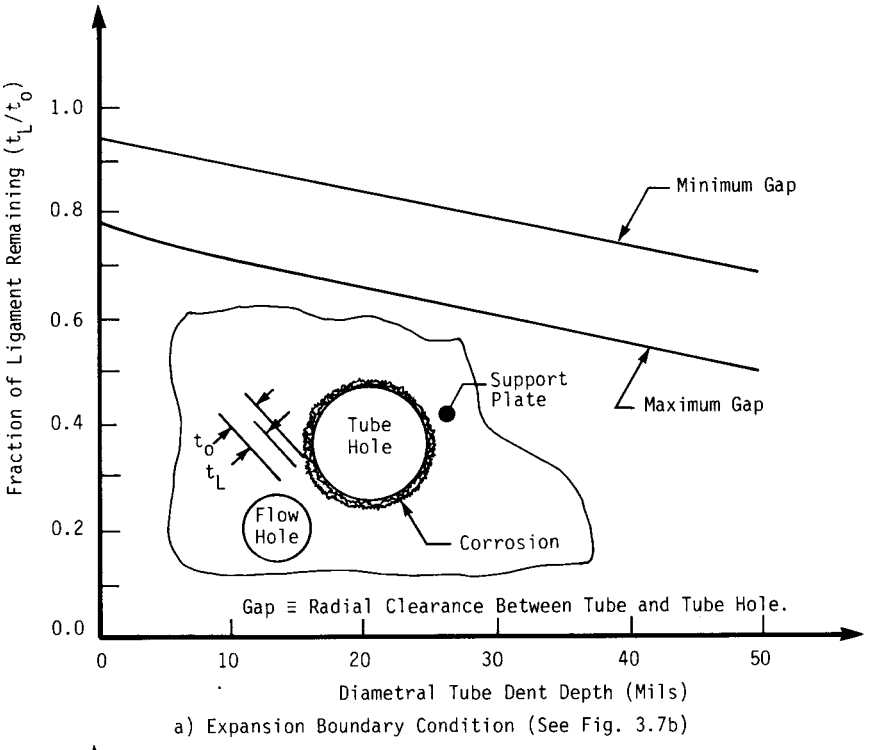

a) Expansion Boundary Condition (See Fig. 3.7b)

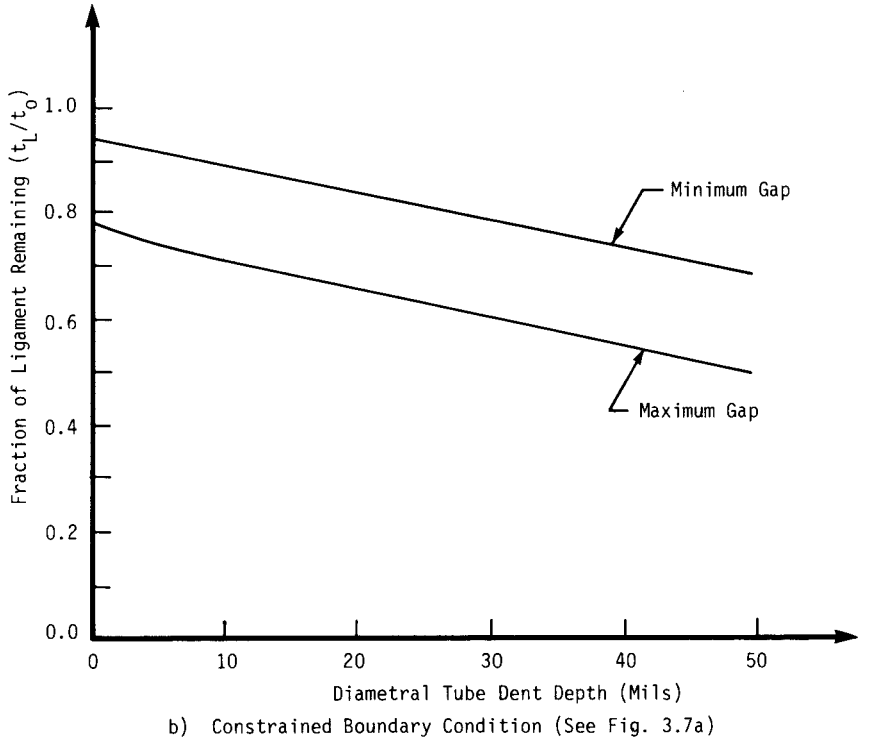

b) Constrained Boundary Condition (See Fig. 3.7a)

Figure B.1 - Effect of Corrosion on Support Plate Ligament Thickness.